UNIVERSITA' DEGLI STUDI DI PARMA

Dottorato di ricerca in
Scienza e Tecnologia dei Materiali Innovativi

Ciclo XXVIII

Organic memristive devices towards biocompatible interfaces

Coordinatore: Chiar.mo Prof. Enrico Dalcanale

Tutor:
Dott. Salvatore Iannotta
Dott. Victor Erokhin
Dott.ssa Tatiana Berzina
Prof.ssa Antonella Parisini

Dottorando: Angelica Cifarelli

SUMMARY

1. INTRODUCTION

The major aim of this thesis work is to explore combination of materials, processes and structures that could pave the way to interfacing memristive devices to biosystems and hence to explore the ability of making neuromorphic artificial systems working together with the natural ones. This aim is strategic from both the fundamental and the technological points of view. The present stage of the art is facing a series of difficulties. The organic, polymer based, memristive systems that are in principle very promising and represent to be natural candidates as biointerfaces but presently require operating conditions, in particular pH, for a functional memristive response incompatible with biosystems and neurons in particular. The present research work focuses on exploring the synergy between polyaniline electrochemistry (the basis of present polymeric memristor devices) and biology introducing other materials at the interface. The experimental work has hence taken advantage from a cross-disciplinary approach including material science, chemistry, physics and biology, reporting also some research results achieved within the framework of the PHYCHIP project, an interdisciplinary, international research project, funded by the EU.

1.1 From Bio-inspired devices to Bio-integrated systems.

Sophisticated structures and functionalities of biological systems in nature have offered unique inspirations in the development of new concepts, diverse classes of functional devices and various materials. The term "biomimetic" was first coined during the 1950s to describe a biological approach to the needs of engineering science [1]. Biomimetic materials, or biomaterials, traditionally defined as materials used in medical devices, today cover a much larger field of research. Biomimetic materials made today are routinely information rich and incorporate biologically active components derived from nature.They have found use in a wide variety of nonmedical applications [2]. The design of bio-inspired devices with tailored properties for actuation, sensing, smart electronics, computation [3], and highly efficient energy harvesting have enabled artificial devices to be endowed with bio-mimicking features among which human nervous system, artificial muscle and electronic skin that can sense and respond to environmental changes by mimicking human ways, have been widely considered as crucially important for new-generation biomimetic devices. Among these bio-inspired devices, artificial synapses are of great significance because they can emulate the signal process and memory functions of biological synapses [4]. Bio-inspired hardware holds the promise of highly adaptive computing systems. One of the major challenges of fabricating bio-inspired hardware is the fabrication of ultra-high density networks from complex processing units interlinked by tunable connections (neuromorphic computing). Their applications span from automatic classification for big data management, through unmanned vehicle control, to control for bio-medical devices. In particular, magnetic tunnel junctions (figure 1) are well suited for this purpose because of their multiple tunable functionalities [5]. A dc current injected through a magnetic tunnel junction creates

a spin torque acting on the magnetization. The resulting magnetization dynamics generate resistance variations, which can help mimic important functionalities of synapses and neurons. Xu et al. [6] proposed organic nanowire (ONW) synaptic transistors (STs) that emulate important working principles of a biological synapse. The ONWs emulate the morphology of nerve fibers with a core-shell–structured ONW active channel and a well-confined channel (figure 1).

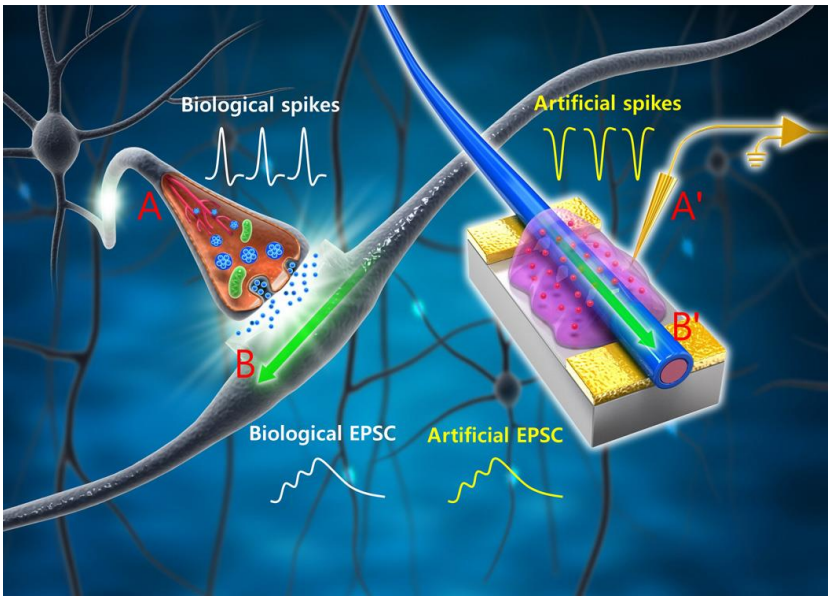

Figure 1 Schematic of biological neuronal network and an ONW ST that emulates a biological synapse.

The conductive lines and probe (A′) mimic an axon (A) that delivers presynaptic spikes from a preneuron to the presynaptic membrane. The mobile ions in the ionic gel move in the electrical field analogous to the neuron transmitters in the synaptic cleft that later induces an excitatory postsynaptic current (EPSC) in the dendrite through the contact of postsynaptic membrane. An ONW (B′) combined with a drain electrode mimics a biological dendrite (B). EPSC is generated in the ONW in response to presynaptic spikes and is delivered to a postneuron through connections to the drain electrode.

Artificial synaptic devices are of great significance for neuromorphic systems because they can emulate the signal process and memory behavior of biological synapses.

From this point of view the development of memristors, memristive devices and systems have been playing a very relevant role and represent one of the best, most promising, pathways towards adaptive and neuromorphic computing. Due to the particular relevance of this specific approach for our work, also pioneered by the Parma group [7], paragraph 2.3 will describe in details this specific field while here I give an overview of the other most relevant perspectives.

Silicon-based integrated circuits have been employed as artificial synapses and neurons, but these circuits consumed considerably more energy than biological synapses [8]. This is a quite critical issue together with the inherent complexity of this approach. It is essential to develop scalable and low-power devices to scale neuromorphic system towards the level of the human brain.

In order to obtain wider support for artificial synapse research from the viewpoint of devices and materials, three-terminal electric-double-layer (EDL) transistors were also creatively designed for artificial synapse applications [9]. For example, excitatory postsynaptic current, dynamic logic, learning and memory functions of biological synapses were successfully mimicked in carbon nanotube transistors gated by proton-incorporated polymer dielectrics [10]. Ion-related EDL modulation and interface electrochemical doping under different pulse voltages are the primary mechanisms for the short-term and long-term plasticity, respectively [11]. The emergency of these

new-concept synaptic transistors greatly enriched the scope of artificial synapses in materials and devices. Stiles et al. [12] stated that binary memories and memristors are interesting for emulating synapses (the point, where a signal passes from one neuron cell to another in the body), while harmonic and stochastic oscillators can mimic some properties of neurons or assemblies of neurons. Two-terminal memristors are the promising candidates for artificial synapses. Wang et al. [13] showed that two-terminal memristors can be implemented by silicon-compatible technology with high density and emulate synaptic plasticity with low power consumption.

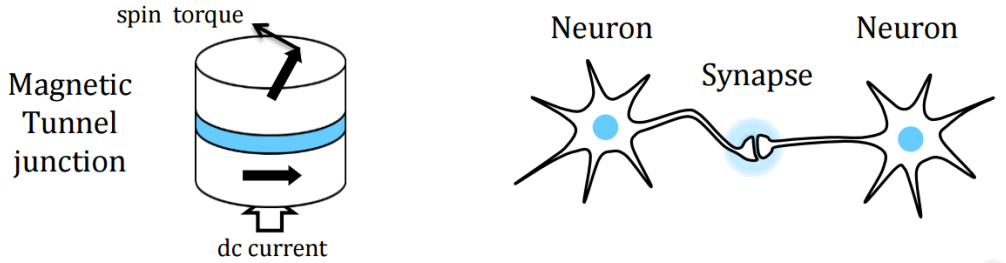

Figure 2 Principle and multi-functionality of spin torque nanodevices [14].

Wang et al. [15] developed a new type of memristive device for computer microprocessors configured more like human brains than traditional computer chips that can mimic the functioning of a biological synapse. Specifically, they developed a diffusive-type memristor where diffusion of atoms offers a similar dynamics and the needed time-scales as its bio-counterpart, leading to a more faithful emulation of actual synapses, i.e. a true synaptic emulator.

Currently, in the literature examples of organic based memristive devices are much less present. Most of the pioneering work done in Parma is based on a polyaniline – polyethylene oxide based two-terminal memristor [7]. This device is able to perform some information processing task, mimicking what happens in real neuronal circuits and the kind of plasticity found in synapses and will be better described in paragraph 2.3. New research frontiers are oriented not only towards biomimetic systems as organic memristors, but also to hybrid systems which can incorporate biological systems as key components, in order to study their properties (biosensors), as well as to exploit their intrinsic features for complex adaptive networks. There is an opportunity for sharply increased synergy between electronics and biology, fostered by both the developments of electronic technologies to the atomic scale on one hand and the rapid advances in system, cell, and molecular biology oh the other. Bioelectronics is the discipline arisen from the convergence of biology and electronics and it has the potential to impact significantly on many areas. Such developments are paving the way in the next future, to make possible to restore vision or reverse the effects of spinal cord injury or diseases. Soon it is expected that a lab-on-a-chip will allow medical diagnoses without a clinic or instantaneous biological agent detection. The application of electronics technology to biology and medicine is not new. In particular the research areas include the understanding of cellular responses and their variability for stimulation (electrical, mechanical, chemical, thermal, and the like); the ability to collect and analyze essential data on the state of biomolecules and cells (chemical, physical, structural, functional). However, nowadays, the term “bioelectronics” is becoming more widely used to describe this multidisciplinary field. A wide range of opportunities and challenges are listed in the table1. It should also be mentioned the fast rise of the Organic Bioelectronic field that is being more and more becoming a novel approach where the interfacing and the specific functionality demonstrate to be a really novel very promising approach [17,18,19].

Category	Highest Priority Research Challenges
Drivers	• Prosthetics, including tissue and neural implants, i.e. vision, hearing, etc. • Disease Prevention, including neural degeneration, cancer, etc. • Disease Detection, including neural degeneration, cancer, etc.
Devices	• Lab on a chip • Protein and DNA chips • Imaging, including cellular • Telemonitoring
Measurements and Analyses	• Noninvasive physical sensing, e.g. vital functions • Concentration of analyte and metabolites, etc. • Real-time & time dependent measurements • Single bio-molecule detection, e.g. in Lab-on-Chip environment (including mass, size, chemical, optical, etc.)
Technologies	• Molecular recognition • Signal processing algorithms • DNA sequencing • Fabrication (electrodes, devices), including patterning • Thin film technology

Table 1 Research challenges of "bioelectronics".

After the vey fist pioneering work in the 18-th by Galvani that could be considered the founder of the field with the famous experiments on the frog, the first reference to bioelectronics, published in 1912, was focused on the measurement of electrical signals generated by the body, which became the basis of the electrocardiogram. In the 1960s two new trends in bioelectronics appeared. One trend, enabled by the invention of the transistor, was focused on the development of implantable electronic devices and systems to stimulate organs, e.g. the pacemaker. Today, bioelectronics focuses on the application of electronics to physically interfacing electronic devices with biological systems (e.g., brain-machine, cell-electrode, or protein-electrode). Applications in this area include assistive technologies for individuals with brain-related disease or injury, such as artificial retinas. A lot of research is devoted to the interaction between bio-molecules and solid surfaces (bio-electronic interface). Examples include bio-molecule immobilization, electron transfer in biochemical reactions and between bio-objects (bio-molecules or cells) and solid surfaces.

Often, biologists and engineers are speaking two different languages which are quite different. Device microfabrication typically employs top-down, monolithic methods to generate patterned surfaces from hard materials (e.g., silicon wafers). In contrast, biology self-assembles from the bottom-up often using soft matter. Manipulation of biological macromolecules, i.e. nucleic acids and/or proteins, implies the use of buffered solutions (usually pH ~ 7), controlled salinity, and regulated temperatures. Interfacing these biological salt solutions with electronics and sensor architectures seems to be an oxymoron. Thus, the conversion or push of biological materials away from solution to solid-state processing has been a key technology. The way to overcome this seemingly insurmountable incompatibility is the use of "bridging" materials systems. These approaches make possible to implement biocompatible materials that do not destroy tissue or cells but maintain the native structure of biomolecules, and possibly at the same time do not compromise the device operation. The electronics-biological matter interface has been identified as one of the frontiers of biophysics that is expected to gain prominence in the next decade (figure 3). The best approach to reconcile the differences between biology and fabrication is to develop methods that allow the biological components to be incorporated into the device after the device has been fully microfabricated [20, 21]. For example, Kim et al. [22] proposed to use the aminopolysaccharide chitosan to Connect Biology to Electronics by fabricating the bio-device interface for the assembly of the biological components at device addresses, using chitosan derivatives to promote such communication across the bio-device interface. Another example that recently highlighted the potentiality of biological

materials for hybrid devices was achieved by integrating the latter into a common electrical construct like a light emitting diode (LED). Researchers have processed the discarded DNA into a surfactant complex and have scaled the process up on a multi-gram scale [23]. At the scale and in the form used, the DNA can now be spin-coated into tradition electronics architectures. A DNA electron blocking layer spin deposited on the hole injection side of the electron-hole recombination layer greatly enhanced LED efficiency and performance [24].

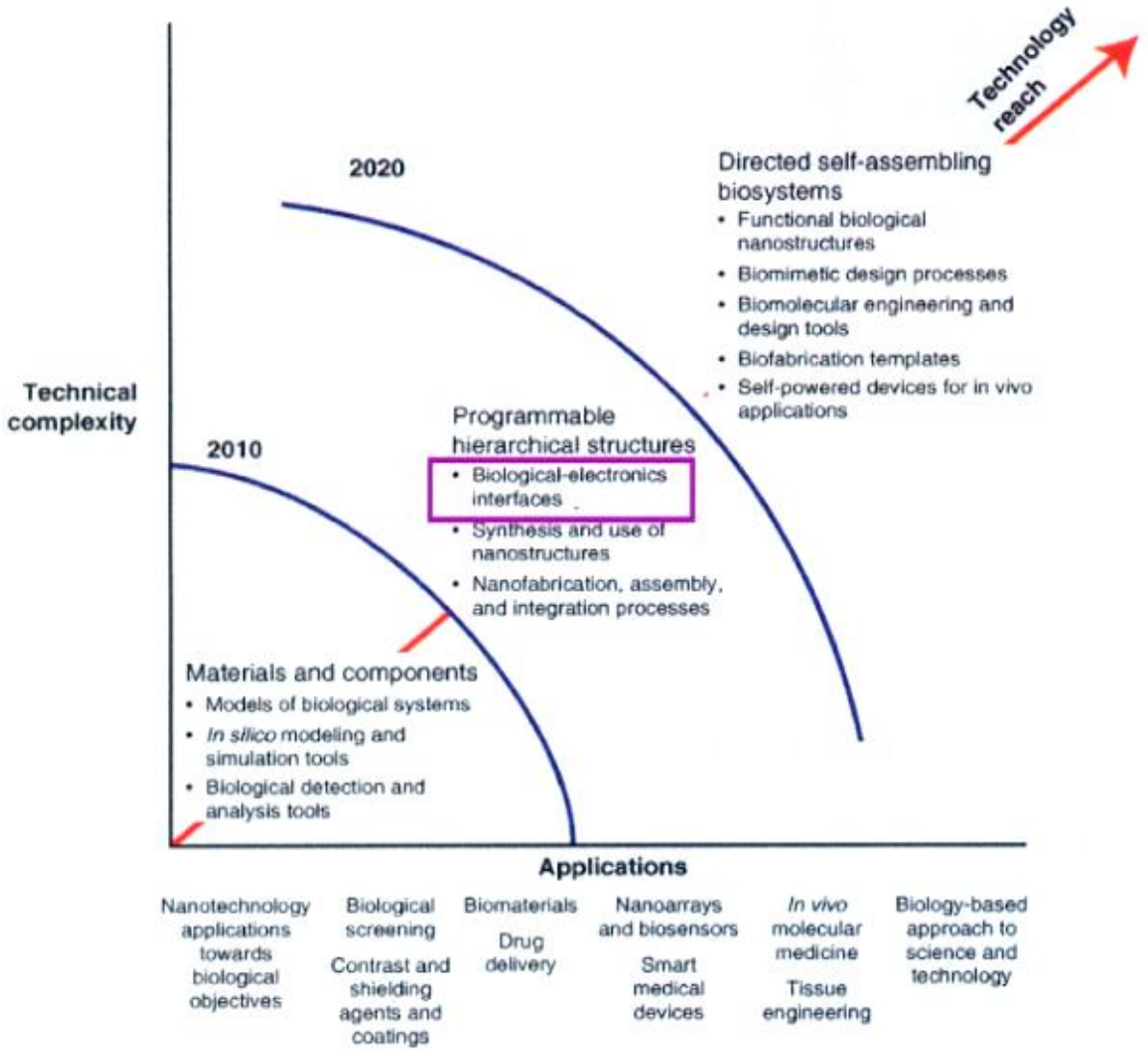

Figure 3 Research frontiers for biophysics and biotechnology in the life science from [25].

Area	Possible Applications
Analysis	Biosensors—multiplexed analysis in hand-held devices Lab-on-a-Chip—high-throughput screening Smart fabrics—remote monitoring of first-responders
Energy	Biofuel cells—efficient conversion of chemical and solar energy Nanostructured batteries—compact storage of energy
Medicine	Devices to personalize medicine—theranostics Prosthetics—effective repair or restoration of function

Table 2 Examples of opportunities enabled by bio-device integration.

Figure 4 illustrates our broad vision for integrating biology and electronics. At the left, a bio-device interface fabricated by assembly step(s) that physically localize the biological components (e.g., proteins, nucleic acids or cells) to an electrode address in a microfabricated system (e.g., an electrode array or microfluidic device) is shown.

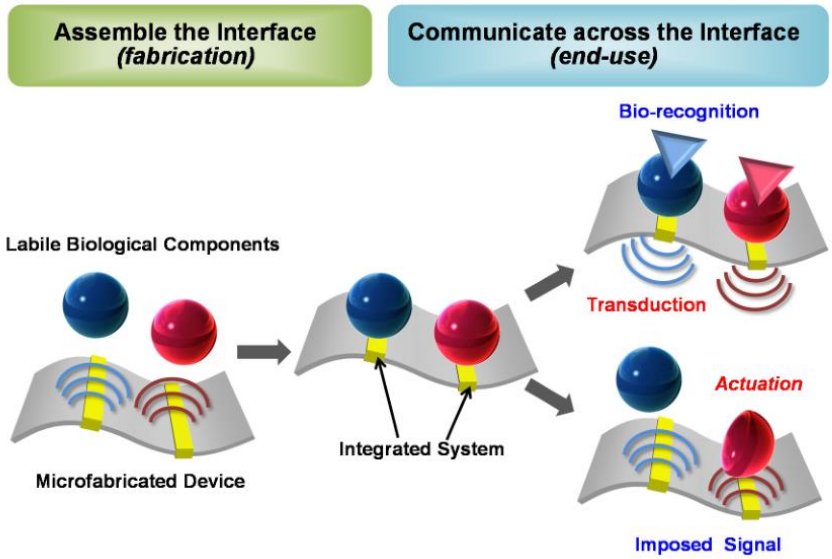

Figure 4 Broad vision for interfacing biology with electronics [26].

An ideal bioelectronic device would allow ready communication between the biology and the electronics. Communication will allow the interconversion of biological and electronic signals Since many envisioned applications of bioelectronics involve sensing/analysis, communication should allow biological recognition events to be transduced into device compatible (e.g. electrical) signals. Alternatively, communication in the opposite direction could allow device-imposed signals to actuate biology. For instance, if the assembled biological component is a protein, actuation could involve triggering of its release from the interface (e.g. for controlled delivery) or actuation could involve inducing of a conformational change to exert a force or to alter biological function (e.g., alter enzymatic activity) [27].

However electronic and biological systems use entirely different information processing approaches. As implied by the name, electronic systems employ electrons (or photons) to process information. In contrast, biology rarely uses electrons or photons for information processing. Usually, ions (e.g., Ca^{+2}) and molecules (e.g., hormones and neurotransmitters) are used in biology information processes. Thus, in order to establish effective communication between electronics and biology it is necessary to bridge somehow these different signal processing modalities.

The obvious obstacle of using electrons for communication between biology and electronics is the fact that free electrons do not exist in aqueous solutions characteristic of biological systems. Bio-

device communication using electrons essentially means the linking of electrochemistry at the device-water interface with redox-biology. Electrochemistry focuses on the electrical potentials and currents at an electrode-solution interface and links the transfer of electrons across this interface to the oxidation-reduction (redox) reactions occurring on the solution side of the interface. Because electrical potentials and currents can be readily measured and controlled, electrochemical methods are highly sensitive and rapid, while the instrumentation is relatively inexpensive. From a biological perspective, redox reactions may provide an important "interface" with biology. A very promising approach within organic bioelectronics is the one based on Organig Electrochemical Transisotrs (OECT) proposed by Berggren, Malliaras and further developed also by Parma and Trento Groups [28-30].
The great strength of this approach is that such devices are direct amplifying transductors of ionic to electronic currents and hence are ideal systems to interface biological signaling into standard electronic devices and systems that is our current technology. They represent ideally suitable systems for bioelectronics. In this thesis, we report the first OECT operating in tandem with a cell and demonstrating memristor properties [31].
In initial study with a culture of Escherichia coli, two biological mediators were added. For reductive redox-cycling the pyocyanin, produced by the bacteria Pseudomonas aeruginosa, was added and reported to be both a virulence factor and a signaling molecule [32-35]. Meanwhile, recent progresses in using natural biomaterials to construct functional synaptic devices was achieved. [36-38]. In the past few years, proteins were generally employed to fabricate functional electronic devices, such as field-effect transistors, resistive switching memory and diodes [39-41]. Chen et al. [42] proposed, natural chicken albumen films with high proton conductivity as the electrolyte dielectrics for fabrication of indium-zinc-oxide (IZO) synaptic transistor. Important synaptic functions including paired-pulse facilitation, dynamic filtering, short-term to long-term memory transition, and spatial summation/shunting inhibition were successfully mimicked by the albumen-gated synaptic transistors (figure 5).

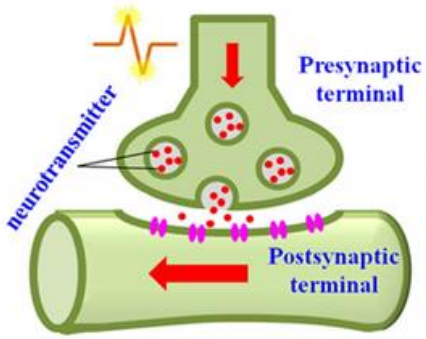

Figure 5 Schematic diagram of a biological synapse [42].

Bioinspired, biomimetic and biomaterials are emerging as the most promising area of research within the area of materials science and engineering. The technological significance of this area is immense for applications as biosystems to biomimicked sensors and devices.

1.2 Thesis Outline

As mentioned above, the main purpose of this thesis was to develop an interface between polyaniline (PANI) Langmuir-Blodgett film and biological environment, in order to preserve the electrical conductivity of the polymer, extending to wider pH range the functioning of PANI-based memristive devices. In this thesis, interfaces based on polysaccharides films are proposed.
First of all the biopolymers, materials never used before in organic memristive elements, were tested in combination with LS- PANI films in standard configuration (ST-OMD).

Then, several trials on ST-OMD were carried out in order to identify the chemical species and components responsible for the electrochemical switching of PANI in OMD. This step was necessary to develop the "double-layer solid polyelectrolyte" technology as well as to choose the formulation of polysaccharide gels suitable for intermediate layer in bio-integrated systems.
Verification and proof of "double-layer solid polyelectrolyte" technology for OMD were carried out by the integration of Physarum Policephalum (PPM) in this organic architecture. PPM peculiar properties were fully characterized in this thesis.

The thesis has the following structure:
Chapter 2 presents a general review of the literature relative to this research. This review is focused mainly on the memristive systems, the properties of PANI, redox reactions and ion transport properties of polyelectrolytes in gel phase and their potential applications.

Chapter 3 is focused on the choice of biocompatible materials suitable to be implemented in electronic architectures as "bridging". In addition, this chapter presents the motivations of choosing hydrogel-based interfaces as intermediate layer between the biology and the electronics.

Chapter 4 presents the electrical characterization of devices in which biopolymers are used as solid polyelectrolytes. Pectin and chitosan films are tested in combination with LS- PANI films in standard configuration (ST-OMD). The electron/ion transport processes that occur at "the contact area" (see par. 2.3) between PANI film and solid polyelectrolyte are discussed in detail and a possible explanation of electrochemical process occurring in the electronic architecture is proposed.
In addition, the morphological, spectroscopic and electrical characterization of the double-layer architecture is reported.

In Chapter 5 the Physarum Policephalum, chosen as model organism, was integrated in the multilayers architecture. In particular, for the first time the unique properties of cellular systems are interfaced with the electronic/ionic responses that characterize PANI organic memristive elements based on PANI layers.

2. Conductive polymers, polyelectrolytes and memristive devices.

2.1 Π-conjugated polymers and devices.

Conducting polymers belong to a particular family of compounds composed of monomer units with conjugated chemical bonds that, under certain conditions, ensure the electron/hole conductivity of the polymer. From the commercial point of view, these polymers are promising for the production of materials suitable for various applications; they can replace metals and semiconductors, because they feature conductivity, low density, and easy processability. Electronically conductive polymers are conjugated organic materials, sharing the same signature. Since the orbitals of successive carbon atoms along the backbone overlap in the π bonding, the electron delocalization can be realized along the polymeric chain [43]. This electronic delocalization provides a vehicle for charge mobility along the backbone of the polymer chain. The simplest possible form of electronically conductive polymers is the archetype polyacetylene $(\text{-CH})_n$. Electronically conductive polymers are particularly attractive due to the doping induced insulator-metal transitions. Doping is the unique, central theme that

distinguishes conductive polymers from all other types of polymers [44]. Reversible doping of conductive polymer, associated with control of the electrical conductivity over the full range from insulator to metal (typically from 10^{-10} S/cm to 10^{5} S/cm), can be accomplished either by chemical or by electrochemical methods [45]. Upon doping, the Fermi level of electrons is moved into a region of energy where there is a high density of electronic states either by a redox reaction or an acid-base reaction [45]. The initial discovery of the possibility to dope conjugated polymers involved charge-transfer redox chemistry: oxidation (p-type doping) or reduction (n-type doping) [46]. The doping via protonation can be fulfilled in polyaniline, where the number of electrons associated with the polymer chains is neither reduced nor increased and the charge neutrality of the polymer matrix in the doping process is maintained by the insertion of counterions. Polarons and bipolarons are charge carriers generated upon doping or photo-excitation in conjugated polymers with non-degenerated ground state [47]. Both are structural defects that are introduced into the conductive polymers upon charge injection. The polaron is a radical cation, which is a kind of quasiparticle consisting of a single electronic charge dressed with a local geometrical relaxation of the bond lengths [45]. The bipolaron is a spinless dication, which is the doubly charged state of two polarons bound together by the overlap of a common lattice distortion or enhanced geometrical relaxation of the bond [45]. The study of the energetics of the separation of the radicals induced upon doping of polyparaphenylene indicates that the two defects tend to remain in close proximity, resulting in the formation of a polaron [48]. At higher doping levels, interaction between polarons leads to the formation of bipolarons (doubly charged defects) that requires a stronger deformation of the lattice [48]. The commercialized applications of conjugated polymers have covered wide fields such as electrolytic capacitor, rechargeable batteries, magnetic disk, special electrode and printed circuit [49]. Doped polyaniline has been used for electromagnetic shielding [50] and for corrosion inhibition. Polypyrrole has been tested as microwave-absorbing "stealth" screen coatings and as the active thin layers of various sensing devices. Polythiophene derivatives are widely used for or field-effect transistors [51]. Poly (ethylenedioxythiophene) doped with polystyrenesulfonic acid has been manufactured as an antistatic coating material to prevent electrical discharge exposure on photographic emulsions. Poly (phenylene vinylidene) derivatives have become major candidates for the active layer in production of electroluminescent displays.

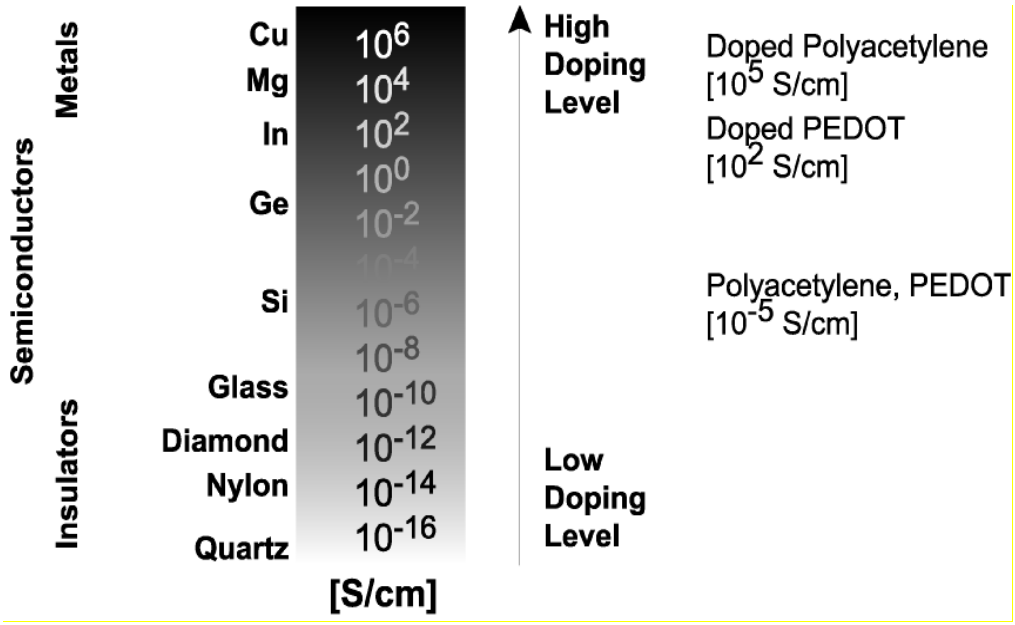

Figure 6 Comparison between the electrical conductivity of conductive polymers and inorganic materials.

2.2 Memristors and memristive devices

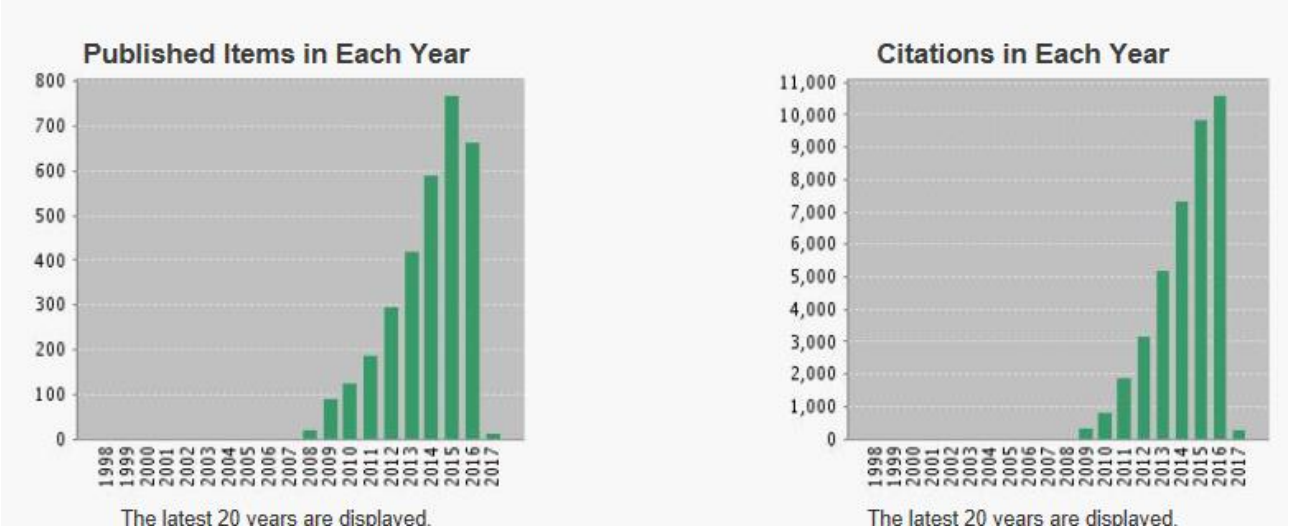

Figure 7 Results per year when searching for "memristor" in ISI – Web of Science

The concept itself of a device called "memristor" was introduced in 1971 [52] by Leon Chua in his paper in IEEE – Transaction on circuit theory, however, without demonstration that it was even physically possible to build such a device. Few significant advances on the topic were made in the following 35 years, with one or two publications per year about memristive systems, until in May 2008 the researchers of HP Labs in Palo Alto claimed, to have built the first memristor, a nanoscale two electrode device based on titanium dioxide [53]. Figure 7 shows the exponential growth in terms of publications and citations that has been experienced from that year reaching more than 700 hundreds of publication and more than 11000 citations per year in 2015/16., two international symposia on memristors and memristive systems, with a large number of symposium and two sessions dedicated to memristors at the 2010 International Symposium on Circuits and Circuits systems, and even a science fiction short story where the memristor features as a ground-breaking technology advance.

In his pioneering work, Chua argued about the existence of the memristor in 1971 by noting that there are four fundamental circuit variables: the current i , the voltage v , the charge q , and the magnetic flux ϕ. There are six possible pairings between these variables; each pairing save one is used in the definition of either the quantities themselves ($q = \int_{-\infty}^{t} i(t)\,dt$ and $\phi = \int_{-\infty}^{t} v(t)\,dt$) or in the axiomatic definitions of resistors ($dv = Rdi$), capacitors ($dq = Cdv$) and inductors ($d\phi = Ldi$) (figure 8). The only pairing left out is the relationship between ϕ and q. Chua proposed that the relationship $d\phi = Mdq$ should be adopted as the axiomatic definition of a fourth basic circuit element, called memristor as a contraction from memory resistor.

Figure 8 is a diagram showing the possible relations between i, q, ϕ, and v [53] Chua showed in the paper that if the memristance M is constant, a memristor behaves exactly like a conventional resistor; however, if the memristance is itself a function of the charge q but not explicitly of time t, i.e. if the magnetic flux depends nonlinearly on the charge, the relationship between the voltage at the terminals of a memristor and the charge through it is:

$$v(t) = M(q)i(t) = M\left(\int_{-\infty}^{t} i(t)\,dt\right)i(t) \qquad (Eq.1)$$

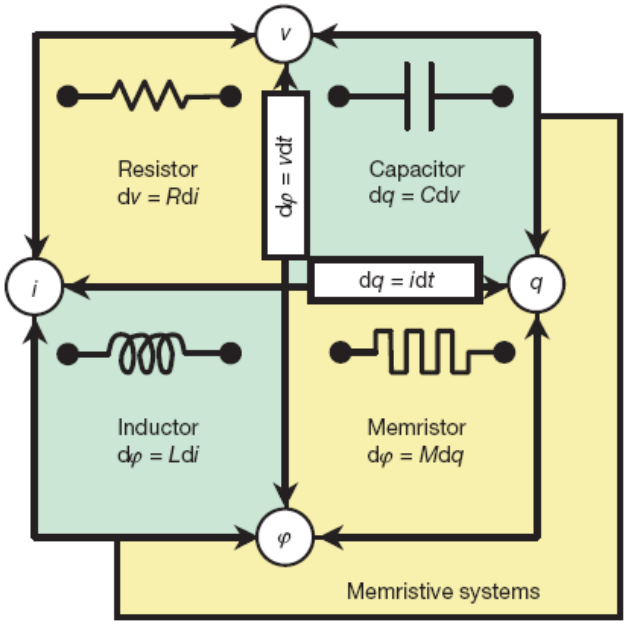

Figure 8 diagram showing the possible relations between i, q, ϕ, and v [53].

In other words, while at each instant in time a memristor behaves like a resistor, the actual value of the resistance depends on the whole history of the currents that have passed through the device: the device shows a kind of "memory", hence the name "memristor" [54].
Some years later, the first definition of memristor was expanded by Chua himself introducing the definition of memristive system [52], a device in which the memristance is a function of an internal state variable, of the input, and possibly an explicit function of time too. In the same paper it was also shown that a large number of systems could be modelled using a suitable memristor, amongst which the neurons' sodium channel, using the biologically accurate Hodgkin-Huxley formalism. In 1995 Chua also proposed a model of cellular neural networks [55].
Actually different research groups observed hysteretic current-voltage characteristics and memristive behaviors in AgI nano-particles assembly [56] claimed to have built a functioning memristor, although there are reports of resistive switching phenomena, especially when dealing with metallic oxides at the nanoscale, dating back to the late nineties [57, 58]. Researchers from the same group that eventually claimed the memristor, were already looking in that direction, by exploring the resistive switching effects in metallic oxides thin films and the possible applications of an array of many, unreliable switching elements within a structure called a crossbar [59, 60]. Here the main goal of the research was to find a high density memory element, but some papers already envisioned the possibility of a new computation paradigm using what we would now call memristors [61].
The first memristor model was proposed in 2008 by Strukov et al. [62]; they showed how memristive effects are bound to come up naturally in materials at the nanoscale, where there is a strong interplay between ionic and electronic transport.
The proposed model consists of a thin semiconductor film, in which there is a region with high concentration of dopants and, therefore, it is highly conductive, and a region where the concentration of dopants is lower and the resistance is higher (see figure 9). The film is attached to two electrodes. When a voltage bias is applied to the film, the doping ions move in the semiconductor, expanding one region of the expense of another, and changing the global resistance of the film.

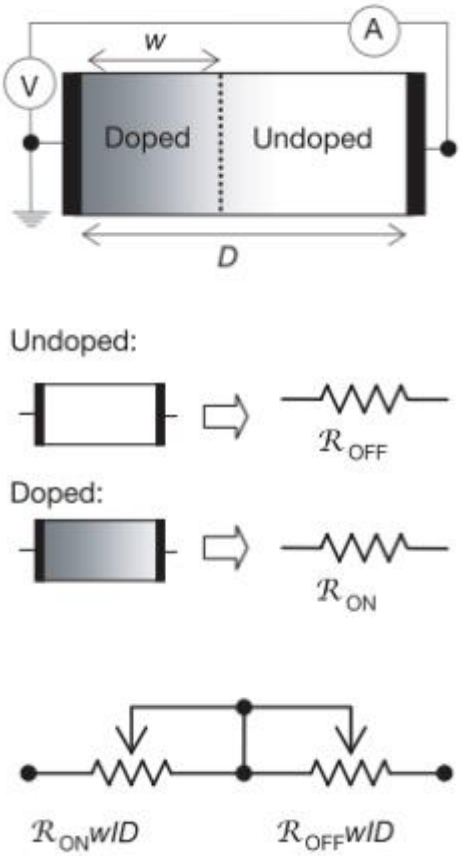

Figure 9 Diagram of a TiO2-based memristor as proposed by Strukov et al.[62].

Stukov et al. demonstrated also, that by varying the frequency or the amplitude of the input signal and by adjusting the nonlinear correction it is possible to reproduce the hysteresis found in the I-V characteristic curves that had been already observed in a range of different materials, from organic films to metal oxides. Furthermore, they provide their own experimental result of a TiO2 – TiO2-x device, in which the dopants are oxygen vacancies, that behave very closely to the model proposed, and which therefore they claim to be the first example of a single, passive memristive device.
Titanium oxide memristors were investigated also at the Imperial College [63], where the memristive behavior, with a contrast in resistance of two orders of magnitude, was present even in devices of several microns in size. Some highly innovative approaches permitted to build a titanium-based memristor also on a flexible support [64] using spin-coating of titanium solution on a polymeric substrate, in order to achieve an amorphous TiO2 film that is cheap to produce and can be utilized in disposable "smart" sensors. Recently an Albanian group of scientists proposed a method allowing to selfassemble a network of titanium based memristors [65].
There are some approaches that rely on different physical processes in order to obtain a memristive device. Amongst them, the one based on the phase transition of vanadium oxide is has already shown some possible applications [66-68]. In VO_2, a phase transition from insulator to metal occurs in proximity of room temperatures. In these conditions, the applied voltage pulse can trigger the transition of nanoscale regions from insulating to metallic, gradually forming a conductive network that percolates through the insulating medium, ionic drift, is that the polarity of the potential applied does not affect the resistance change, so positive and negative potentials have the same effect on the total conductivity.
The panorama of techniques used to achieve memristive effects however is not restricted to these three mechanisms: [69] the formation of conducting wires is followed by the movement of doping

ions and vacancies. Schottky barrier manipulation, finally, is the source of memristive behavior found in Schottky Barrier FETs with poly-Si nanowire channel [70,71].
There is also a large interest on theoretical aspects of memristor circuitry. Lahio and Lehtonen [72] showed that, in principle, two memristor are enough to compute any Boolean function.
The possible applications and architectures of memristors inside a circuit are numerous, and research nowadays is just starting to explore all the possibilities that the new circuit element can provide [73,74]. Phase transition-based memristors have been used to create analog circuits in which the frequency response can be modified by the input to the circuits, for example by shifting the resonance frequency [75]. Broadly speaking, however, two classes of applications are emerging as dominant in the field; the first one consists in high density, low power information storage, and the second one concerns adaptive circuits with a focus on neuromorphic technology [75]. The Parma group presented the first evidence that memristive device-based organic materials show adaptive behavior similar to biological cognitive systems, using learning in the feeding neural network of the pond snail, Lymnaea stagnalis, as a specific biological reference [76,77].
The literature reports also applications of memristors as memory units. A significant advantage of memristor-based RAMs is given by the lower power consumption; this is because memristors are passive elements, thus they do not require power to operate, and to their non-volatility, that eliminates the necessity to refresh periodically the content of a single cell. A study on the power consumption performed using the linear drift memristor model showed that the RMS power consumed by a memristor-based CAM (Content Addressable Memory) is 95% lower than the power consumption measured in a standard SRAM device. For example, Jo et al [78] claimed that their 1KB device based on Silicon has a density of 2 Gbits/cm2; the device has a pitch between electrodes of 120 nm.
One of the most interesting features of a memristor, however, is the ability to function at the same time as information storage and as signal processing unit. Snider, one of the authors of the 2008 HP labs paper, had already explored in two papers the possibilities of using a hysteretic resistor array for computing [79]. His first approach to the problem used the crossbar architecture and a convenient model for the memristor linking the two electrode planes, with a positive voltage threshold that would put the memristor in a conducting state, a negative voltage threshold, and two "breakage" thresholds and, one positive and one negative, that would damage the memristor and leave it permanently in the insulating state if reached. With this approach, every memristor in a crossbar can be used as a latch, an element that can read and store the state of another element, or as an inverting latch, provided that the right voltages are sent to both; the state can be set as "open"(that is insulating), or "closed" (that is conducting), corresponding to the binary values 0 and 1. The right combination of latches and manipulation of input voltages, in combination with a clock system, can provide a universal computation: Snider proposed a circuit for an XOR gate, that uses 9 clock cycles to perform the operation, as well as a way to join together different logic gates and operate further on their outputs.

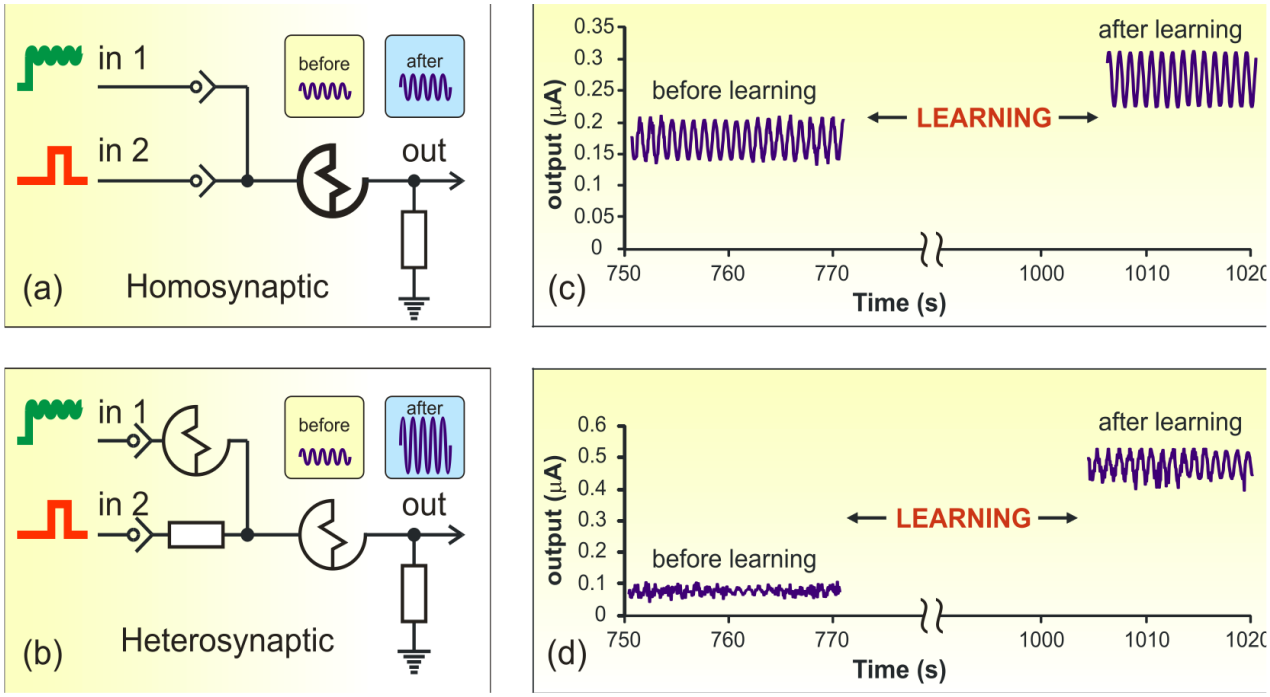

Figure 10 Artificial memristive circuits emulating synaptic response with homo and heterosynaptic junctions [77].

2.3 Organic memristive device in standard configuration (ST-OMD)- State of the art.

This section is dedicated to standard organic memristive element proposed by Erokhin at al.[80], which was considered synape analog. This element must provide weight function variations according to learning of the system. In other words, it has the property to increase its conductivity with the time (or voltage) and its involvement into the signal propagation process [80].

The organic memristor is a three-electrode device, wherein the electrodes are named by analogy to the field effect transistor (FET), although their role in this case is not quite the same. Furthermore, there are differences in the structure, principle of operation, and especially in the properties of the element, as compared with a FET.

A thin layer of PANI between two metal electrodes (figure 11) is used as a conducting channel; it is deposited onto a non-conductive substrate (glass). The two metal (Cr) evaporated electrodes are called (in accordance with the terminology used for FET) source (S) and drain (D) electrodes. In the central part of the PANI channel, a stripe of solid electrolyte (PEO doped with lithium perchlorate-$LiClO_4$) is placed. A silver (Ag) wire 50 μ in diameter electrode is attached in the PEO stripe it is called gate (G) or, the reference electrode. Then, the structure is dried at ambient temperature. Schematically, the device is shown in figure 11. PANI –PEO junction, or the area where PANI channel is in direct contact with the PEO polyelectrolyte, is called the "active zone". All redox reactions and, hence, the changes in conductivity occur in this area. The technology of organic memristor manufacturing is of great importance, since the choice of methods at the manufacturing stage can affect the performance of the element. The concentration of dopants in PEO-gel must be sufficiently high to provide a noticeable effect on the conductivity of PANI, but should not make the electrolyte too conductive. The thickness of the conducting channel (PANI layer) is extremely important because all redox reactions (the driving force of the device operation) are diffusion dependent: ions penetrate the film by several tens of nm [81]. If on one hand, a thick film provides a better conductivity, on the other hand the use of too thick film hinders ion diffusion. Therefore, the

Langmuir-Blodgett technique is the most suitable method for the formation of the conductive channel, allowing you to create structures with a resolution at the level of a single monolayer [82]. The choice of material for reference electrode plays also an important role in the operation of the element, as it will be shown later in this thesis (par. 4.6.1).

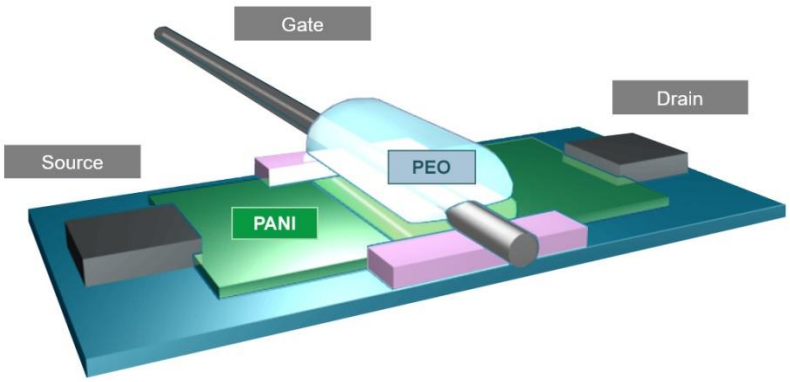

Figure 11 Schematic representation of organic memristive device

The elements are characterized by measuring simultaneously two V/I characteristics of the dependences of the drain and gate currents on the variation of applied drain voltage. These characteristics are shown in figure 12. The drain current contains both ionic current in electrolyte and electron current in the channel. The third characteristics (that is not shown) is the dependence of differential current (drain-gate) on the applied voltage.

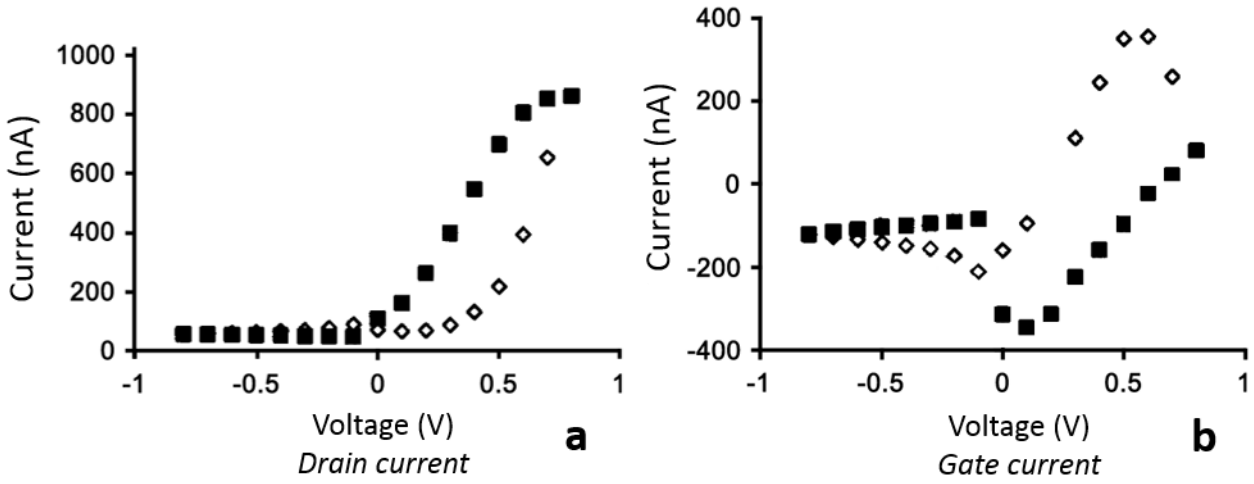

Figure 12 V-I characteristics of memristor, based on PANI-PEO junction. a) V-I characteristics of the drain current, b) V-I characteristics of the ion current. Empty rhombus represent portions of the curve acquired in direct sweep, the filled squares represent the one in reverse sweep [81].

At ~ 0.5-0.6 V the ionic current (I_G) characteristic presents a peak (figure 12b), which is accompanied by a significant increase in the electron current (I_e) (figure 12a), indicating the change in redox state as well as in conductivity of PANI film. The value of the peak voltage corresponds to the oxidation potential of PANI film. Its value is ~ 0.5-0.6 V, which is higher than the oxidation potential of PANI in the solution (+0.3 V) [83]. This phenomenon can be explained as the following: when the oxidation

potential is applied to the film, the drain voltage is distributed along the whole length of PANI film. Therefore, the actual potential of the active zone is always lower with respect to the applied voltage. However, the applied voltage should not exceed a value of 1.5 V, because an irreversible overoxidation of PANI film occurs in this case. During the reverse potential sweep the electron current decreases (figure 12a), and presents a linear dependence between 0.1 and -1.2 V. In the ion current characteristic (figure12b) for a voltage of +0,1V a negative peak corresponding to the reduction potential of PANI appears, that is, the transition of the active zone to a non-conducting state. The presence of hysteresis loop provides a "memory" property to the system: the output is not the same in the direct and reverse potential sweep. And the rectifying behaviour of element is analogous of synapse: the information (the output) flows only in one direction (for positive bias and not for negative one).

The most important characteristic of the memristor element is the gradual but slow increase in conductivity during a direct voltage sweep and a gradual rather fast decrease in conductivity during a reverse voltage sweep. The temporal dependences of the drain current at fixed drain voltages equal to +0.6V and -0.2 V are shown in figure 13.

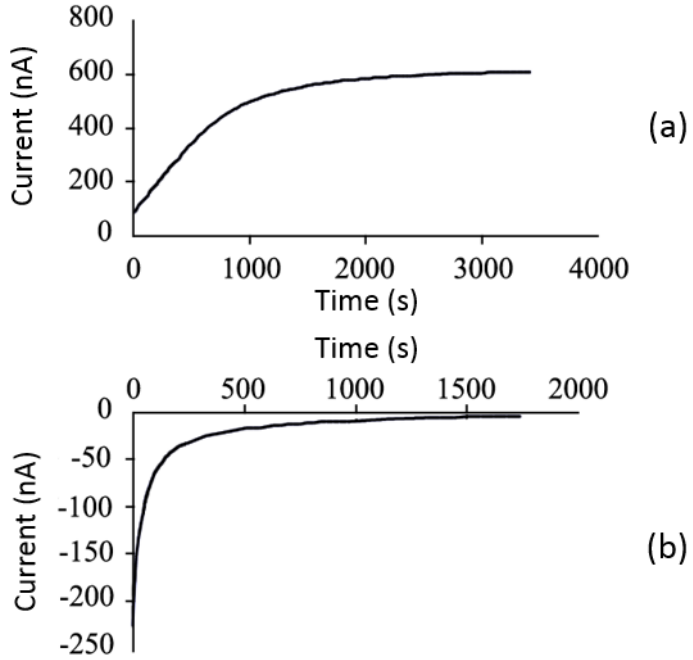

Figure 13 Time dependences of the current at fixed drain voltage of (a) +0.6 and (b) –0.2 V. Both dependences reveal the saturation [80].

For positive bias, the conductivity of element slowly increases and then goes to saturation. In the case of applying a positive voltage to the memristor, which is in a non-conducting state, only a part of the active area is under the oxidation potential. Thus, a gradual transition of the active area to the conductive state takes place. Conversely, by applying a negative voltage, the entire active area is under the reducing potential, the conductivity changes process throughout the active zone, which defines a more rapid kinetics (figure 13).

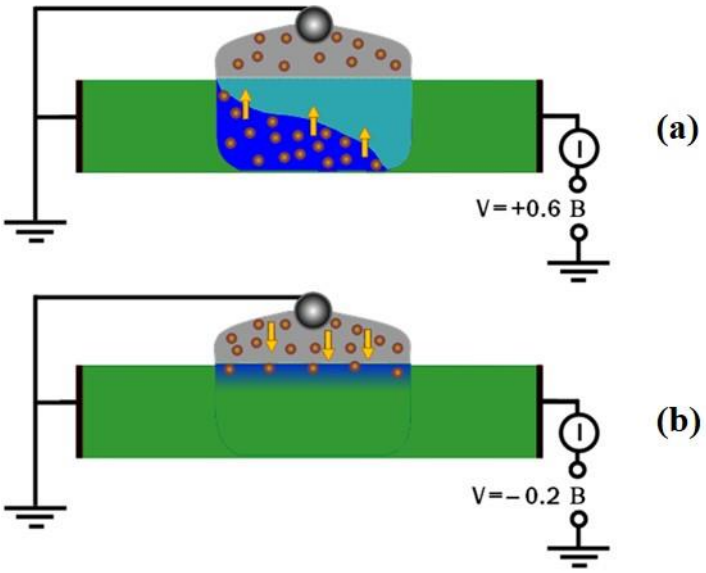

Figure 14 Model illustrating the changes of the state of the active zone, depending on the polarity of the applied voltage: a) behavior of the active zone under positive voltage (+0.6 V) application; b) the active zone behavior under negative voltage (-0.2 V) application.

The temporary dependence represents the basis of adaptive behavior of the devise. In fact, the increase of conductivity in time during a positive potential application is a basic property necessary for self-adaptation or training, according to rule of Hebb [84]. The Hebb rule states on the strengthening of synapses and ensuring the signal transfer from one neuron to another. The behavior of the structure will lead to the formation and strengthening of the preferential signal paths in a network consisting of a large number of the memristors. Thus, such element can be used as a main tunable node of adaptive polymeric network.

In such a network, the conductivity of the signal propagation paths increases proportionally with the frequency of signal propagation through these paths. The possibility of sharply decreasing the conductivity at negative voltages (figure 13b) is likewise very important for constructing adaptive networks; the application of the negative voltage across particular pairs of input–output electrodes serves as a forced training of the system by blocking the signal transmission paths arising from a priori improper connections. As follows from the foregoing, the aforementioned nonlinear electrochemical element can be used for constructing adaptive networks, i.e., systems that are able to change the conductivity of signal transmission paths depending on the frequency of their participation in the signal transmission process under the external training action.

2.4 Memristor Bulding-Blocks

The choice of materials for the realization of organic memristor is an important point. A priori, it is clear that at least two materials are necessary. One must possess a sufficiently high electronic conductivity and the ability to change the value of the conductivity by several orders of magnitude during the redox reactions, such as conductive polymers. The second material should provide the necessary environment (medium) for the electrochemical reactions. Consequently, it must be an electrolyte, namely, a solid polyelectrolyte, as it should be implemented in solid-state systems. The following polymers: polyaniline (PANI) and polyethylene oxide (PEO) were proposed in the “state of art” fabrication of organic memristive device in standard configuration.

2.4.1 Polyaniline

Polyaniline is one of the oldest known conducting polymers, discovered in the 19th century [85] Polyaniline, was originally known as "aniline black" [86,87] and was extensively reviewed.[44, 86,88-90]. In the material family of π-conjugated polymers, polyaniline spurred intensive scientific interest in the last decades due to its good environmental stability, controllable electrical conductivity, intriguing redox properties and sufficient mechanical properties. Polyaniline shows also an excellent electrochemical reversibility [91]. The conductivity of polyaniline is known to exhibit hysteresis, which is illustrated in the current versus potential sweep characteristic plot [92], where the current response to the potential sweep in the positive direction is different from that one to the reverse potential sweep. This hysteretic behavior is more closely related to the level of doping than to the electrochemical potential or pH value of the polymer [93] and has been identified as a "memory effect" and attributed to structural relaxations [94]. This is not the case for other types of conducting polymers such as polypyrrole, polythiophene or PEDOT. Polyaniline for its unique ability to possess excellent electrochemical reversibility presents many advantages in nanoscale devices [95]. Mainly polyaniline has three distinguishable oxidation states, with an infinite number of possible oxidation states virtually existing in between. Therefore, in principle, polyaniline can exist in a continuum of oxidation states ranging from a completely reduced to a completely oxidized form. A general chemical structure of polyaniline is shown in figure 14 where the polymer chain consists of two types of repeating units, namely, the reduced (y) and the oxidized (1- y) blocks (figure14, where $0 \leq y \leq 1$).

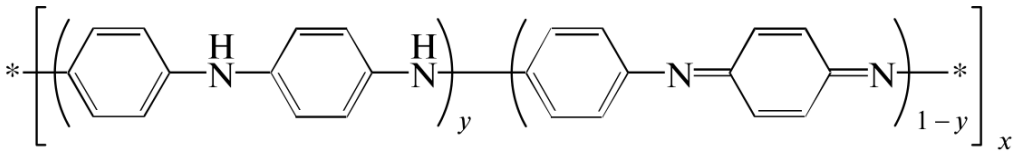

Figure 14 Monomer units of polyaniline chain [96].

The redox state of the polymer is determined by the value of y , which may vary continuously from zero to unity. At y = 0.5, polyaniline occurs in the form of emeraldine (half oxidized); y = 0 corresponds to the fully oxidized form, pernigraniline, while y = 1 corresponds to the fully reduced form, leucoemeraldine [96]. Pernigraniline and emeraldine may occur as either salts or bases [97, 98] The forms of PANI have not only different conductivities but also different colors, stabilities. Pernigraniline base is violet, emeraldine base is blue, protonated emeraldine salt is green, leucoemeraldine base is a pale yellow substance. Among various electroconductive polymers, PANI holds a unique position for its electrical and electrochemical properties which can be reversibly controlled both by charge (electron) doping and by protonation, i.e. acid doping. Indeed two completely different types of doping for polyaniline exist: oxidative doping (redox process) or protonic acid doping (a non-redox doping process). The imine nitrogen atoms, which do not have hydrogen bonds, can be protonated in an acidic environment where protons can be attached to these nitrogen atoms to generate radical cations (polarons) and/or divalent cations (bipolarons). The latters represent the charge carriers responsible for the electronic conductivity increase in PANI [91]. Hence, the majority charge carriers in polyaniline are holes (p-type doping). The degree of protonation depends strongly on the oxidation state of polyaniline and on the pH of the aqueous solution in which the polymer is immersed. PANI has been reported to be switched to the "on" or "off" state by a shift of electrochemical potential. MacDiarmid (1987) [97] found that PANI film has various intrinsic domains with different length of π -conjugated fragments. Each domain has an individual redox potential and they are distributed over a mean redox potential. Later these data were confirmed using potential-step chronocoulometry; the mean redox potential of PANI was 0.71 V and 0.16 V in different acidic solutions, these value were determined by measurement of doping level at different oxidation potentials vs. Ag/AgCl for pernigraniline/emeraldine base and emeraldine base/

leucoemeraldine base, respectively [99].The polymer is conductive in the oxidative state between 0.2V (versus Ag/ Ag + in acetonitrile) and 1.6V, where degradation of the material begins to occur.

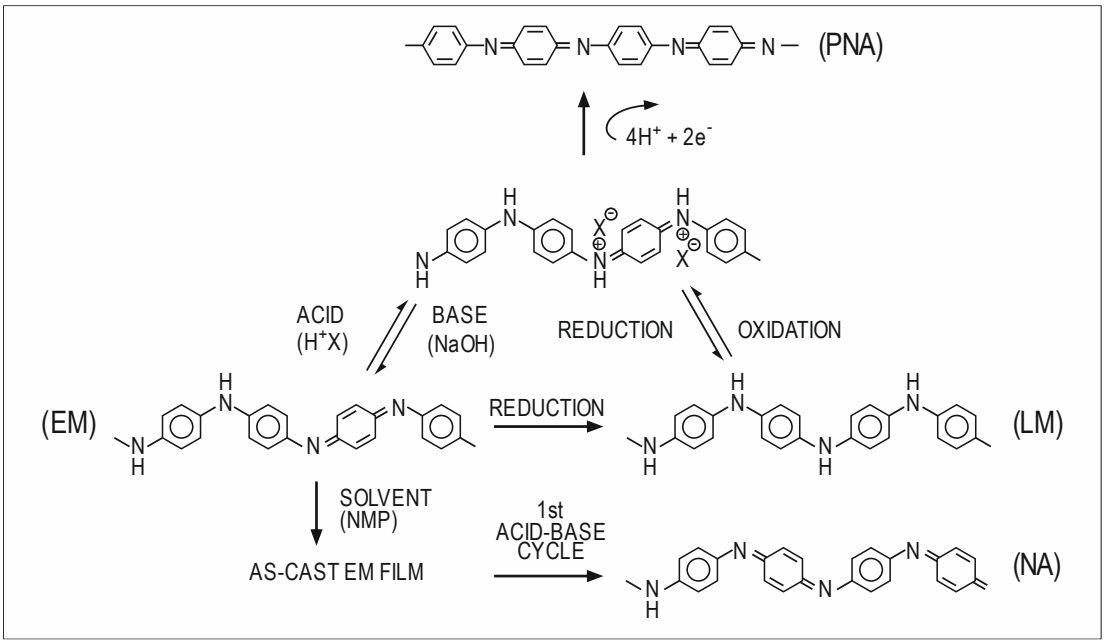

Figure 15 Electrochemical redox states and the corresponding doped form of polyaniline [93].

2.4.2 Polyaniline in organic electronics

Polyaniline was studied for use in a wide range of applications [100]. The possibility of using PANI for electroanalytical purposes stimulated the development of potentiometric [101] and voltammetric anion-selective sensors in which oxidized fragments of a conducting polymer matrix are cationic centers [102]. The practical application of polyaniline inspired the most interests is in the area of electrochemical batteries. Many groups [103, 104] also discussed the application of polyaniline for rechargeable lithium battery. Polyaniline is a promising material for positive electrodes in lithium secondary batteries, since polyaniline electrodes synthesized by electro-polymerization exhibits good specific capacity, stability, reversibility, and low self-discharge in a $LiClO_4$ /polycarbonate (PC) electrolyte.

Composite materials based on PANI are used more frequently to manufacture supercapacitors, owing to the high specific capacitance of the material, 450–900 F/g [105, 106], and the stability during recharging (up to 1000 cycles). PANI electrodes electrochemically deposited on steel, as well as composite materials based on manganese oxide, likewise possess high capacitance and can endure a large number of recharging cycles [107]. The electrochromic properties of polyaniline coated electrodes have been extensively investigated because of their possible applications in display devices [108, 109].

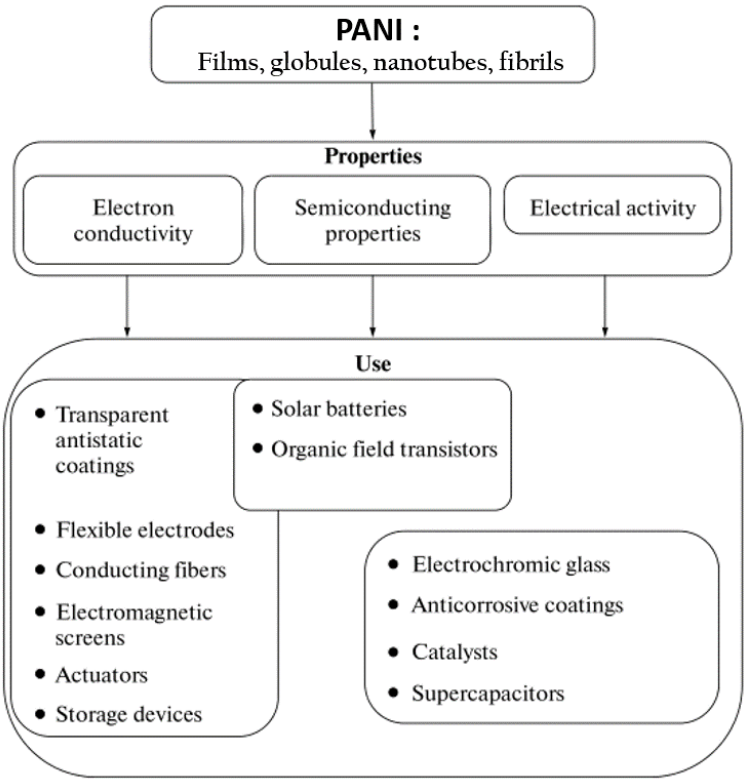

Figure 16 Uses of polyaniline in organic electronics.

Another application area of PANI in organic electronics includes the design of organic field-effect transistors [110, 111], and polymer light diodes [112-114]. The use of composite materials based on conducting polymers for transistor manufacturing of is often limited by the low mobility of charge carriers and grainboundary effect. Nevertheless, the available techniques make it possible to prepare materials with a rather high mobility of charge carriers reaching the values up to 3 cm^2 /(Vs) and a ratio of switch-on/switch-off currents above 10^4 [115]. A technique of vacuum deposition of oligomeric PANI and fullerenes to create organic field transistors was developed [116]. Light-emitting diodes designed with the use of the graft copolymer PANI–poly(4-styrene-sulfonic acid) [117] surpassed the known similar polymers in terms of performance and stability because of the high chemical stability of the material. Polyaniline doped with camphorsulfonic acid has found use as an element of electrically programmable permanent storage device [118]. Polyaniline deposited onto tin fluoroxide is used instead of platinum as internal electrode in photoelectric solar cells [119]. When PANI is used as a component of an electronic device, special conditions of synthesis or modification of this conducting polymer are used to impart the desired properties to it. The employment of nanostructured PANI in photoelectric cell permits to increase the efficiency of these devices [120].
Another application area of PANI includes the design of fuel cells [121], separation membranes [122] anticorrosion coatings [123], memristors. The first organic memristive device based on polyaniline as a conductive polymer, was proposed by Erokhin et al.[80].

2.4.3 Problems and limits of polyaniline for applications in organic electronics.

The use of polyaniline in various areas of electronics and engineering is limited because its conductivity is unstable at neutral pH and temperatures above 150°C owing to dedoping of polymer chains. Extensive investigations of the proton-induced insulator-to-metal transition of PANI have been carried out. The protonation of PANI does not occur at pH above 3, when the polymer remains

essentially an insulator ($\sigma \leq 10^{-8}$ S/cm) [124, 125]. At lower pH the conductivity increases logarithmically with decreasing pH, and levels off at pH≤0 with $\sigma \sim 10$ S/cm. This phenomenon is due to the specific structure of PANI where carbon rings and nitrogen atoms both lie within the conjugated path. The deprotonation process occurs in the presence of nucleophiles, specifically water. If PANI is doped with HCl, the dopant anions can be released from polymer network [126]. Because of the bulky size, Cl^- anions are essentially capable to diffuse out of the PANI film, which correlates with the depressed electroactivity of PANI-HCl film in neutral or alkaline solutions. Since the polymer can be deprotonated, it loses, thus, its electroactivity in neutral media. This may restrict the possible applications of this kind of processes, such as biological processes, biosensors or biological integrated systems, where the most enzymatic and cellular activities are pH sensitive, and can properly function only in neutral pH environment, typically between pH 6 and 8.

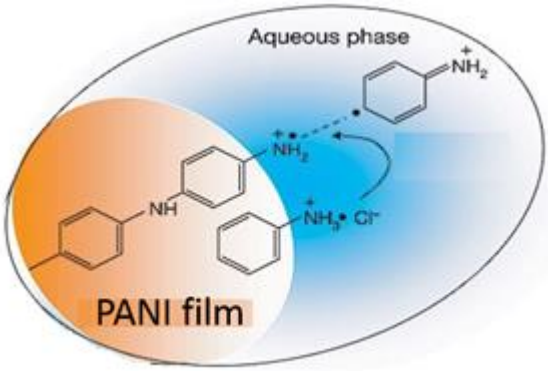

Figure 17 Scheme for ideal electron transfer in polyaniline film at interface with aqueous phase.

2.4.4 Polyethylene oxide, solid polyelectrolyte and gel phases.

A polyelectrolyte is made of a polymeric backbone covalently bonded with repeating electrolytic groups which can be acids, bases or salts. The electrolytic groups can dissociate with the formation of charged polymer chains and oppositely charged counter ions in a polar solvent, such as water. Polyelectrolytes can be classified into two types, polycations and polyanions, in terms of the chemical structure of the polyelectrolyte. Polycations comprise positively charged polymeric backbones and negatively charged counter ions. Conversely, polyanions are composed of negatively charged polymeric backbones and positively charged counter ions. In the solid phase, the charged polymeric backbones are considered as effectively immobile since they are relatively much larger than the counters ions. Therefore, the ionic conductivity of solid state polyelectrolyte is represented by transport of the atomic or molecular counter ions. This unique feature of polyelectrolytes is exploited in electrolyte-gated organic field-effect transistor in order to avoid possible electrochemical doping in the semiconducting channel [127]. Due to the counter ion condensation phenomena [128] in solid polyelectrolytes, not all counter ions are dissociated from the polymeric backbones and can be transported freely. The activation energy of the dissociation process depends strongly on the amount of solvent content in the solid polyelectrolyte. Polyelectrolytes are usually hydroscopic, because of their polarity characteristics, and thus become promising candidates for humidity sensing [129, 130]. When the counter ions are dissociated from the polymeric backbones, solvent molecules form a shell around mobile ions. Then, the ions can move together with their solvent shells. The ionic charge transport in polyelectrolytes is mainly attributed to the diffusion along concentration gradients and migration under electric fields. During ion transport, the dissociated ions are subjected to frictional forces, which are proportional to the viscosity of the solvent and the size of the solvated ions [131].
Poly(ethylene oxide) is a polymer with formula $(-CH_2-CH_2O-)_n$ and it is one of the most studied polymeric electrolytes. It is commonly used in industrial applications, especially as solid

polyelectrolyte in lithium batteries. In [80] it was used by Erokin et al. as a solid polyelectrolyte in organic memristive device.

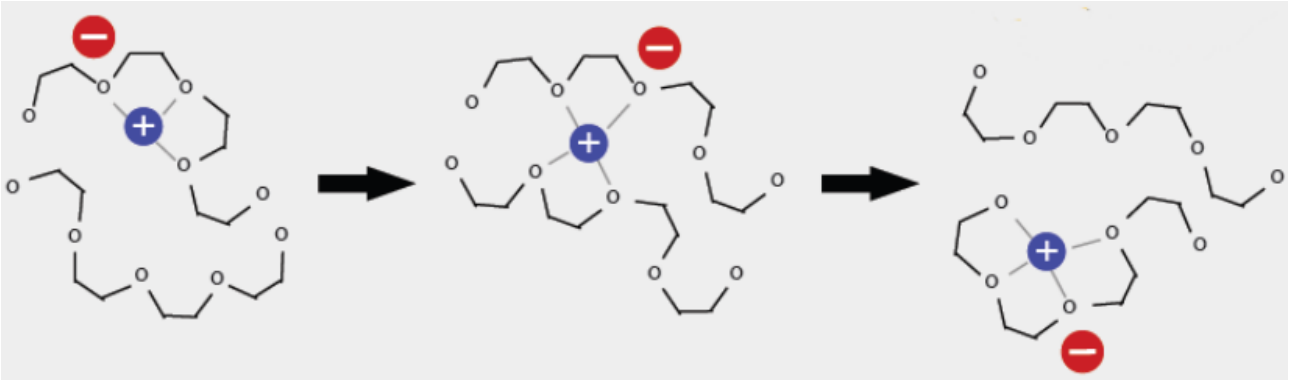

Figure 18 Transport of ions from one chain to the next in PEO.

Solvent-free solutions of salts in PEO are amongst the most studied polymeric electrolytes [132-134]. These substances have a conductivity that ranges between 10^{-8} and 10^{-4} S/cm at temperatures between 40 °C and 100 °C, because of the high crystallinity of the solid PEO/salt compound and of the low solubility of the salts in amorphous PEO [135]. PEO aqueous solution where lithium salts were solved, the positive ions are the mobile charge carriers to which the PEO's conductivity is due [136]. Often polymeric electrolytes are used in a gel phase, which allows to reach higher conductibility even if at the expense of worse mechanical properties. A gel is a phase that has the cohesion properties usually associated with the solids while having the diffusion properties of the liquids. A polymer gel is usually defined as a polymer network, in which the polymer chains are linked, containing some solvent [137]: it is important to note that it's the solvent solved in the polymer, not the other way around.

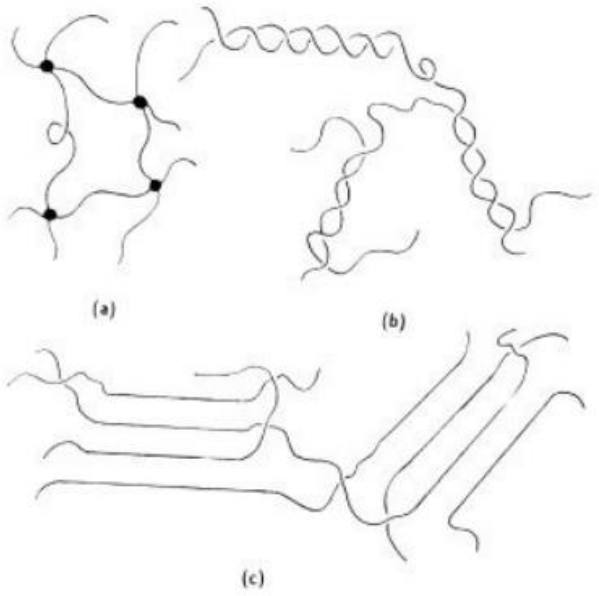

Figure 19 Polymer gels showing a) chemical cross-linking, b) entanglement, c) fringe micelles [137].

A gel is obtained by a physical or chemical cross-linking process between different polymer chains; during the gelification the compound goes from a more or less viscous polymer solution to an infinitely viscous liquid; a gel in a tube does not flow if the tube is tilted. Figure 19a shows the effects of covalent cross-linking: a chemical reaction binds two atoms belonging to two different polymer

chains with covalent bonds. Gels formed in this way are called irreversible and the number of junctions between polymers does not usually change as a function of physical parameters like temperature, mechanical stress or solvent concentration. On the other hand, the number of inter-chain bonds depends on these parameters in the physical cross-linking gels, also called "entanglement networks". There are two main ways in which polymer chains can bind, even if sometimes the ions in the solution can add further gelification mechanisms. Figure 19b shows chains where the interaction takes place between the end zones; figure 19c shows a case, where the interaction is between the central part of the different chains, creating configurations called "fringe micelles", in which there are some small crystalline zones weakly interacting between themselves [138]. In technological applications, the use of polymeric electrolytes shows some remarkable advantages with respect to the traditional liquid or solid electrolytes, and it has greatly influenced the development of lithium batteries for portable devices [133]. Polyelectrolytes are generally safer than liquid electrolytes, with a reduced chance of reacting with the metal electrodes; the electrolyte is actually wrapped in a thin plastic film instead of being held in a metal container, and this reduces the risk of corrosion of the metal parts and of explosion, besides attenuating the battery's vulnerability to thermal or mechanical shocks [139]. Compared to solid electrolytes, polyelectrolytes are more compact and less porous, and they can avoid the formation of metallic dendrites from the electrodes, which over time impede the efficiency of the charge/discharge cycles and can even lead to shorts in the battery itself [140]. Moreover, polyelectrolytes are better suited to deal with the changes in volume that happen at both electrodes during the charge/discharge cycles.

3. Materials and Methods.

The choice of materials endowed with memristive properties is an on going, quite relevant research subjet by itself. Polyaniline (PANI) and polyethylene oxide (PEO) were the first one proposed and represent still now the "state of art" in the fabrication of organic memristive device in standard configuration (as reported in par. 2.3-2.4).
Although the use of these "building blocks" in a standard organic device has demonstrated to very successful, for some aspects, they show strong limitations in some applications including biosensors or biological integrated systems, where most activities are strongly pH sensitive. As already mentioned, the study proposed in this thesis aims at exploring the synergy between PANI electrochemistry and biology in organic memristive devices.
The basic approach here is based on the standard configuration (par.2.3) introducing previously unexplored multilayer structures that could preserve the memristive response of the PANI while interfacing a biosystems. One of main issue that has been faced was the identification of suitable materials to realize this complex architecture. Natural-origin polymers are proposed as new "building block". The developments achieved in this thesis work, allow overcoming some of the limitations of the state of art of organic memristive elements and pave the way to the feasibility of bio-integrated memristive devices.

3.1 Choice of Materials for Bio-Organic devices.

The combination as well as the integration between biological solutions (usually pH ~ 7) and electronics is a key goal of this thesis; in particular, the combination of PANI-HCl films with biological elements was studied.

Implementing biocompatible materials, as "bridging" elements, in electronic architectures is at the basis of the approach chosen here in order to achieve and maintain suitable conditions for the bio-integration while maintaing device function and operation. Since the biological medium is water, obviously the electronic device fabrication methods must embrace and guide interactions in water. For this reason, the present work focuses on the study of hydrogel-based interfaces between the biological object and the active polymer film. The idea is to use polymer host materials to capture and maintain the biological functionality.

Many polymer systems are qualified as hydrogels because they incorporate and maintain an enormous amount of water, e.g., poly(vinyl alcohol) (PVA), PEO, Chitosan, Alginates, Pectins. In particular, we chose polymers of natural origin, that have already been qualified for an high degree of bio-compatibility and solubility in dilute solutions of organic acids, at a pH between the value necessary to avoid the de-doping of the conductive form of polyaniline and the pH value suitable to preserve biological functionality. Bio-polymers fulfill both the biological requirements by the incorporation of water, and, on other hand, they preserve the conductivity of polyaniline. In addition, the use of these bio-materials, which are classified as polyelectrolytes, will allow in the future the development of even more complex device architectures, more efficient from the technological point of view, using, for example deposition methods compatible with scalable technologies (polymer systems can be spin-coated, lithographically patterned, and subjected to other treatments). Thus, polymers represent a truly bridging material system in making biological macromolecules mesh with synthetic technology.

The interface suitable to be used as "bridging" material should have specific characteristics and properties that can hardly be fulfilled. It should be bio-compatible and able to produce a sort of buffering effect on pH at interface, avoiding, in this way, the emeraldine salt de-doping. In addition, it should support the "communication" as well as the ion- exchange processes to allow the interconversion of biological and electronic signals.

The electronic systems rely on electrons to process information, while biology information processes uses ions, molecules, and biopolymers. Thus, establishing effective communication between electronics and biology requires somehow bridging these different signal processing modalities. The redox reactions may provide an important "interface" for biology, to communicate between biology and electronics in the aqueous medium.

The materials mainly adopted are presented in the paragraphs 3.1.1 and 3.1.2. It is important to note that plasticizers and additives as crosslinking agents were avoided in the final formulations of polysaccharide-based gels because the most common plasticizers (glycerol, glutaraldehyde etc.) could affect both the electrical characteristics and the biocompatibility of the gel.

In this work, it was preferred to optimize the texture and mechanical properties of materials by modulating the inorganic salts concentration and the variation of acids, rather than by additives. Moreover, the idea of simplifying as much as possible the formulation of the gels was a key factor that has allowed to investigate the electrochemical mechanisms at the basis of the devices operation (see chapter 4), as well as bringing advantages in terms of feasibility and cost.

3.1.1 Chitosan.

Chitosan (poly-β(1,4)-D-glucosamine) is a linear aminopolysaccharide, it is an abundant, naturally occurring biopolymer. Chitosan (CS) is generated by the partial de-acetylation of chitin, the main component of the exoskeleton of crustacean shells, such as shrimps. Formally it is a co-polymer of glucosamine and N-acetylglucosamine residues. The distinguishing structural feature of chitosan is its primary amine at the C-2 position of the glucosamine residues (figure 20). At low pH, these amines get protonated and become positively charged, that makes CS a water-soluble cationic polyelectrolyte. On the other hand, as the pH increases above 6, CS's amines become deprotonated and the polymer loses its charge and becomes insoluble. The soluble–insoluble transition occurs at its pKa value: pH between 6 and 6.5. As the pKa value is highly dependent on the degree of N-acetylation, the solubility of CS is dependent on the deacetylation degree (DD) and on the method of

deacetylation used [141]. The degree of ionization depends on the pH and the pK of the acid with respect to studies based on the role of the protonation of CS in the presence of acetic acid and hydrochloric acid [142]. The following salts, among others, are water-soluble: formate, acetate, lactate, malate, citrate, glyoxylate, pyruvate, glycolate, and ascorbate.

The dissolution constant K_a of the amine group is obtained from the equilibrium:

$$–NH_2 + H_2O \leftrightarrow –NH_3^+ + OH–$$
$$K_a = [–NH_2][H_3O–]/[NH_3+] \quad \text{and} \quad pKa = –\log Ka.$$

The dissociation constant for polyelectrolytes depends on the degree of dissociation at which it is determined. CS can easily form quaternary nitrogen salts at low pH values. Therefore, organic acids such as acetic, formic, and lactic acids can dissolve CS [143]. The most commonly used solvent is 1% acetic acid (pH ~4.0). CS is also soluble in 1% hydrochloric acid and dilute nitric acid but insoluble in sulfuric and phosphoric acids. But concentrated acetic acid solutions at high temperature can cause depolymerization of CS [142]. Solubilization of CS with a low DA occurs for an average degree of ionization of CS around 0.5; in HCl, it corresponds to a pH of 4.5–5. It is reported that at higher pH, precipitation or gelation tends to occur and the CS solution tends to form gels with anionic hydrocolloids [144]. The concentration of the acid plays a great importance to impart desired functionality [145]. Solubility also depends on the ionic concentration and a salting-out effect was observed in excess of HCl (1M HCl), making it possible to prepare the chlorhydrate form of CS. When the chlorhydrate and acetate forms of CS are isolated, they are directly soluble in water giving an acidic solution with pKa=6±0.1 [146] in agreement with previous data [147]. It is known that the amount of acid needed depends on the quantity of CS to be dissolved [142]. The concentration of protons needed is at least equal to the concentration of $–NH_2$ units involved.

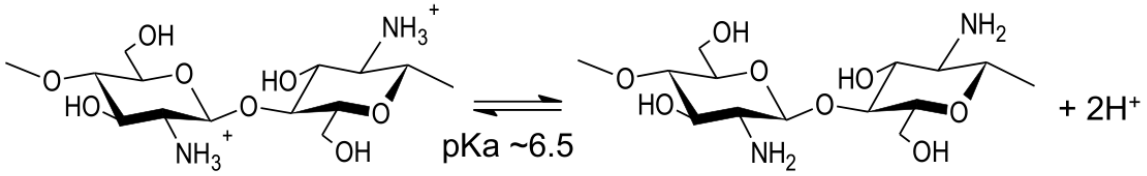

Figure 20 Equilibrium of protonation and deprotonation in chitosan.

Chitosan chains can undergo self-associations to form a three-dimensional hydrogel network. [148-150]. The process of chitosan's hydrogel formation can be viewed as either a reversible sol-gel transition that results from the formation of physical (i.e., non-covalent) crosslinks, or a triggered self-assembly of a supramolecular network. Irrelevant to the words used to describe this process, hydrogel formation serves to organize structure over a hierarchy of length scales from individual macromolecular chains to the macroscale. There are important points concerning chitosan's self-assembly that are not well understood. Unresolved questions include; the solution conditions (e.g., salt concentration) that modulate the chitosan chain conformation, the sol-gel transition pH, and the hydrogel network and the competition between intramolecular and intermolecular associations that affect network structure aggregates vs. gels).

Chitosan possesses a unique combination of properties to meet challenges and to act as an effective bio-device interface material. For assembly, chitosan's pH-responsive film-forming properties allow it to "recognize" electrode-imposed signals and respond by self-assembling as a stable hydrogel film Chitosan has important properties for building the bio-device interface and establishing communication across this bio-device interface.

Due to the presence of amino groups, chitosan is a weak polyelectrolyte that possesses pH-responsive properties (figure 20). Chitosans as integrative biomaterial for lab-on-a-chip devices is reported in literature [151].

Chitosan is not only a biocompatible, non-toxic material, but due to its porous structure and dense amine groups, chitosan is well-suited for attachment of biomolecules. Chitosan films can be modified with proteins, enzymes, antibodies, and DNA. The typical application of chitosan films with biomolecules are the selective coatings for biosensor [152].
Several applications of chitosan, also in the form of a hydrogel, has been found in literature. For example chitosan hydrogels are employed in wastewater treatment [153], separation membrane [154], food packaging [155], wound healing [156, 157], and a drug delivery system [158, 159]. Even if the use of chitosan as integrative biomaterial for lab-on-a-chip devices was reported in literature [151], the combination of chitosan with synthetic polymers, i.e. polyaniline, for electronics has been not extensively studied and it is missing for polyaniline. Thus, an innovative application is proposed in this thesis, which consists of the combination between chitosan and polyaniline films in organic (and bio-organic) memristive devices. In this thesis the chitosan gel was tested as a solid polyelectrolyte because it forms gels in solutions of weak organic acid, at intermediate pH value that is suitable both for emeraldine salts of polyaniline and biological environment. The chitosan is deposited over polyaniline layers by casting and then is dried at room temperature (25°C) forming a solid film.

3.1.2 Pectin.

Pectin is a linear polysaccharide consisting of a few hundred to one thousand saccharide units. The average molecular weight of pectin varies from 50,000 to 150,000 Da [160]. Pectins are primarily a polymer of D-galacturonic acid ~85% and L-rhamnose. The molecule is formed by α-1,4glycosidic linkages between the pyranose rings of D-galacturonic acid units. Depending on the pectin source and the extraction mode, carboxyl groups of galacturonic acid units are partially esterified by methanol and, in some cases, hydroxyl groups are partially acetylated. Neutral sugars such as D-galactose and D-xylose may also be present and bounded to the galacturonic acid as side chains or inserted into the main chain [161].
Pectins are a class of complex polysaccharides that are present in the primary cell walls and in the middle lamella between plant cells, where they function as a hydrating agent and cementing material for the cellulosic network. The amount, structure and chemical composition of the pectin differs between plants, within a plant over time and in different parts of a single plant. Although pectin occurs commonly in most of the plant tissues, the number of sources that may be used for the commercial manufacture of pectin is limited. Various sources of pectin include citrus peels, dried apple pomace, sugar beets, sunflower heads, residues of mango, guava, papaya, coffee and cocoa processing [162, 163].
Pectin is an important polysaccharide with applications in foods, pharmaceuticals, and a number of other industries. In the food industry, pectin is used as a source of dietary fiber in preparation of jams, jellies, frozen foods, and more recently in low-calorie foods as a fat and/or sugar replacer. In the pharmaceutical industry, it is used to reduce blood cholesterol levels and gastrointestinal disorders. Other applications of pectin include use in edible films, paper substitute, foams and plasticizers, etc.
Dry powdered pectin has the tendency to hydrate very rapidly and form clumps on addition of water. These clumps consist of semi dry packets of pectin contained in an envelope of highly hydrated outer shell. Further solubilization of such clumps is very slow. Based on solubility, two different types of pectins exist: water-soluble or free pectin and water-insoluble pectin. Solubility in water is a function of the degree of polymerization and the number and distribution of methoxy groups. Generally, solubility increases with decreasing molecular weight as well as with the esterified carboxyl groups. Solution pH, temperature, and the nature and concentration of the solute present have a marked effect on solubility [164].
Dilute pectin solutions are Newtonian but at moderate concentration, they exhibit non Newtonian, pseudo plastic behavior characteristics.

Pectins have many applications because of their ability to form gels usable as water binder and stabilizer [165]. The physical characteristics of gels are the consequence of the formation of a continuous three-dimensional network of cross-linked polymer molecules [166]. The molecular level, an aqueous gel consists of three elements: junction zones where the polymer molecules are joined together; interjunction segments of polymers that are relatively mobile; and water entrapped in the polymer network. A junction zone may involve a single covalent bond between two chains or a combination of hydrogen bonds and hydrophobic interactions between two polymer chains running side by side.

Factors that increase gel strength will increase the tendency to gelification, decrease solubility and increase viscosity. These properties of pectins are a function of their structure. Solutions of monovalent salts of pectins exhibit stable viscosity because each polymer chain is hydrated, extended and independent. Reduction in the pH (increasing acidity) reduces the ionization; the polysaccharide chains no longer repel each other over their entire length and can associate and form a gel.

Gel strength depends on the length of molecule. At very low molecular weight, pectin is unable to form gels [167].

Different parameters affect the pectin networks properties: the concentration, hydration level, cross-linking degree, swelling [168].

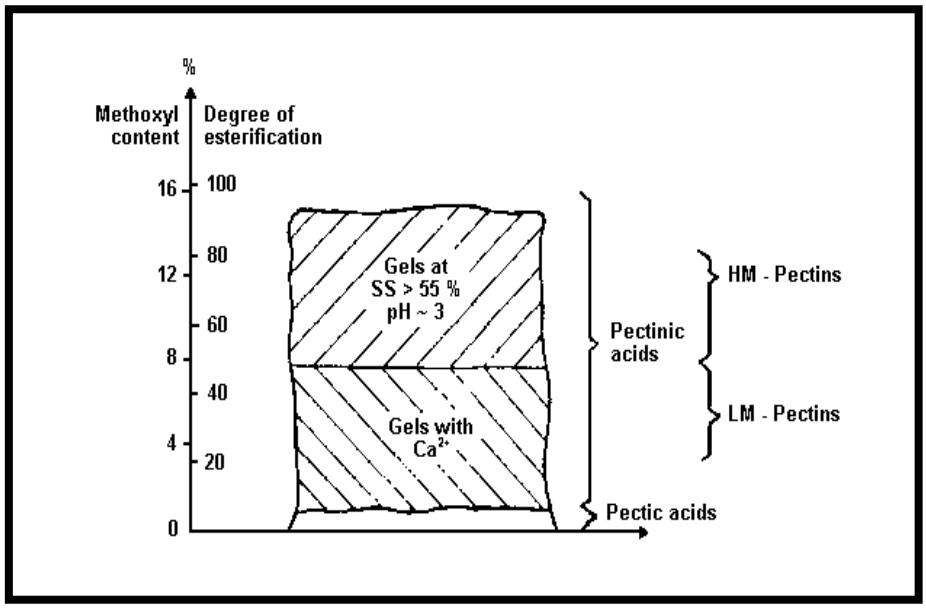

Figure 21 Gelification of pectins.

Depending on the degree of methoxylation, pectins are classified as follows: lower degree of esterification (LM) (25 to 50%) and high degree of esterification (HM) (50 to 80%). Apparent pK-values (pH at 50% dissociation) vary with the esterification degree DE of the pectin; a 65% DE pectin has an apparent pK of 3.55, while a 0% DE pectic acid has an apparent pK of 4.10. However, pectins with increasingly larger degree of methylation will gel at somewhat higher pH, because they have fewer carboxylate anions at any given pH.

Gels have different texture in both HM (hard texture) and LM (softer texture) pectins. The mechanism of gel formation is different in both HM and LM pectins. Noncovalent forces (i.e., hydrogen bonding and hydrophobic interactions) are believed to be responsible for gel formation in HM pectins [169]. HM pectins form gels if the pH is below 3.6 and some cosolute, typically sucrose, is present. With decreasing of the pH value, the ionization of carboxylic groups is suppressed, and this results in the reduction in hydration of the carboxylic acid groups. As a result of reduced ionization, the polysaccharide molecules no longer repel each other over their entire length, and can associate and form a gel phase. The function of sugar in the formation of gels of HM pectins is to stabilize junction zones by promoting hydrophobic interactions between ester methyl groups. In HM pectins the

hydrophobic effects arise from the unfavorable interactions between water molecules and the nonpolar methoxyl groups of pectin molecules [170]. The methoxyl groups induce changes in water structure, decreasing its entropy. To minimize this change, the methoxyl groups are forced to coalesce, reducing their surface area of contact with water. This removal of nonpolar groups from contact with water makes a major contribution to the free energy of conformational stabilization [171, 162, 163].
LM pectins, jellify is formed over a wide pH range in the presence of Ca^{2+}, which acts as a bridge between pairs of carboxyl groups of pectin molecules. In this way, two carboxyl groups belonging to two different chains are in close contact with each other [172].

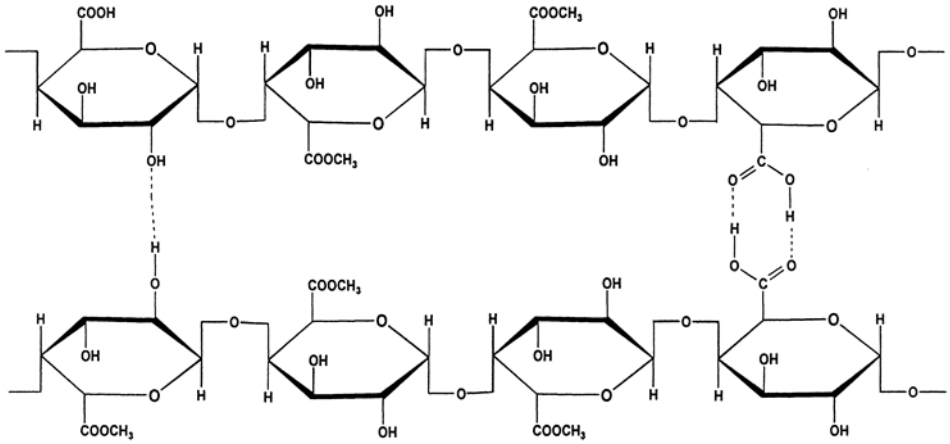

Figure 22 High DE pectin at low pH.

A number of factors influence the gelation of pectin such as pH, presence of other solutes, molecular size, degree of methoxylation, number and arrangement of side chains, and charge density on the molecule, the ionic concentration.
In this thesis, pectin with high degree of esterification was used as solid polyelectrolyte because it forms gels in presence of weak organic acid. Results that the pH value of interface is closed to 7 (suitable for biological elements). The pectin gel is deposited over polyaniline layer by casting and than is dried at room temperature (25°C) forming a solid film.

3.2 Materials and Methods.

Chitosan (poly(D-glucosamine) medium molecular weight (Mw~100KDa), from Pandalus Borealis, 77% deacetylation), pectin (poly-D-galacturonic acid methyl ester, Mw 30000-100000 Da, from apple etherification degree 70-75%), polyethylene oxide (PEO) (Mw~8000000 Da), emeraldine base polyaniline (Mw~100000 Da), polystyrene and $MnCO_3$ microparticles (3 μm) were purchase from Sigma-Aldrich. N-methyl pyrrolidone (Sigma-Aldrich, anhydrous, 99.5%), toluene (Sigma-Aldrich, ACS reagent, ≥99.5%), acetic acid (Fluka, ACS reagent, 0≥99.7%), hydrochloric acid (Fluka, ACS reagent, 37%) were used without further purification. BaFe 12 O 19 nanoparticles were obtained by a sol-gel method [173].
Water (for film deposition, solution preparation, washing) was purified by Milli-Rho-Milli-Q (resistivity: 18.2 MΩ cm).
Strain of slime mold Physarum polycephalum (Order Physarales, class Myxomecetes, subclass Myxogastromycetidae) was obtained as a sclerotium from Bristol University (UK). The mold was grown in humidity-controlled chamber with 1.5% Agar non nutrient gel.

Polystyrene and $MnCO_3$ microparticles were used in an aqueous dispersion (5 mg/mL). Barium hexaferrite $BaFe_{12}O_{19}$ nanoparticles (2 mg/L) were solved in a homogeneous aqueous. The solutions was sonicated before its deal.
The morphology of the polymeric layers was studied by scanning electron microscopy (SEM). SEM images were acquired with high resolution Scanning Electron Microscope Zeiss Supra 40 at an accelerating voltage of 1-10 kV and 30 μm aperture. For elemental analysis of the samples in this thesis we used a microanalysis system INCA (OXFORD Instruments) based on the EDS (energy dispersive spectroscopy) Detector X-MAX.
The spectroscopy analysis of polymeric films deposited on quartz substrates was carried out in the visible spectral region (between λ = 400 nm - 750 nm), near the IR (between λ = 750 nm - 1200 nm) by means of commercial Spectrophotometer UV-VIS: model Jasco UV/VIS 7850. Jasco 7850 is a high resolution UV-visible double-beam spectrophotometer with double monochromator.

3.3 Device fabrication.

The technology of organic memristor manufacturing is of great importance, since the choice of methods at the manufacturing stage affects the performance of the element.
The thickness of the active channel (PANI layer) (as reported in par.2.4) is extremely important because all redox reactions (the driving force of the device operation) are diffusion dependent: ions penetrate the film by several tens of nm [81]. Thus, even though a thick film provides a better conductivity, which facilitates the current measurement and reduces electrical interferences, the use of a too thick film leads to a decreasing conductivity. Thus, the optimal thickness of the PANI layer is a critical parameter. In order to take full advantage of the electrical properties of the semiconducting polymers in the field of molecular electronics, it is often useful to have the polymer layer as ordered as possible, so to maximize its conductivity. The deposition of the polyaniline layer using a Langmuir-Blodgett technique is one of the best ways to obtain ordered and ultra-thin films [174-176].
Therefore, in this work the Langmuir-Blodgett technique is adopted, because it seems the most suitable for the formation of the channel, allowing creating structures with a resolution at the level of a single monolayer [177-178].
In experiments reported here typically, the PANI film has a total thickness of about 60 nm (sixty monolayers of PANI).
The PANI Emeraldine base (MW 100,000) powder was dissolved in 1-methyl-2pirrolidone (NMP) at a concentration of about 0.1 mg/mL and filtered carefully. 10% of toluene was added to NMP solution of PANI in order to improve the solution spreading on water interface.
Deposition of Langmuir layers was carried out using the KSV 5000 LB trough with a modified method of Langmuir-Schaefer (Langmuir-Schaefer (LS)) (horizontal lift). Deionized water (resistivity of 18.2 MΩ×cm) prepared using Milli-Q system, was used as a subphase.
250 μl of PANI solution was spread onto the subphase surface of the LB-trough. Surface pressure-area isotherm is shown in figure 23.

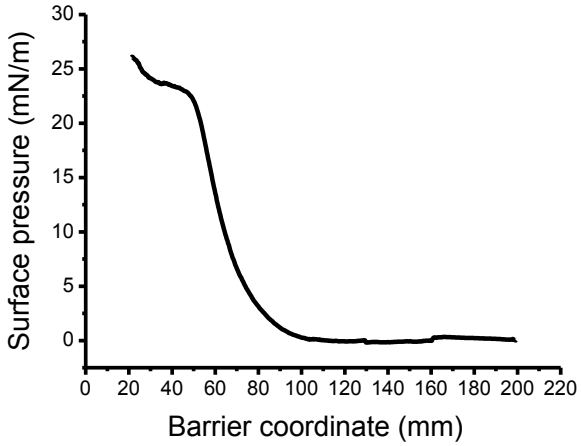

Figure 23 Surface pressure-area isotherm of polyaniline monolayer spread onto the surface of pure water.

The graph (figure 23) reports the area per repeated unit of PANI but it show only the barrier coordinate in mm. This is explained by difficulties to determine precisely the concentration of PANI in solution, because PANI is very poorly soluble in NMP, moreover there is inevitable loss of the compound caused by NMP dissolution in water subphase during its spreading.
PANI monolayer was compressed at a rate of 0.5 cm/min to a surface pressure of 10 mN / m. Then the barriers were stopped and a formed monolayer was divided into independent sections by means of a plastic greed. Each section was used for transferring the monolayer onto the substrate by the Langmuir-Schaeffer method (LS-method) (figure 24). The substrate used cut are glass cover slip rectangles (12x8 mm), with sputtered chrome electrodes (source and drain). A PANI strip (4.3 mm) was formed on the substrate surface through a special mask. The PANI strip is connected to two electrodes.

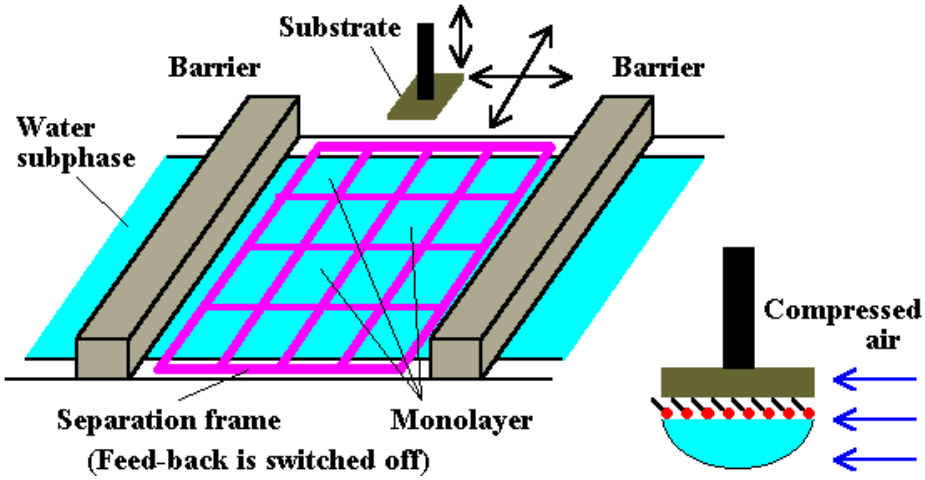

Figure 24 Scheme of Langmuir-Schaeffer method of deposition.

The quality and uniformity of the deposited films was controlled by Scanning Electron Microscopy (SEM). Figure 25 shows the typical morphology of LS PANI film. The polyaniline multilayer has a granulated morphology typical for polymer films, and quite similar to other literature data.

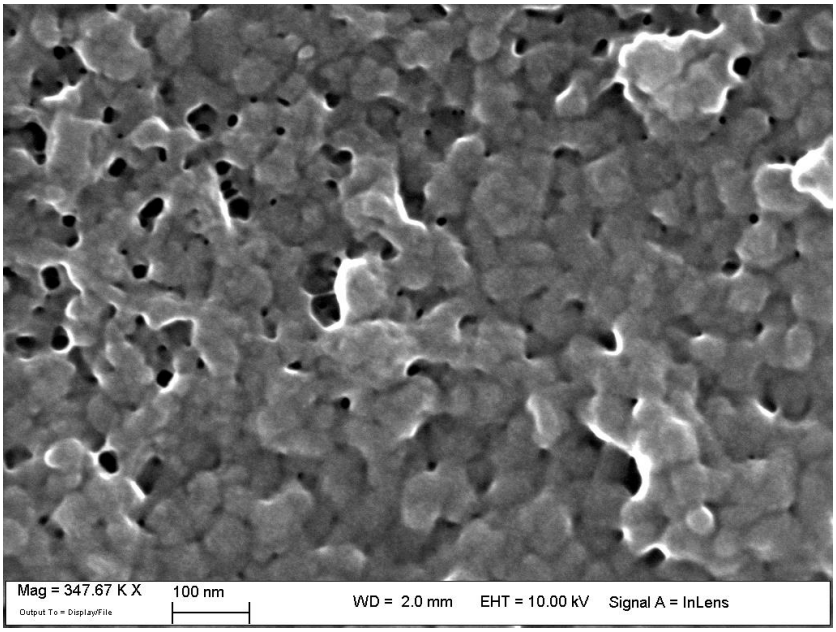

Figure 25 SEM image: morphology of 36 LS-PANI layer.

The resulting film was doped in 1M hydrochloric acid (1M HCl) for one minute. Doping process was repeated after 20 minutes to achieve obtain a higher and stable conductivity. After deposition the film has a blue colour, while after the doping in HCl the colour of the PANI film changes from blue (non-conductive, emeraldine base) to green (conductive state, emeraldine salt). The conductivity of the film is within the range of kΩ after doping twice.

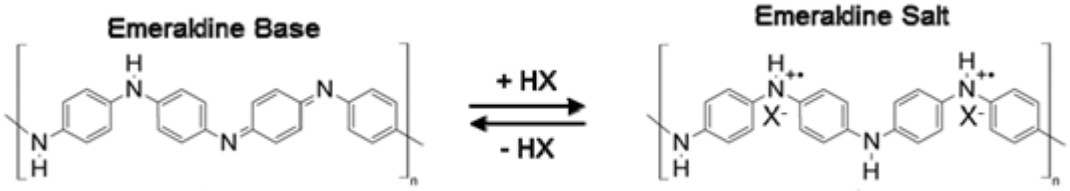

Figure 26 Acid doping of Langmuir-Sheafer PANI film.

As noted earlier, another important element in organic memristive device is the medium for redox reactions.
Chitosan-gel (30 mg/mL) and high methoxyl pectin (HM-PEC) gel (50 mg/mL) were prepared in 2% acetic acid. 30 mg / ml PEO solution was prepared dissolving it in 0,1 M water solution of $LiClO_4 \times 3H_2O$. After 24 hours of swelling and dissolution of the powders, the formation of a transparent gel was achieved in all cases.
A thin gel stripe of 1.2 mm width, was placed onto the central part of PANI layer between source and drain electrodes (S-D). A silver wire (gate electrode, G) with a diameter of 50 microns was positioned above the polymeric stripe and covered with an additional layer of gel. Contact zone PANI-polyelectrolyte is an active junction of the above-described device (par. 2.3).
In devices with standard configuration (par. 2.3), at the moment of the formation of physical contact between a stripe of PEO-gel (prepared in water solution) and a layer of PANI (doped with hydrochloric acid), the PANI de-doping immediately occurs, due to water diffusion from gel to PANI layer. To return to the initial value of conductivity of PANI film, the additional doping of vapours of concentrated HCl (37%) solution to the whole structure was carried out.

The figure 27 shows a schematic representation of organic memristive device, in which PEO has been replaced with a bio-polymer.

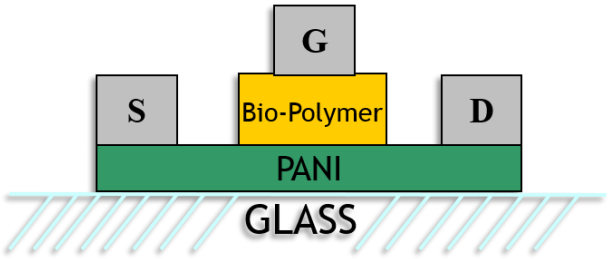

Figure 27 Schematic representation of organic memristive device.

3.4 Electrical characterization

The electrical measurements were performed using a Keithley 236 source measure unit and a Keithley 6514 system electrometer. The 236 unit was used to apply a potential difference between the source (S) and the drain (D) electrodes of the device, keeping the source at the ground level, and to measure the total current ID passing through the device. The 6514 unit was used to measure the current passing from the gate to the drain electrode IG, i.e. the ionic current. The subtraction of this value from the one measured by the 236 unit gives the value of electronic current passing through the PANI layer. The voltage–current characteristics were measured between −1.2 V and +1.2 V Measurements started at 0 V at the drain. The sampling period was 1 second. Voltage was applied in steps of 0.1 V. Readout of the current value was performed after 60 s delay after the voltage application (in standard configuration). This time delay is necessary to balance the electrochemical processes occurring in the active zone and to equilibrate the state of the element. Initially, the active zone is maintained in a non-conductive state, as evidenced by a low electron current value (voltage range from 0 V to +0.4 V) [81]. Each experiment was performed at least in triplicate.

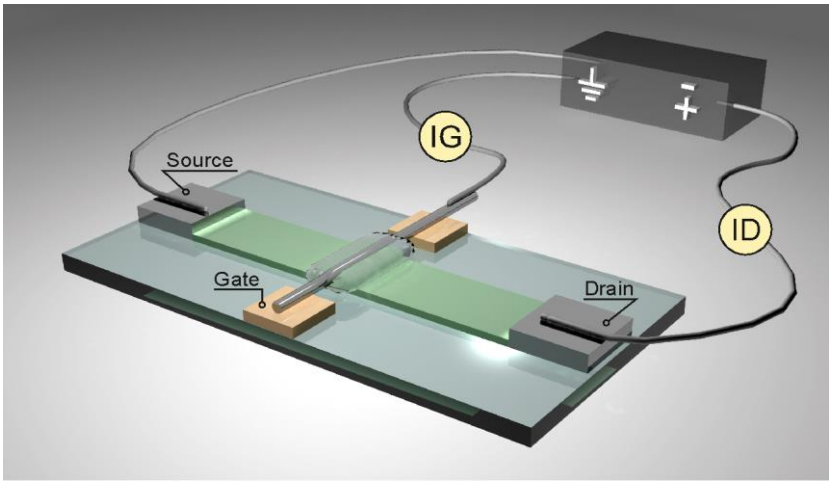

Figure 28 Schematic representation of organic memristive device and circuit for measuring of its voltage-current characteristics.

4. Results and discussion.

The main aim of this thesis is the identification of a strategy to achieve a functional matching between polyaniline and biological system. The key idea is to introduce an intermediate layer between polyaniline and a biological counterpart making a multilayer architecture. The interface layer should be a "solid buffer" able to retain the PANI conductivity. Moreover, it should be electrochemically "inert", thus it should not interfere with the ion exchange between biological components and PANI in bio-organic devices (see chapter 5).
The first step of this study consisted in substituting the PEO used in ST-OMD (see par. 2.3) with chitosan and pectin.
Hence the suitable conditions as well as doping agents (salts, organic or inorganic acids e.g.) for the interface layer were studied and optimized. Therefore, it was necessary understanding and identify the chemical species and components in ST-OMD responsible for the electrochemical switching of PANI.
All the chemical components able to induce a memristive behavior should be eliminated from formulation of gel used in multilayers hybrid structure (see chapter 5).
In order to obtain the largest information possible about the parameters necessary to build the interface, the research work focused on several experimental parameters that could influence the electrochemical characteristics of devices. In particular, the following factors have been studied:
-The chemical nature of the solid polyelectrolytes used in active area of the organic memristive element (comparison between biopolymers and PEO).
-The effect of hydrochloric acid and acetic acid on voltage-current characteristics of organic devices;
-Comparison between chloride salts and acetates as doping agents in solid polyelectrolyte;
-Role of cations on memristive behavior of devices including pectin as solid polyelectrolyte;
-Effect of electrode materials on voltage-current characteristics of organic devices;
-The equilibration time (delay between the voltage application and the readout of the current value).

4.1 Organic memristive elements with chitosan as solid polyelectrolyte.

The devices studied in this section were prepared using chitosan as solid polyelectrolyte and HCl as doping agent without addition of any lithium salts.
First of all, I prepared the devices following the procedure that was described in paragraph 3, replacing PEO with a Chitosan stripe. Chromium was used for source (S) and drain (D) electrodes while silver wire was used as gate (G) electrode. The cyclic V-I characteristics for using a delay of 180 s is shown in figure 29. The resulting characteristic curve is not significantly different from previously reported ones for standard device (see par. 2.3). It exhibits a pronounced rectifying behavior and significant hysteresis loop of the conductivity in the positive voltage branch. The time delay of 180s used results to be long enough for completing the processes of oxidation and reduction of PANI in the active zone under chitosan stripe. These results strongly indicates that, there is not any influence of the chitosan layer on memristive behaviour of the device. When compared to the typical PEO characteristics, Chitosan does not produce significant modifications of the current major trends (the memristive behaviour and the rectification of current in negative voltage branch were observed in both cases), even if there are kinetic effects that is worth discussing further.

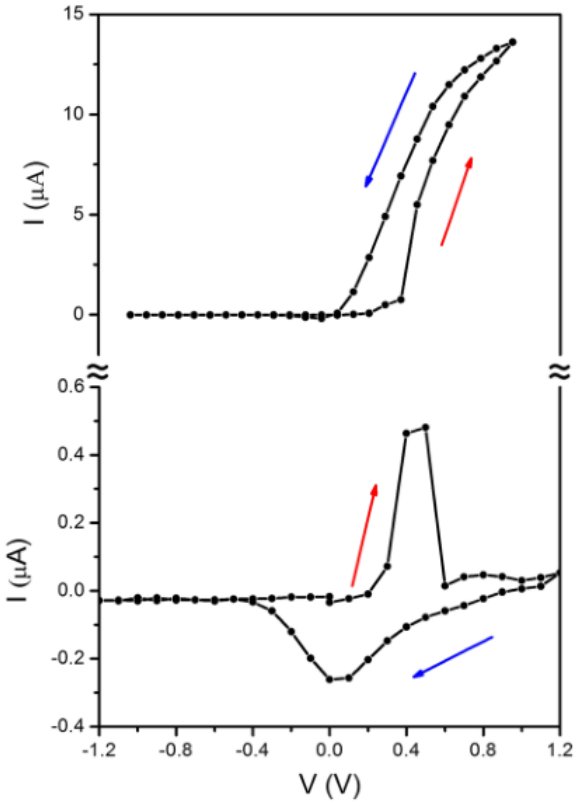

Figure 29 Typical cyclic V-I characteristics of a device with chromium S, D electrodes and silver G electrode. (Chitosan stripe). Delay time is 180s. Arrows indicate the direction of the voltage cycles.

It is worth noting that the absence of lithium ions in the gel formulation does not influence the electrical characteristics of devices: the response of the OMD with chitosan does not differ from that of ST-OMD, although in this case there was not any addition of a lithium salt into organic polyelectrolyte which is fundamental in the ST-OMD. The chitosan casting solution was hence characterized by EDX analysis to check whether some metal ions may be present by accident. No metal ions were detected by means the EDX analysis, in the limit of the sensitivity of the technique, even if, it is possible that some salt are present in traces in commercial chitosan (see. par. 3.2).

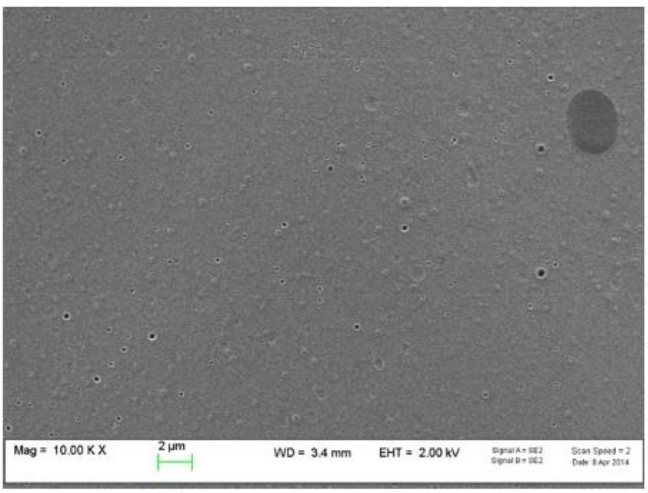

Figure 30 Morphology of Chitosan cast film.

Note that just hydrochloric acid and the acetic acid were added in gel formulation; they are practically enough for supporting the processes of oxidation and reduction of PANI in the active zone under chitosan stripe. This is a strong indication that lithium ions could not be the only key components in the mechanism of PANI switching in organic memristive elements.

4.1.1 Kinetics of Organic memristors with chitosan as solid polyelectrolyte.

As shown in paragraph 4.1, changing PEO with chitosan in a standard device does not changes the basic electrical features. In other words, the chemical nature of the solid polyelectrolyte does not modify the memristive properties. Nonetheless, some differences in the kinetics of redox processes have been observed and thus, a kinetic study was carried out for organic element with chitosan as solid polyelectrolyte.
Cyclic voltage-current (V-I) characteristics were measured as described in paragraph 3.4; and different experiments have been carried out changing the delay time.
At each voltage step, the delay times of 60 and 180s were used respectively to equilibrate the transient processes in the devices at each test.
First of all, the electrical features of devices with chitosan in standard condition were studied: applying the delay of 60s at each voltage step. Figure 32 reports subsequent measurements of I-V cycles. Subsequent cycles seem quite different from the first one. In fact in the first cycle the trend of electronic current shows a plateau (a saturation of current) at ~ 1.2V and at least a peak in reverse potential sweep at the positive voltage branch. In addition, a perfect rectification of the current in the negative potential branch is absent in above-mentioned curve. These peculiar behaviours are a first indication that the delay of 60s is not enough to complete the redox processes in PANI film in contact with chitosan stripe. In any case, the measurements carried out for subsequent cycle show that the device with chitosan as solid polyelectrolyte has good stability and reproducibility.
Thus, in a second set of experiment a delay time of 180 s was tested. The figure 31 shows the comparison between the curves of electronic current for both delays.
At this much longer delay times no significant differences were observed during subsequent I-V cycles. A better rectification of the current in the negative branch of the voltage was also observed with 180s delay (figure 31B) with respect to the 60s delay time

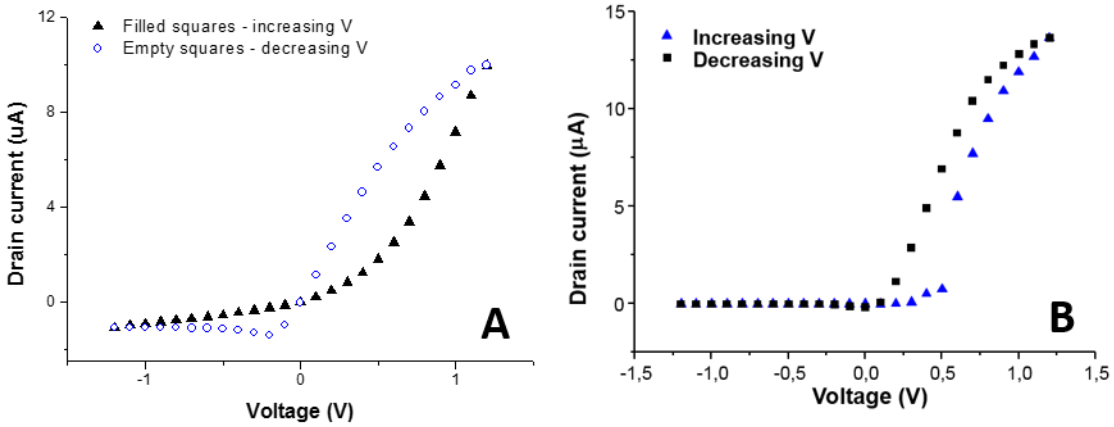

Figure 31 Comparison between the electronic current trends of organic memristive elements with chitosan as solid polyelectrolyte. (A) Delay time is 60s; (B) delay time is 180s.

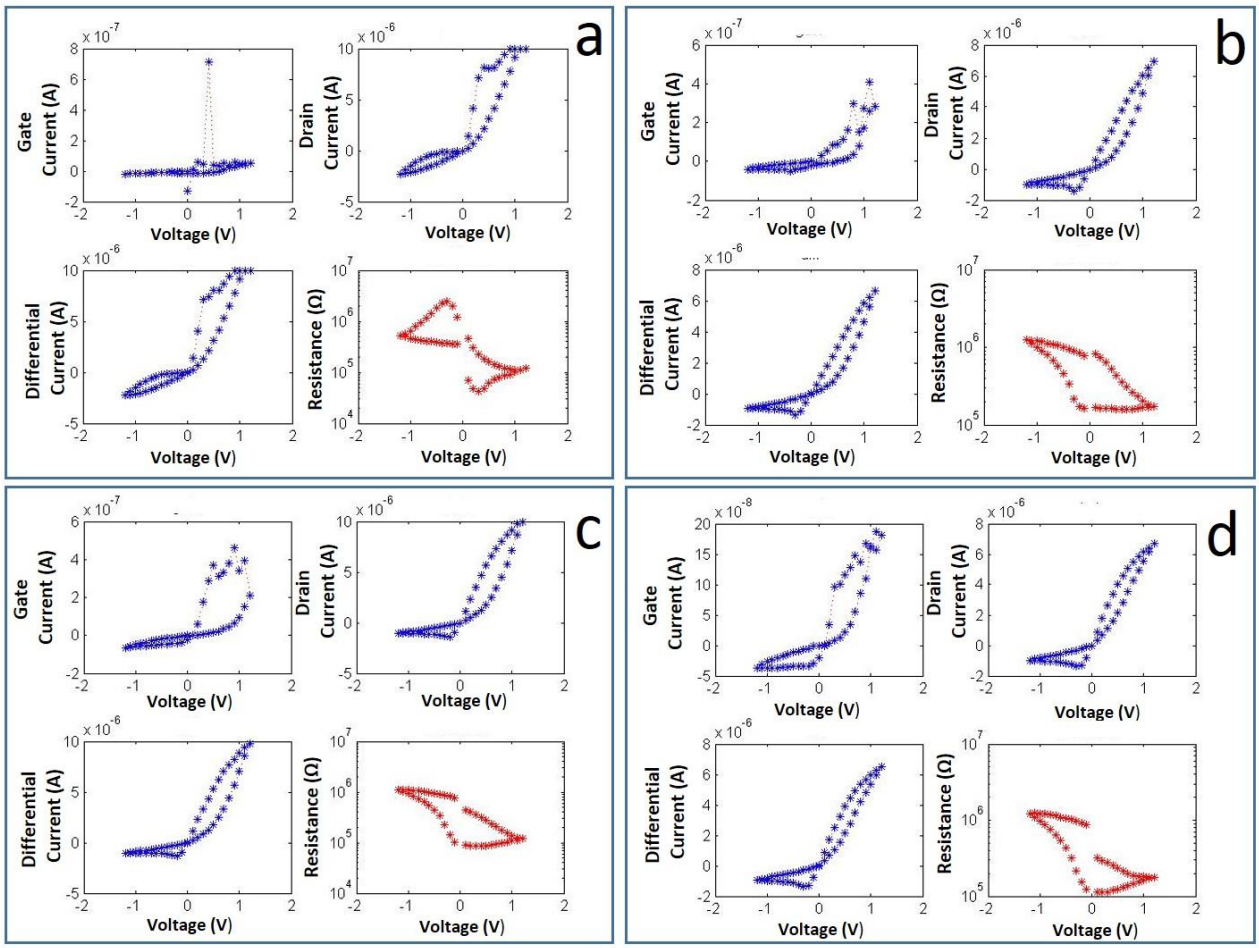

Figure 32 Subsequent cycles of I-V measurements of organic memristive elements with chitosan as solid polyelectrolyte; the delay time is 60s.

These data compared to the results obtained with PEO (both 30 mg/mL) strongly support that the processes of ion migration in Chitosan are significantly slower than in PEO, under the conditions explored here. The two polymeric matrix in quasi-dried state are different.

4.1.2 Optimization of Chitosan gel formulation.

In order to optimize the texture, the homogeneity, the brightness and the drying conditions of gels I tested several gel formulations for both chitosan and pectin, changing for example the bio-polymer concentration (in the range between 20 and 50 mg/mL). Of course, as expected, the polymer concentration greatly influence the type of matrix both in gel phase and in solid state while the crosslinking degree and the strength of chain-chain interactions in the dried polymer (see par. 2.4.4) influence the ion conduction in polyelectrolyte. Increasing the concentration gives rise to a denser polymeric matrix, that will hinder ion migration.

The concentration of the polymer and the delay time are a couple of non-independent and correlated parameters that, working synergically, influence together the electrical features of the current in organic memristive elements.

It was hence necessary to test different combinations chitosan concentration/ delay time in order to define the best conditions and parameters for the preparation and characterization of organic memristive devices. Figure 33, shows an example of the V-I characteristics of a device with chitosan (50 mg/mL) in acetic acid 10% w/w, which is doped by LiClO4 (0,1M). The figure shows the V-I

characteristics for delay of 60, 180 and 300s that was used to equilibrate the transient processes in the devices in each test respectively.

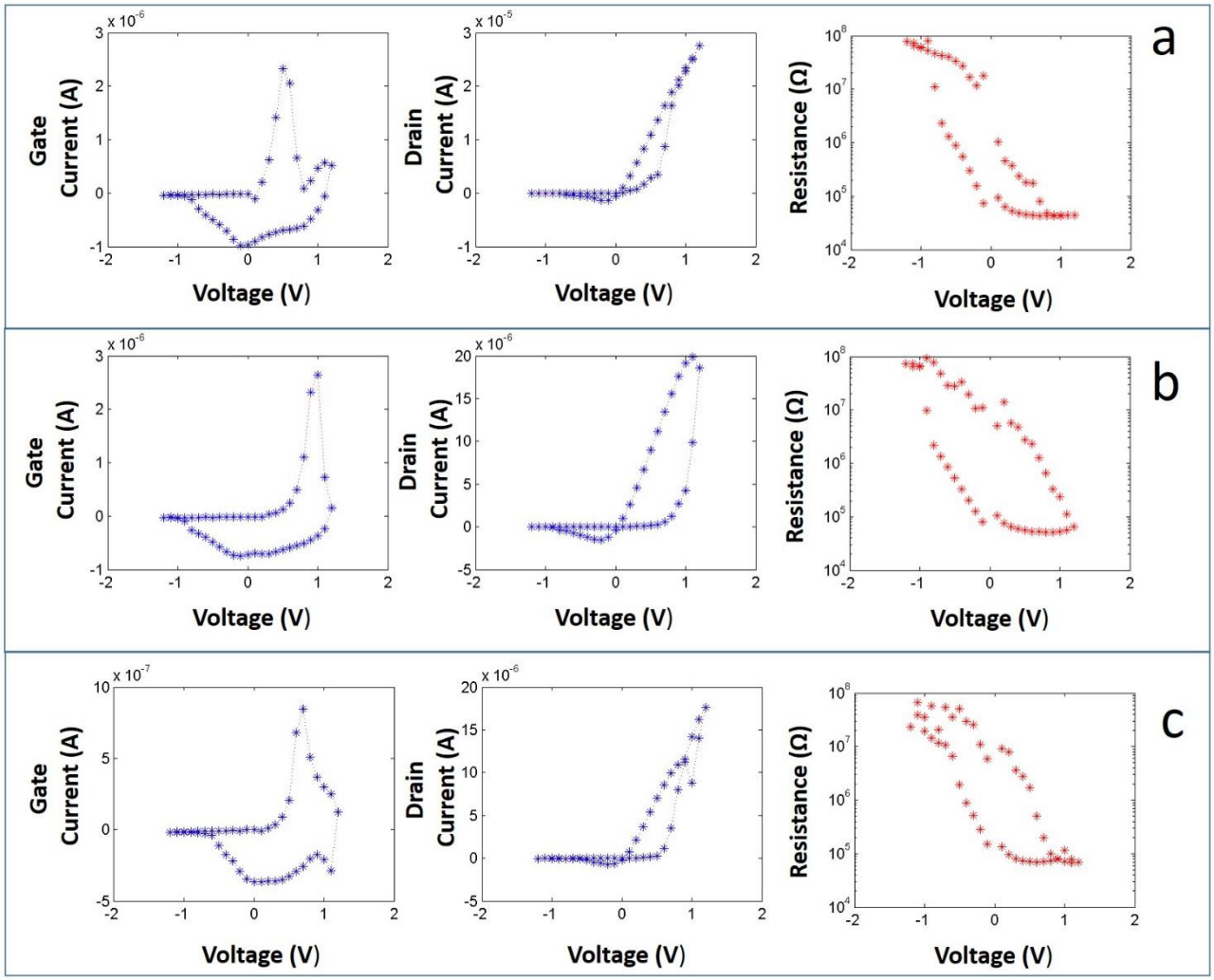

Figure 33 Cyclic V-I characteristics of the organic memristive device assembled with chitosan (50 mg/mL in acetic acid solution 10% w/w) doped by $LiClO_4$ (0.1M) and HCl (0.1%). The delay time is (a) 60s; (b) 180 s; (c) 300s.

Comparing the cyclic voltage-current (V-I) characteristics for each device, results that the best electrical features are obtained with the following combination chitosan concentration/ delay: 180 s delay with chitosan (30 mg/mL) (figure 33B).

4.1.3 Effect of electrode materials on voltage-current characteristics on Chitosan based.

The devices characterized in this section were fabricated using the chitosan as solid polyelectrolyte and HCl as doping agent without addition of any lithium salts as above (par. 4.1) while the material used as gate electrode was changed with respect to ST-OMD, in order to study the role of the electrode materials on V-I characteristics of OMD.
When the platinum (Pt(0)) wire is used as gate electrode, and chromium was used for source (S) and drain (D) electrodes, no memristive behaviour is observed in V-I characteristic of OMD with

chitosan. The drain current exhibits linear Ohmic behaviour, the current presents the suppression of the ionic conductivity around 0V, and there is no evidence of any peaks associated to PANI redox processes. The dependence of resistance as a function of the applied voltage for the device with all platinum electrodes confirms that electrochemical switching of PANI does not occur. There is not any observable variation in the current trend (shown in figure 34) increasing the delay time (from 60 s to 360 s). Results indicate that platinum is not suitable as gate electrode in organic memristive devices. Even if the concentration of protons (H^+) is high, they does not promote the electrochemical switching of PANI in presence of platinum as gate electrode, although the Pt(0) has a lower overvoltage hydrogen than Ag. In other words, if the the H_2 evolution is the driving force of the PANI electrochemical switching (that should be based, in this case, mainly on the protons exchanging and migration), the memristive behavior should be more easily observed with platinum electrode. Nevertheless, these results confirm that the organic memristive elements require silver wire as gate electrode. These aspects will be depth in par. 4.7.2.

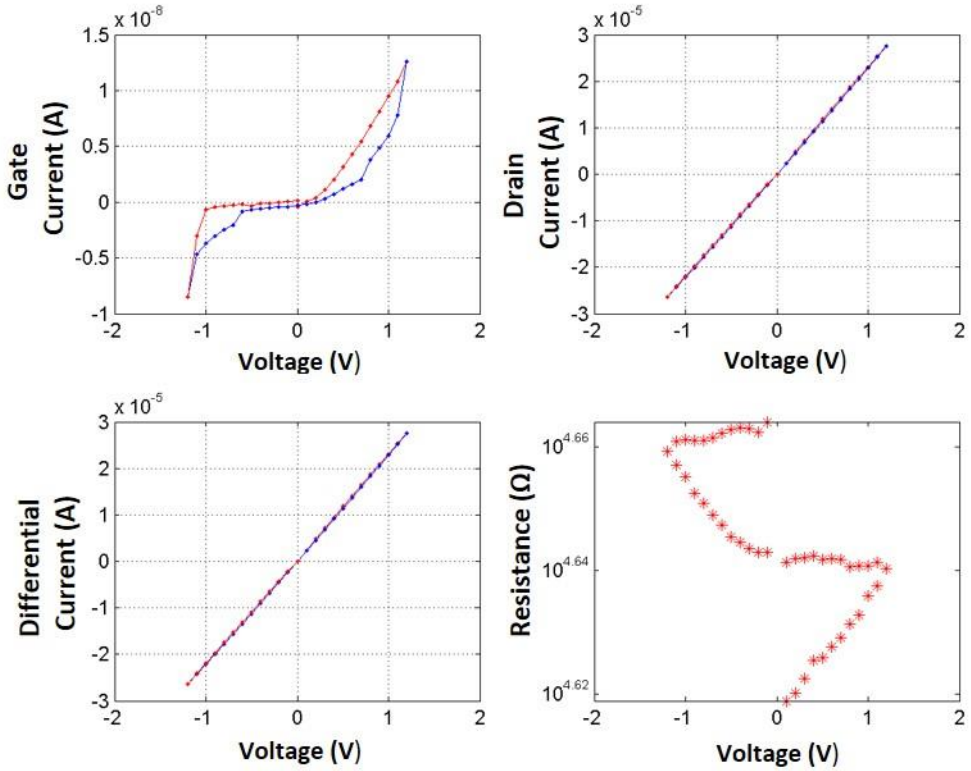

Figure 34 Cyclic V-I characteristics for the device with chromium S, D electrodes and a platinum G electrode. (Chitosan stripe). Delay time is 180s.

In order to verify if the PANI redox processes however occur with the Pt gate electrode but at different potentials compared to ones with Ag wire, I widened the voltage window in which the measurements were acquired. The platinum has a higher working function (in other words, a different reduction standard potential (E0)) than silver. The V-I characteristics of devices with platinum gate electrode were recorded in the potential range between +2V and -2V (figure 35).

Also in this case the PANI redox processes seem not to take place. Also the variation of resistance confirms that electrochemical switching of PANI does not occur in the tested conditions (figure 35). Figure 35 shows peaks in drain current that are probably due to secondary processes such the electrolysis of water that is bounded to the polymeric matrix of polyelectrolyte.

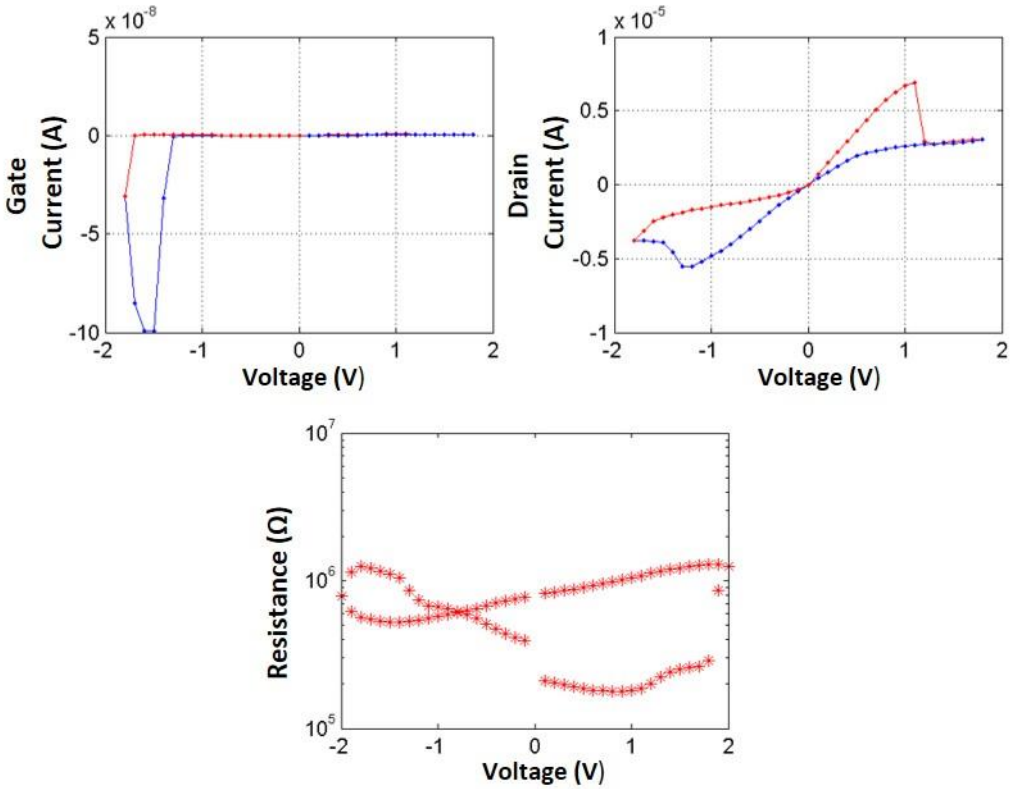

Figure 35 Cyclic V-I characteristics for the device with S, D and electrodes and platinum G electrode. (Chitosan stripe). Delay time is 180s, potential range from -2V to +2V.

The experimental data showed that the material of the gate electrode has a great influence on memristive behavior of electronic elements. Results indicate that silver is the best suited, if not the only, gate electrode in organic memristive element. Memristive behavior was not observed with platinum gate electrode, also in presence of hydrochloric acid.

4.2 Chitosan films (without PANI layer) in direct current (DC) mode.

The current-voltage characteristics of chitosan-gel stripes in contact with different electrodes (silver, chromium, platinum) were studied also without PANI in direct current mode, in order to understand if any redox reaction at the biopolymer-electrode interface takes place inducing asymmetric I-V characteristics. In fact it is necessary to verify that secondary redox processes would not occur alternatively to the redox reaction at the PANI-biopolymer interface.
In other words, this is very important to ensure that any process causing a non-linear behavior of currents (see par 4.1 and 4.3) due to secondary reactions would not interfere with the electrochemical processes occurring at the contact area between PANI layer and the polyelectrolyte.
Figure 36 (bottom) shows the I-V characteristic of a chitosan-gel layer doped with HCl and $LiClO_4$, where a Direct Current mode was used applying voltages between +1.2 V and -1.2 V for several delay times in the range from 3s to 360 s. In this case, the different delay times do not influence the V-I characteristic. Only one example (for 60 s of delay time) is shown in figure 36.

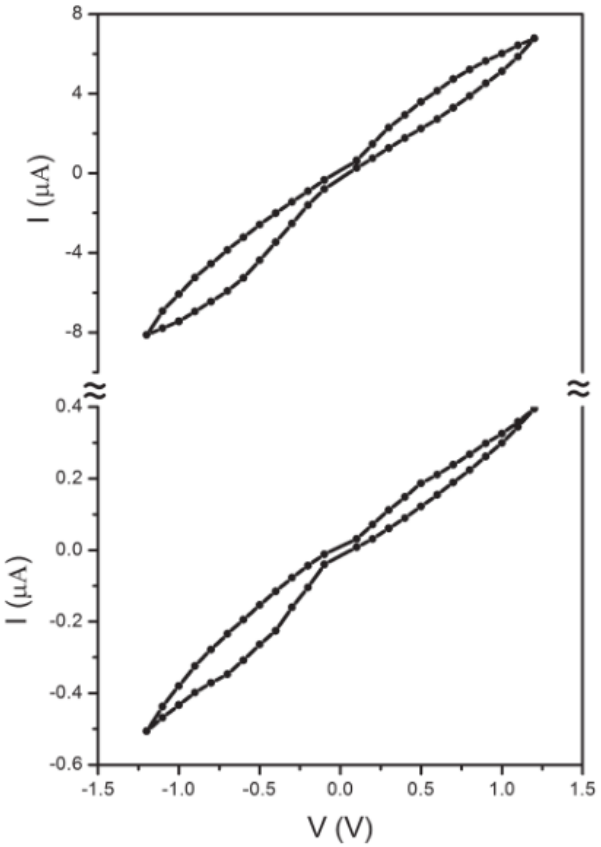

Figure 36 Cyclic voltage-current characteristics of solid polyelectrolyte stripe, made of chitosan-gel (bottom) compared to PEO-gel (top), with addition of HCl and $LiClO_4$. Delay time 60s.

Essentially linear current-voltage characteristics were observed (figure 36); this excludes that reactions at electrodes or the degradation phenomena of polyelectrolyte would affect the memristive behavior (figure 29). Therefore, chitosan resulted suitable as electrochemically "inert" material. No significant differences in the electrical data were observed, in comparison, for PEO (figure 36 top) and pectin (results do not shown).

4.3 Organic memristive elements with pectin as solid polyelectrolyte

As already mentioned Pectin is a quite promising candidate as interface between PANI film and biologic objects in bio-integrated multilayer structure.
As mentioned in a previous paragraph (par. 3.2) gelation of Pectin differs from that of Chitosan, since the presence of mono- and bivalent cations is crucial for the process of pectin gel forming. Therefore, in this part of the work I devoted much attention to the study of the composition of pectin gel and the impact of its structure on the electrical characteristics of OMD.
As in the case of chitosan, I prepared different formulations of Pectin gel with and without the addition of 0.1M HCl in its composition (see par. 4.3 and 4.3.1), because the previous results indicated that the Cl^- could greatly affect the electrochemical features of devices. In addition, the effect of the presence of ions such as Li^+, Na^+, K^+, Ca^{+2} in gel formulation on the memristive behavior was also studied (see par. 4.4.1).
For each composition of the solid polyelectrolyte based on Pectin the OMD were fabricated and the behavior of the current-voltage characteristics of devices were studied. These characteristics were recorded for at least three structures for each type of devices.

The figures 37 and 38 show the results obtained with the following formulations:
-Pectin (50 mg/mL in acetic acid solution 2% w/w) with $CaCl_2$ (1M) and HCl (0.1%) as doping agents;

-Pectin (50 mg/mL in acetic acid solution 2% w/w) with $CaCl_2$ (0.1M) and HCl (0.1%) as doping agents.
Figures 37 and 38 show, respectively, the cyclic V-I characteristics recorded for a delay-time of 300 s in both cases. In presence of high calcium concentrations, the ionic current shows two couple of peaks due to the oxidation and reduction processes of PANI, while in system with calcium 0.1M the second couple of peaks is not clearly distinguished. The variation of resistance upon the potential applied is about three orders of magnitude in both cases; the trend of electronic current is memristive-like.

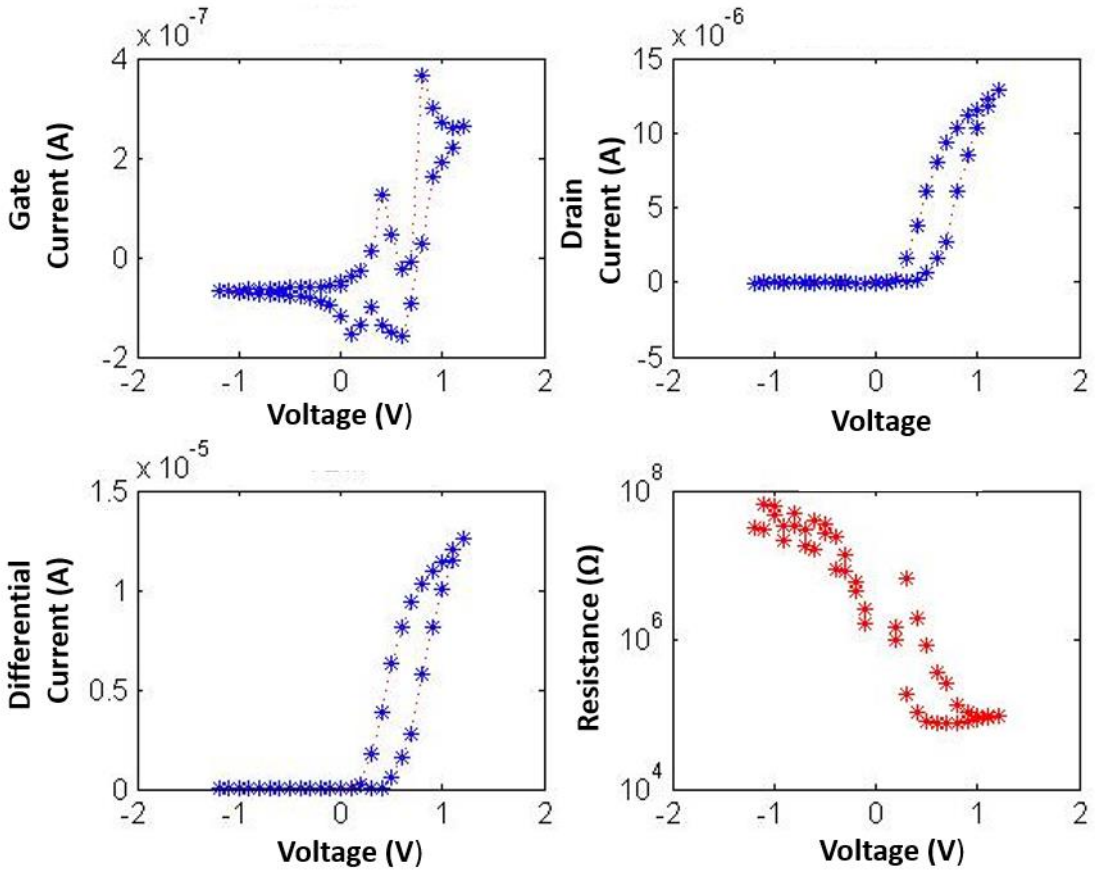

Figure 37 Cyclic V-I characteristics of the organic memristive device assembled with pectin (50 mg/mL in acetic acid solution 2% w/w) doped by $CaCl_2$ (0.1M) and HCl (0.1%). The delay time is 300s.

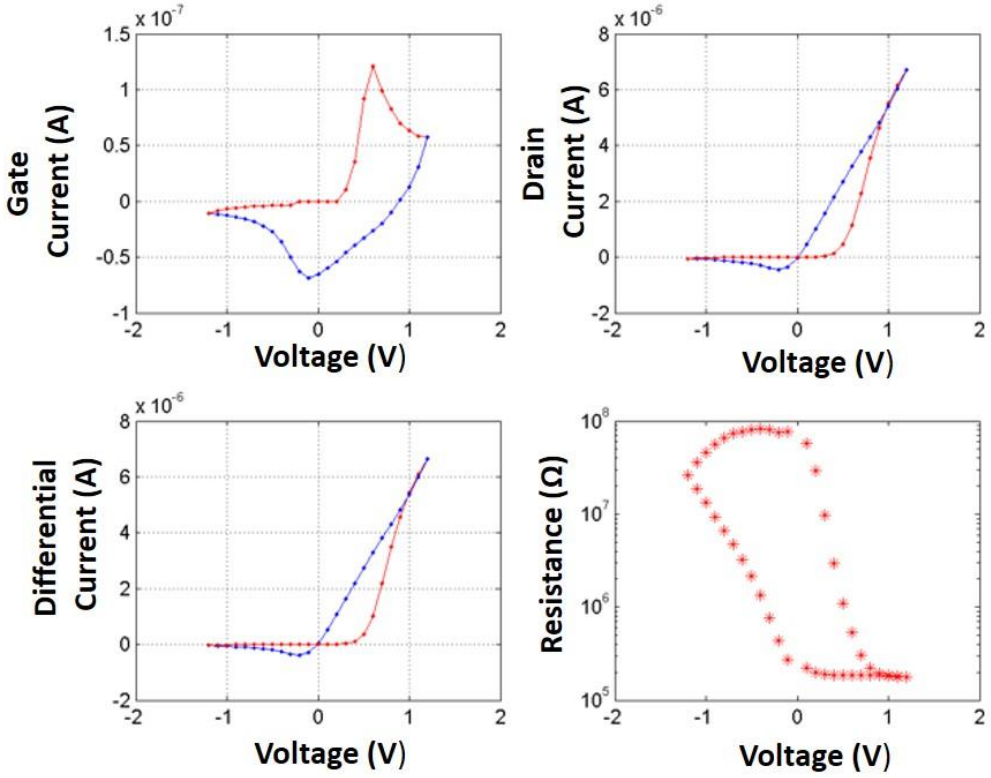

Figure 38 Cyclic V-I characteristics of the organic memristive device assembled with pectin (50 mg/mL in acetic acid solution 2% w/w) doped by $CaCl_2$ (0.1M) and HCl (0.1%). The delay time is 300s. Direct sweep (red line); reverse sweep (blue line).

A first analysis of these data brings to a first important conclusion that it is possible to develop memristive-like structures by replacing PEO, used in the ST-OMD as solid polyelectrolyte, with Pectin a bio-polyelectrolyte. It's worth noting that a much larger delay time (300 seconds) it is necessary for structures based on Pectin in comparison with the standard (60 seconds are enough for ST-OMD).

4.3.1 Effect of hydrochloric acid on Pectin based memristors.

Devices with a pectin (solubilized in acetic acid, see par.3.3) layer and HCl as doping agent are described in this section. The cations such as calcium ions are absent in this case.
The cycle V-I characteristics (figure 39), recorded in these experimental conditions, are very similar to the previous ones (see figures 37 and 38).

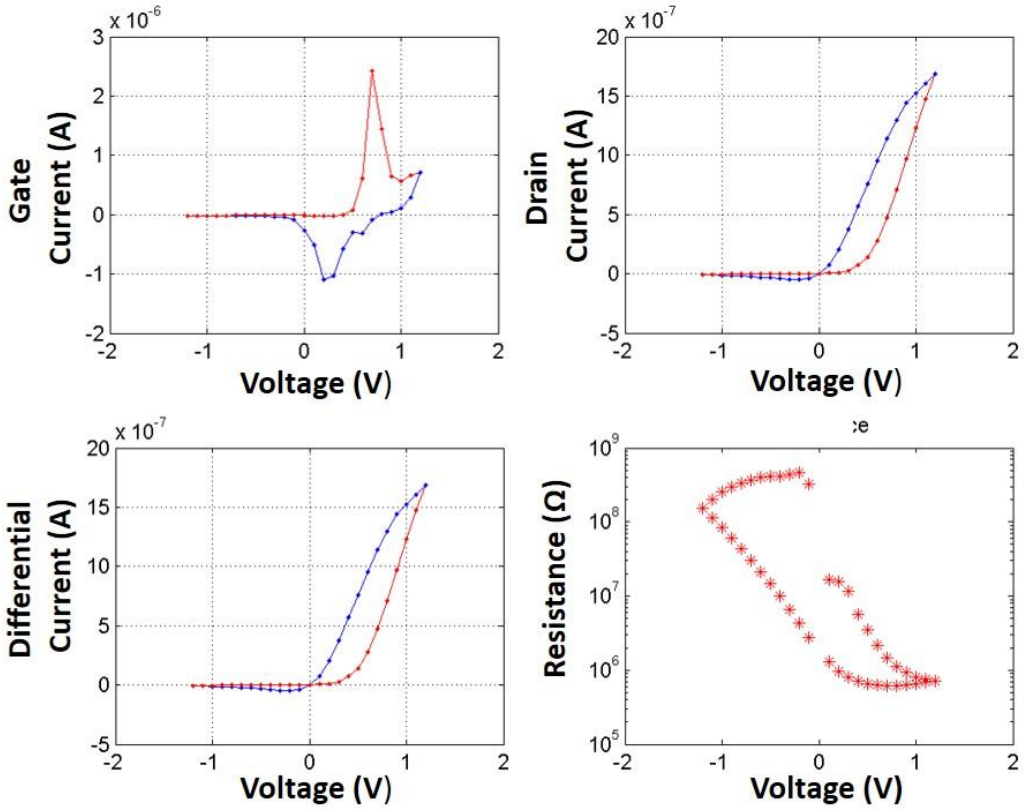

Figure 39 Cyclic V-I characteristics of the organic memristive device assembled with pectin (50 mg/mL in acetic acid solution 2% w/w) doped by HCl (0.1%). The delay time is 300s. Direct sweep (red line); reverse sweep (blue line).

The experimental data show hence that the presence of calcium ions is not fundamental for memristive feature of the systems. In order to separate the contributions, on memristive behavior, of the hydrochloridric acid and acetic acid, I prepared some devices in which the HCl was used both as doping agent and for dissolving pectin in aqueous solution. Even in this case, the V-I curve of (figure 40) exhibits a pronounced rectifying behavior and significant hysteresis in the positive voltage branch. Both the peaks in the ionic current curve (figure 39) show a shoulder, this feature was also observed in other samples (see figure 37), and it will be discussed further later on (par. 4.7.4). The V-I characteristic was recorded with a delay time of 300s, which is long enough for accomplishing the oxidation and reduction processes of PANI in the active zone. Note that both Pectin and Chitosan (see par. 4.1 and 4.3) show a slower kinetics for ion conduction processes, in comparison to PEO in a standard device.

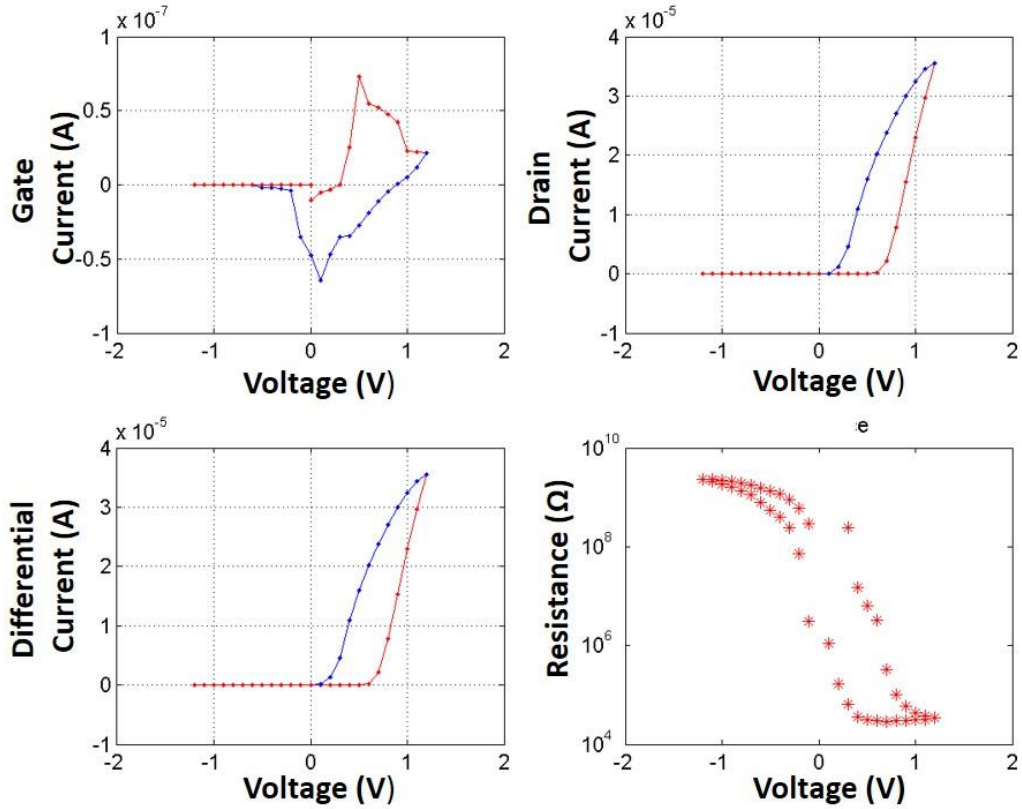

Figure 40 Cyclic V-I characteristics of the organic memristive device assembled with pectin (50 mg/mL in HCl (0.01N)) doped by HCl (0.1%). The delay time is 300s. Direct sweep (red line); reverse sweep (blue line).

The experimental data shown in this section (par.4.3.1), confirm that the hydrochloric acid has a key role in PANI electrochemistry, not only for chemical doping (see chapter 3), but also in the redox processes involving PANI.

4.4 Memristors with Pectin in gel phase as solid polyelectrolyte: towards biointerfacing and biosensing.

In biological systems the ionic conductivity is the result of synergic activity of different ions that have different characteristics (charge, ionic radius, hydration enthalpy). The migration of ions in polymeric matrices is tightly interconnected to these chemical-physical parameters. The rate of ion diffusion affects the electrochemical switching of PANI. Here I studied the effect of different ions (as chloride salts or acetates) as doping agents in OMD with pectin.

4.4.1 Role of doping agents (chloride salts) on memristive behavior.

The communication between biology and electronics is supported by exchanges of ions in electrochemical devices and biosensor. In particular, the cations have a key role in biologic events. From the point of view of the main aim of this thesis that is to find a suitable architecture for bio-integrated device, Pectin is a promising candidate that can be used as a solid matrix in which the ionic (in particular cations) migration could occur.

Devices with Pectin, doped by different chloride salts, were fully characterized from the electrochemical point of view. In particular, the correlation between the chemical nature of doping agents and memristive behavior was studied.
The cyclic V-I characteristics of the devices assembled with Pectin, doped by different chloride salts (NaCl, KCl, LiCl and $CaCl_2$ respectively) and HCl, showed a memristive behaviour, regardless of the added salt. HCl in the polyelectrolite produces a kind of "leveling effect", so that, any kind of selectivity for cations was not observed. These results are in good agreement with the experimental data previously shown (see par.4.3.1).
Then, a second set of experiments were carried out: the same chloride salts were employed at the same concentration (0.1 M) (NaCl, KCl, LiCl and CaCl2 respectively), but in this case the HCl was not present in gel composition while the pH was decreased only by addition of acetic acid (2% w/w) in the Pectin gel. It has been verified, in this case, a strong dependence of electrical features of device from type of metal ions, that were added in the gel formulation as chloride salts (figures 41). The V-I curves clearly show these differences. The corresponding curves (figure 41) were recorded with the same rate sweep (delay time 300s in all cases) and following the already discussed standard procedure (reported in par.3.3).

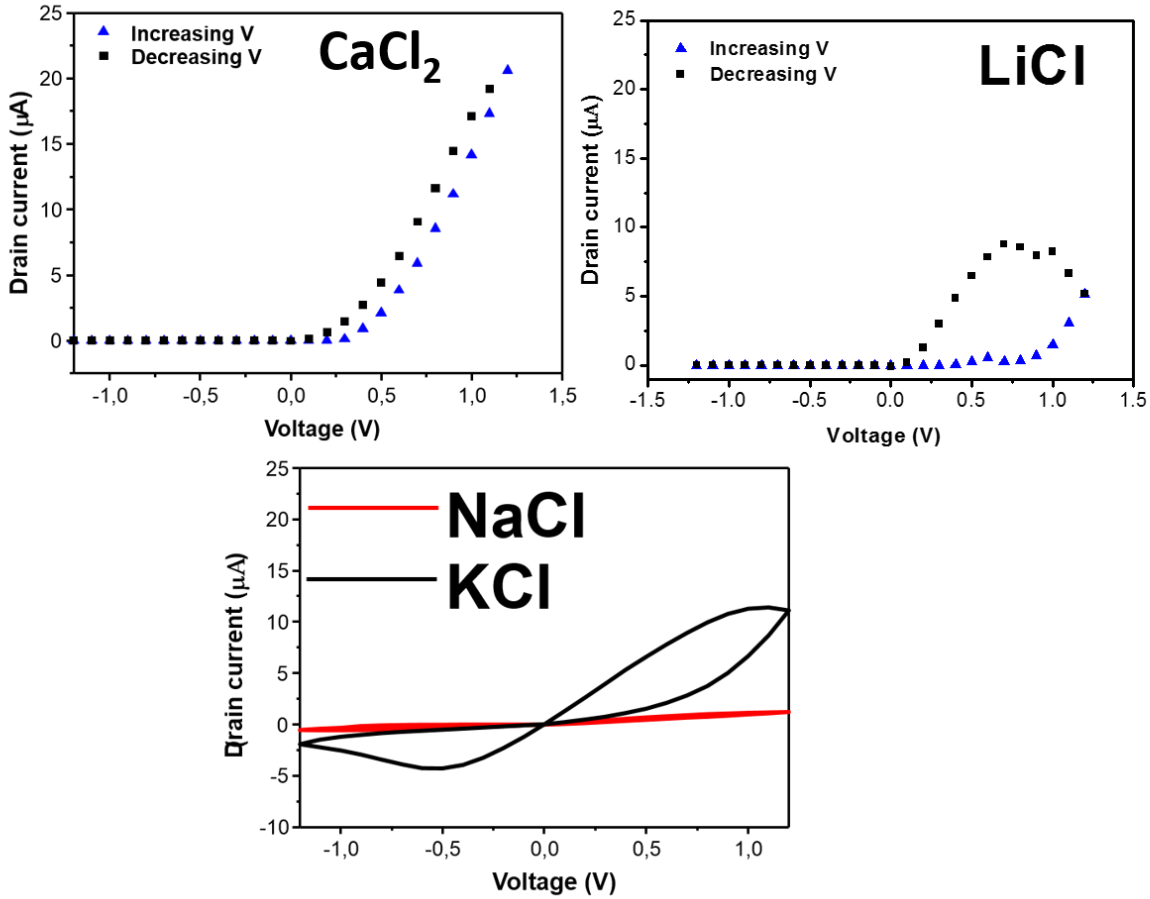

Figure 41 Cyclic V-I characteristics for the drain current of devices assembled with Pectin (50 mg/mL in acetic acid 2% V/V) doped by NaCl, KCl, LiCl and $CaCl_2$ (0.1 M) respectively. The delay time is 300 s.

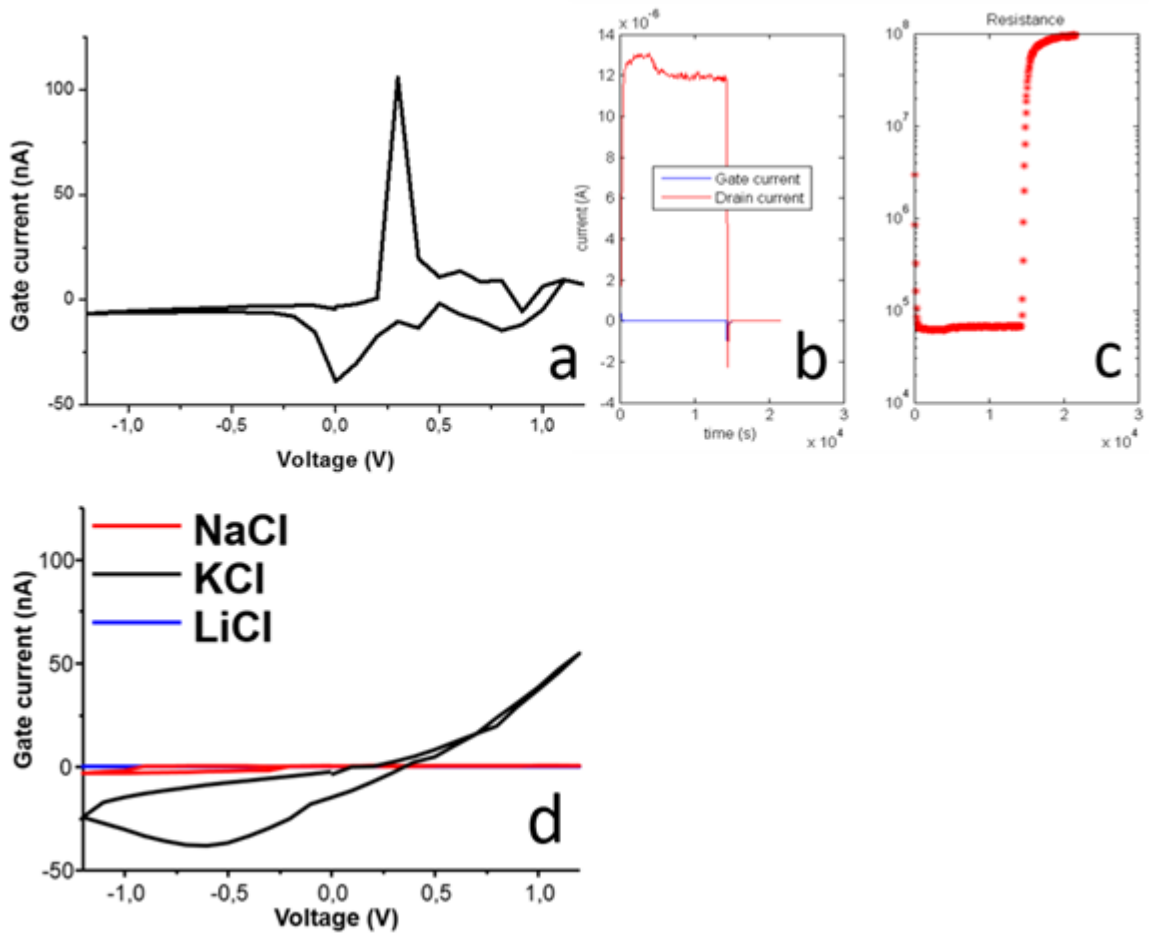

Figure 42 Comparison between cyclic V-I characteristics for the ionic current of the organic memristive device assembled with Pectin (50 mg/mL in acetic acid 2% V/V) doped by (a) $CaCl_2$ (0.1 M) and (d) NaCl (0.1 M) (red line), KCl (0.1 M) (black line), LiCl (0.1 M) (blue line). The delay time is 300 s. The dependence of (c) resistance vs time and (b) drain and gate current for the memristor assembled with $CaCl_2$-doped pectin.

As shown in figures 41-42 only the devices with $CaCl_2$ salt used as doping agent, showed the typical "classic" memristive behaviour. The major difference that appears with respect to previous measurements (figures 37-40) regards the hysteresis loop: the hysteresis loop breadth is tighter without HCl. In other words, lowering the Cl^- ions concentration, the kinetic of the process that occur is faster, because the current in reverse sweep is quite the same that in direct sweep. Steric effects could explain this peculiar feature: conductivity due to anion migration will be drastically decreased, at too high concentrations (figures 37-40), as a consequence of the energy landscape and of migration kinetic of Cl^- ions that have a large size (167 pm) [179]. The V-I curves, both for the ionic and electronic current (figure 41-$CaCl_2$ and 42b), of the devices assembled with Pectin doped by $CaCl_2$ show trends that are very similar to ST-OMD ones.
The V-I characteristic for the electronic current of the devices assembled with Pectin doped by LiCl shows a non-linear characteristic, with a hysteresis loop broader than standard. Even peak appears to grow on reverse sweep that proves that the oxidation process of PANI was not fully completed during direct sweep. This behavior could provide a supplementary information about the ionic conductivity. At the first we consider the hypothesis that positive ions should be the majority extrinsic charge carriers. Lithium ion should have a much higher mobility than calcium, considering their ionic radii (76 and 106 pm, respectively). This hypothesis is in contradiction with the experimental evidence. In other words, if the positive ions are the majority charge carriers, the devices with LiCl should work

much better than the devices with $CaCl_2$. Note that the ionic current in LiCl-doped devices are very low and it does not show any PANI oxidation or reduction peaks (figure 42d, blue line). This is also reason why the electronic current is lower than the currents recorded for $CaCl_2$-doped devices. So, we can resume the experimental evidence, considering a large number of replicates, that V-I characteristics of LiCl-doped devices are different from $CaCl_2$-doped devices.
The electronic current curves recorded for KCl-doped devices shows a quasi-symmetric characteristic; in particular they shows a negative hysteresis at positive potential. This trend of the current, which cannot be considered as memristive (figure 41-KCl black line), shows a non- rectifying behavior in the negative potential sweep. The ionic current (figure.42d black line) shows a current drift at voltage values different from "standard" reduction potential of PANI. This current trend proves that the processes occurring are not enough to switch the PANI state.
The cyclic V-I characteristic for the electronic and ionic current of the NaCl doped device showed a linear behaviour both in negative and in positive potential sweep while none of the features typical of memresistivity was observed in any case (figure 42d, red line). Even the ionic current of these devices does not show any PANI oxidation or reduction peak.
The selective memristive response observed for calcium ions is a feature that if further explored and applied could be very important for developing a novel class of biosensors and bio-medical devices where the transduction will be based joined to a memristive electronics. In fact, today it is widely recognized that Ca^{2+} ions are central to a complex intracellular messenger system that is mediating a wide range of biological processes: muscle contraction, secretion, glycolysis and gluconeogenesis, ion transport, cell division and growth [180,181].
The advanced and futuristic goal to develop devices were the selective memristive response induced by calcium ions could be the transduction mechanism would pave the way to relevant developments in bio-electronics applied to medical and nano-medicine fields.
Furthermore, the connection between memristive systems and the recognition of calcium is appealing. In fact, a memristor is a system that mimics the synapses properties, while calcium is closely involved in the regulation of numerous important cellular events as well as the transmission of electrical signals al neuronal level: the release of ($[Ca^{2+}]$) has important roles in the triggering of neurotransmitter release and the regulation of short-term plasticity [182].
In the following, we propose a preliminary, qualitative explanation of the experimental data and of selectivity for calcium ions, considering both the features of different chloride salts and the peculiar properties of Pectin, which differently from Chitosan is able to induce this selectivity.
Considering the key role of chloride ion in the electrochemistry of the device, the first consideration concerns the stoichiometric ratios between cations and chloride in salts. In the comparative study already described, the same concentration of each salt (NaCl, KCl, LiCl and $CaCl_2$) was used as doping agent in Pectin. Differently from other chloride salts, the stoichiometric ratio between Ca and Cl in the $CaCl_2$ is 1:2. But a thorough analysis suggests that the difference between the V-I characteristics shown in figures 41-42 can not just be ascribed to the different stoichiometric ratios between mono-and bivalent ions and Cl^- in chloride salts. In fact, the V-I characteristics that were obtained with different monovalent salts are quite different among them, even if the stoichiometric ration are the same (ratio1:1 between cation and Cl in monovalent chloride salts). For this reason, other parameters and factors should be taken into account: interaction between polymer chains, cations (mono or bivalent), counterions, and water. In literature, it was no possible find a model fully suitable to our materials and our experimental conditions. In particular, it could not be easily explained and described the solid polyelectrolyte (Pectin) characteristics, its ionic conduction mechanism, the cations coordination on the basis of common models suitable for Pectin aqueous solutions in semi-diluted regime [163]. One difficulty arises from the fact that in most applications both polymer and salts are used at much lower concentrations compared with our experimental conditions (par. 3.2). In addition, the drying up of the polyelectrolyte stripe (see par.3.3.1) greatly influences the ion conduction mechanism and final proprieties since solvation changes the binding of ions to Pectin chains. In a quasi-dried state ion pairs formation both between ions and the polymeric

chain is promoted. The formation of ion pairs results in the reduction in the number of free ions in solid polymer electrolytes.
In addition it is not too easy to predict the final characteristics of the polymer because several different dehydration mechanisms could occur. During dehydration polymer-polymer ion pairs interaction can substitute water molecules in forming hydrogen bonds (H-bonds) with the polar and charged groups present at the biomolecular surface [183] forming a scaffold upon dehydration. In fact, H-bonds bridging multiple headgroups are labile in the dilute regime but expected to strengthen, as a result of the removal of the water molecules [184]. In addition, the biopolymers could concentrate residual water molecules close to the biomolecular surface, thereby preserving largely its solvation and native properties in the quasi-dry state [185]. Vitrification process are also possible, that involve the formation of amorphous glasses. [186] This gives an idea of how complex are the processes occurring in a dehydrated polymeric matrix which are also affected by a strong variability for each polymeric fragment.
Anyway, it is possible tentatively to try to explain the process within Pectin matrix considering some general properties of solid polyelectrolytes.
Polyelectrolytes in gel phase consist of dissociated ions, ion pairs, solvent, and polymeric chains (i.e. folded, or partially or fully unfolded chains) as reported by several studies [187-192].
Experimentally, there is widespread evidence for ion association (i.e. ion pairs or higher aggregates) in polymer electrolytes. [193-195].
A metal salt MX dissolved in a polymer host results in formation of ion pair [MX]. Aggregation of the ion pair also takes place such as formation of large size $[MX_2]^+$ aggregates called contact ionic clusters. However, such kinds of aggregations lower the mobility within the polymer electrolyte hence affecting the ionic conductivity [195,197].
In general, high salt concentrations are likely to favour ion pairs (or aggregates). As many ions are provided in the polymer host, the distance between the ions become too close and the rate of ion association is higher than the rate of ion dissociation. The recombination of ions forms neutral pairs, which would not contribute anymore to conductivity [198]. In our specific case the formation of ion pairs with different degree of stability could possibly explain the selectivity that was showed by the devices described in this section.
The occurrence of contact ion pairing formation may mirror the solubility of different chloride ions. For example the lower solubility of KCl compared with $CaCl_2$ (table 3) could induce a higher probability of ion paring formation. Therefore, it seems likely that, especially at higher salt concentrations, there will be counterions on the inside of the chloride hydration shell of cations [199]. The hydration energy (in other words the solubility of salts) defines the probability of ionic pairs (solvent-separated) formation. The hydration energy is more negative (more favorable process) for Ca^{2+} than for monovalent ions. Hence the result is that the $CaCl_2$ solubility (-278.7 Kcal/mol) is higher than for the monovalent ions listed in table. The differences of hydration energy (in absolute value) follow the order: $CaCl_2$ > LiCl>NaCl>KCl.

Salt	Lattice energy (Kcal/mol)	Hydration Energy A^{n+} (Kcal/mol)	Hydration Energy X^- (Kcal/mol)	Hydration Energy (Kcal/mol)	Difference (Kcal/mol)	Ionic Radii A^{n+} (pm)
$CaCl_2$	-190.0	Ca^{2+}:-376.9	Cl^-: -91.8	-468.7	-278.7:soluble	106
LiCl	-206.5	Li^+: -119.3	Cl^-: -91.8	-211.1	-4.6 :soluble	76
NaCl	-183.1	Na^+: -93.2	Cl^-: -91.8	-185.0	-1.9 :soluble	102
KCl	-171.6	K^+: -77.0	Cl^-: -91.8	-168.8	+2.8:insoluble	138

Table 3 Chemical and physical parameters of chlorine salts [179, 200].

The three-dimensional diffusion coefficients of ions typically (but not entirely systematically) decrease in the order Cl^- >K^+ >Na^+ >Ca^{2+} in polyuronates matrix [186], which is also the trend

observed experimentally for the free ions in solution (2.03, 1.96, 1.33, 0.79 and 0.71 $nm^2\ ns^{-1}$, respectively) [201] at 298.15 K);
A faster diffusion correlates with a weaker hydration strength. The chloride ion has a greater ionic radius (Cl- 167 pm) and coordinates water molecules less efficiently than other ions listed in table 3. Small ions have high charge densities; in contrast, large ions have low charge densities. In other words, the growth of ion radius decreases the electrostatic forces on water [202].
On the basis of tunable interactions between the Pectin chains and different cations, the selectivity to $CaCl_2$-doped devices could be explained. Following the tight interaction between Pectin and selected cations, the ionic concentration in bulk and the probability of contact ion pairing formation decrease.
And thus, the occurrence of more stable interations between Pectin chains and ions decrease the numer of species (ionic pairs and clusters) that limit the ion conductivity increasing the number of free anions.
Several models [163, 186] confirming the preferential affinity for divalent (alkali-earth) over monovalent (alkali) metal cations in single-chain homopolyguluronate segments (the most important natural derivatives of polyuronates are Pectins), the density and tightness of the distributions of the different cations within the counter-ion surroundings follow the approximate order $Ca^{2+} > Mg^{2+} > K^+ > Na^+$. This selectivity is well known for gels: the divalent cations bound in junction zones cannot be displaced by monovalent cations. [203,204].
The solvent-separated binding of the cations to the carboxyl groups of the chain is frequent, and its occurrence follows the approximate order $K^+ > Na^+ > Ca^{2+} > Mg^{2+}$. Infact, the salts of poluronates with monovalent (alkali) metal cations are typically water-soluble (no gel formation in the absence of divalent cations). The selectivity towards these cations appears to follow the sequence $Li^+ < Na^+ < K^+$ according to Pereira et al. [205].
The model proposed by Perì-chassler [186] indicates that not only the hydration but also the presence of Cl^- anions influences the cation binding to polyuronates chain.
The cation radial distributions of the ions around the polyuronate chain in the absence of Cl^- anions (simulations with Na, K, Mg and Ca) are relatively narrow and tight. In the presence of Cl^- anions (simulations with NaCl, KCl, MgCl and CaCl), the cation distributions tend to be somewhat broader and looser while the corresponding change in the distribution of the divalent cation is much more limited.
Divalent cations form a denser and tighter counterion environment around the chain compared to monovalent cations. Upon addition of one equivalent of the chloride salt of the same ion, the counter-ion atmosphere becomes slightly more diffuse and less tight, as a result of the increased ionic strength (electrostatic screening) and the competition between the chain and the chloride ions (predominantly distributed in the bulk region far away from the chain) for interactions with the cations [186].
Another possible explanation of the observed selectivity for calcium takes into account the hydration energy and the ionic radii rather than the Pectin affinity for bivalent cations.
In this thesis, an interpretation purely qualitative and phenomenological of the processes that take place in a so complex matrix (Pectin doped with a high salts concentration in almost-dried state) is provided. I suppose that the ion-pars formation (probably contact ions pairs and solvent-separated ions pair), the different chemical-physical properties of cations and anions (diffusion coefficients, hydration enthalpy, ionic radii), the affinity of Pectin for bivalent cations, could explain the selectivity and the behavior of $CaCl_2$-doped devices compared to other doping salts (figures 41-42).
The different affinity of Pectin for each cation could influence the free-cation concentration in polymeric matrix, decreasing the formation of neutral species. The suppression of ionic conductivity reset the memristive effect.
A more comprehensive and coherent explanation of the processes occurring in OMD with Pectin requires further specific investigations and will be carried out in future studies by means of specific theoretical models and specifically devoted experiments.

Here however, we have identified some systems in which there is a synergy between a certain selectivity degree towards Ca^{2+} ion and memristivity that could guide further studies. These devices could pave the way after further developments, to a fully novel class of biosensors.

4.4.2 Role of doping agents (acetates) on memristive properties.

In order to verify the role of cations in memristive PANI switching processes, the electrochemical behavior of devices were tested in presence of different acetate salts as doping agents in the Pectin layer.

In this set of experiments, Pectin (50 mg/ml in acetic acid (2%)) was doped with different acetate salts: sodium acetate (NaOAc), lithium acetate (LiOAc), potassium acetate (K(OAc). and calcium acetate ($Ca(OAc)_2$). The PANI layer shows a good conductivity also without using HCl as doping agent in Pectin. This aspect will be discussed in depth in paragraph 4.5.1.

The gate current of acetates-doped devices (figure 43) are very low and do not show any oxidation and reduction peaks of PANI for lithium, potassium and calcium acetates. Even if the ionic radius of lithium (76 pm) is the smallest, the ionic conductivity is low also in this case and hence, the electronic current does not show any memistive feature for lithium, potassium and calcium acetates.

The V-I characteristic for the NaOAc doped device could be considered as non-linear, but also in this case the dependence of resistance upon the voltage confirms that no redox processes of PANI occur. No variations in subsequent V-I cycles were observed in any case.

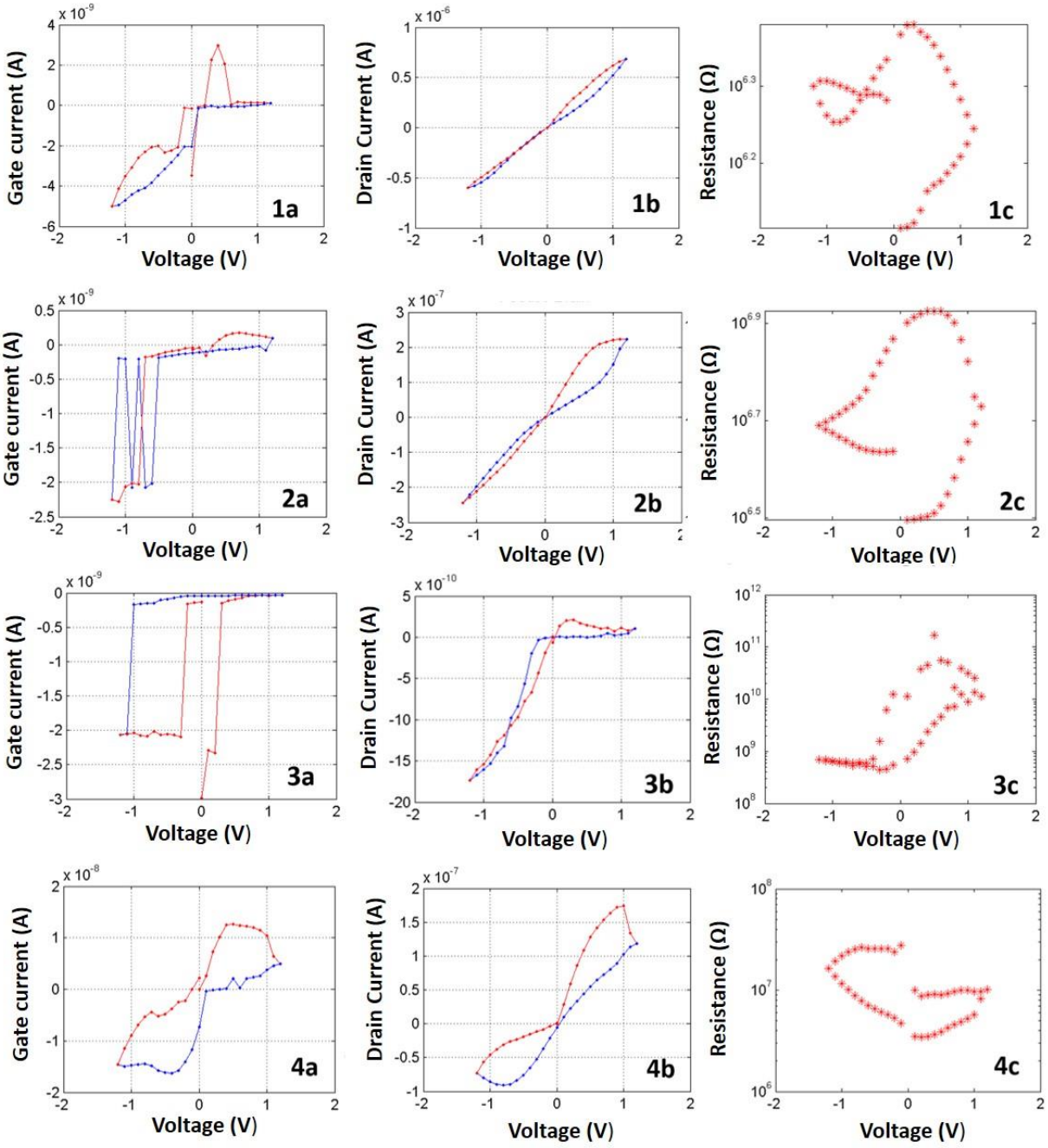

Figure 43 Cyclic V-I characteristics of the organic memristive device assembled with pectin (50 mg/mL in acetic acid (2%) doped by (1) $Ca(OAc)_2$ (0.1 M); (2) Li OAc (0.1 M); (3) KOAc (0.1 M); (4) Na OAc. The figure shows the ionic current (a), the electronic current (b) and the resistance (c) for each device. The delay time is 300s in all cases. Up scan (blue line), reverse scan (red line).

Note that the experimental data obtained in absence of HCl show that, even without HCl as doping agent in Pectin, it is possible to measure a current, even if its behaviour is very different from the trends typical of ST-OMD. This aspect will be described and discussed in detail later on (par. 4.5.1).

4.5 Multilayer architectures: identification of biocompatible interfaces.

Although polyaniline based devices have considerably progressed in recent years, the use of polyaniline in biosensors or biological integrated systems has faced serious limitations because most of enzymatic and cellular activities are strongly pH sensitive. Polyaniline on the other end becomes a very poor conductor at pH higher than 5, required for biological objects. As already stated several times, in this study a strategy to match polyaniline and biological systems in the same device is proposed by introducing an intermediate layer between polyaniline and biological object. The interface layer should be a "solid buffer" able to retain the PANI conductivity. Moreover, the interlayer should be electrochemically "inert", so that it would not interfere with the ion exchange between biological component and PANI. For these reasons it was necessary exclude all the chemical components able to induce memristive behavior in the formulation of the gel. In particular, we excluded from gel formulation chloride salts and hydrochloric acid not only to preserve the biocompatibility, but also to avoid its interference in electrochemical processes that should regard only the PANI film and the biological object. To preserve biocompatibility, strong acids were avoided and polysaccharides-based materials are preferred.

4.5.1 Comparison between the pectin and chitosan properties in polyaniline-junction.

Pectin with a high degree of methylation and Chitosan were tested as interlayer, achieving the best conditions to preserve high conductivity of polyaniline at neutral pH and to assure linear electrical characteristics of the device. The use of HCl as dopant in the formulation of solid buffer was avoided, because HCl is not suitable for the realization of bio-integrated devices: much milder conditions are needed. In addition a high concentration of Cl^- ions (40g/L in standard devices) must be avoided for two reasons. First of all, the chlorinate species are strong oxidants, and on other hand, there is the strong indication, as will be discussed in paragraph 4.7, that the Cl^- ions are the principal regulators of the memristive electrical behavior. The composition of interlayer should not contain any component able to effect the PANI electrochemistry, in order to employ these "solid buffer" as "inert" layer between PANI and the biological object.
A different behavior was observed for Chitosan and Pectin-gels in contact with PANI layer. By using chitosan-gel without a strong acid, PANI layer switched into the emeraldine base insulating form ($\geq$200 MΩ), even if the acetic acid content was increased up to 30%. In these conditions, it was impossible to acquire current-voltage characteristics. Figures 44 and 45 show the comparison for ionic and electronic currents recorded for both HCl doped and undoped samples. In the first case a standard memristive behavior was observed; in the second one the values of currents are very low (~30 nA at 1.2 V, electronic current) due to a de-doping process of polyaniline.

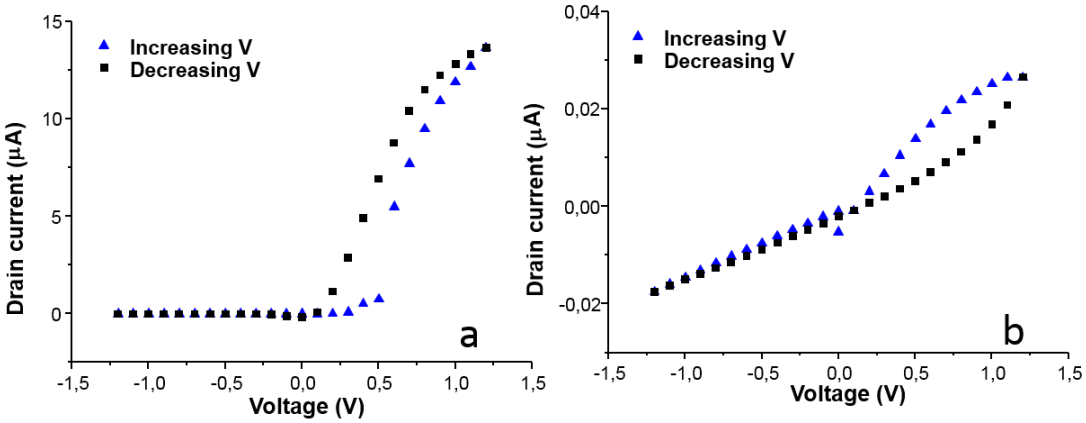

Figure 44 Trend of electronic currents recorded for the samples with chitosan solid polyelectrolyte. (a) CH_3CO_2H and HCl, (b) only CH_3CO_2H doped stripe. Time delay is 180 s.

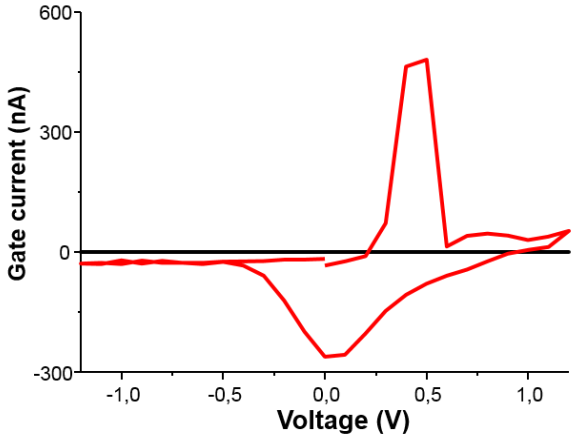

Figure 45 Trend of ionic currents recorded for the samples with chitosan solid polyelectrolyte. (Red line) CH_3CO_2H and HCl, (black line) only CH_3CO_2H doped stripe. Time delay is 180 s.

On the contrary, the Pectin-based gel with acetic acid 2% w/w when combined with PANI did not induce a de-doping of the polymer, in spite of being a water-based gel, but rather decreased its resistance (≤50 kΩ).

The spectroscopic studies of the pectin-PANI junction was carried out in order to confirm the observation described above. The conductivity switching in PANI are due to doping/de-doping processes, and to the subsequent change in the quinoid-benzenoid ratio of the aromatic rings. Such effects can lead to characteristic changes in the optical spectra of the material [206]. The comparison between PANI (emeraldine base, EB) film and HCl-doped PANI (emeraldine salt, ES) film, and pectin-PANI solid junction is reported in figure 46.

These data were obtained for a 60 layer LS film of PANI deposited on a quartz plate. The UV-visible spectra of non-conductive form of PANI (figure46a) and conductive form of PANI (figure 46b) are reported. The experimental data are in agreement to pervious literature [81].

The pectin-PANI junction is formed putting in physical contact PANI-ES film (60 LS-layers) with pectin gel (prepared in acetic acid 2 % w/w, see par. 3.3.1), and then drying it in air. Pectin is transparent in the visible part of the spectrum.

The spectra of the pectin-PANI junction and the PANI-ES film confirms that PANI is in conductive state. (figure 46c) The formation of pectin-PANI junction does not produce a conductivity transitions in PANI. The acetic acid in pectin is enough to avoid the de-doping process of PANI kept in contact with an aqueous medium. The spectra of the pectin-PANI junction and the PANI-ES film show the

same absorption bands: at ~310, 420 and 830 nm for the p– p* transition of the benzenoid rings, the polaron band to p* band transition and the p band to polaron band transitions, respectively [207].
Note that a red-shift of the polaron band (p* band transition) occurs in pectin-PANI junction spectrum (425 ± 5 nm) compared with PANI-ES spectrum (395 ± 6 nm). The origin of aforementioned shift in the junction will be detailed in subsequent studies; reasonably some modifications occur at the interface, which slightly changes the spectroscopic characteristic of PANI in the junction.
In both the spectra the absorption related to transitions in the quinoid rings is suppressed, because the doping of PANI-EB with acids converted it into poly(semiquinone) cation radicals (salt form). The spectrum of PANI-EB is shown as a control. In the EB spectrum (figure 46a), one band was observed at 600 nm (n-π* transition).

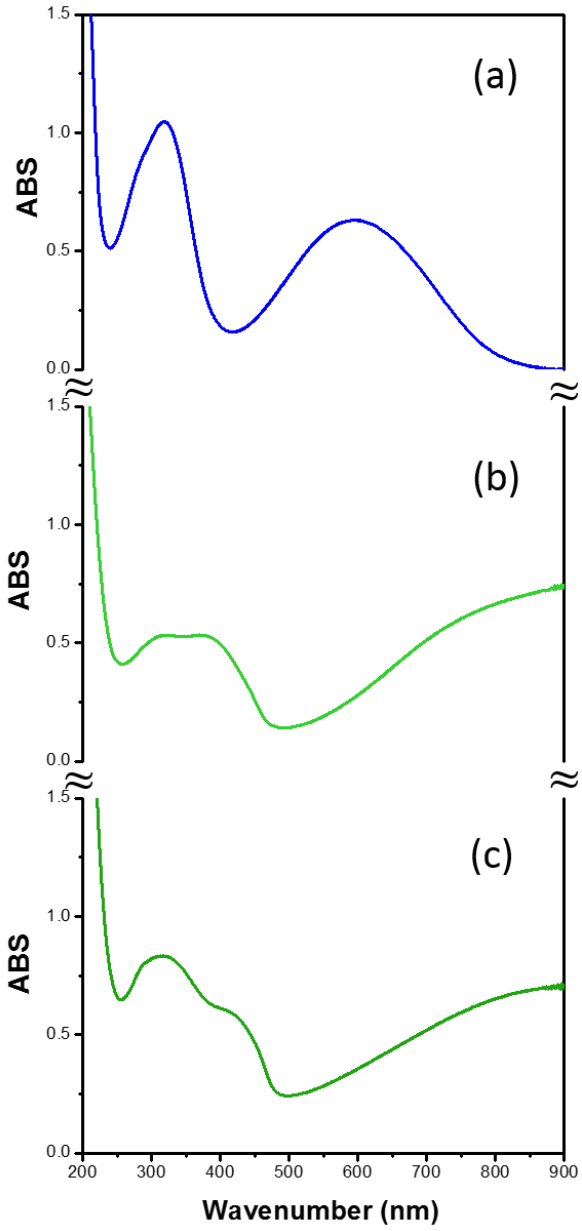

Figure 46 UV-visible spectra of PANI-EB (a) and PANI-ES (b) film; pectin-PANI junction (b). Conducting PANI films (20-100 kΩ) (green lines), non-conducting PANI films (1 MΩ) (blue line).

The cyclic voltage-current characteristic (figure 47) of the HCl-free device with pectin shows a very similar current value to HCl-doped devices (figures 37-40): in both cases, current-voltage

characteristics were detectable, with currents of the order of μA; even if the current trends measured with and without HCl are different: in the first case is asymmetric and memresistive, in the second one is resistive.
Cyclic voltage-current characteristics of devices with a solid polyelectrolyte stripe made of pectin-gel without addition of HCl) were recorded for several delay times in the range from 3s to 360s. The different delay times do not influence the V-I characteristic. One example (for 60 s of delay time) is shown in figure 47.
I provide a qualitative explanation of the different behaviors observed for chitosan- and pectin-gel. The acetic acid concentration (2% w/w) used for chitosan solubilization and gelification should give a pH value (2.4) capable to preserve, in theory, PANI in conductive state. In our experimental conditions, chitosan (pKa 6.3) formed quaternary nitrogen salts becoming a water-soluble cationic polyelectrolyte [208] whose counter ion, being involved in the charge balance, is the anion acetate. The protonation of amino groups of chitosan shifted the acetic acid dissociation equilibrium towards the anion acetate formation. The H^+ concentration, mainly involved in chitosan protonation ,was not sufficient to preserve PANI in the conductive state owing to basic hydrolysis of the acetate ion.
Several experiments proved that even high acetic acid concentration (up to 30% w/w) was not able to preserve the PANI conductivity.
Concentrations of acetic acid higher than 30% w/w were not considered, because they induced over-oxidation of PANI and chitosan depolymerization, as the gel softening showed, according to literature [142, 209]. Thus, we can conclude that chitosan-gel, although it has a good biocompatibility, is not able to preserve the PANI conductivity without adding a strong acid. The pectin-based gel, instead, was prepared using pectin with high degree of methylation (>74.0% HM-PEC), in which hydrogen bonds and hydrophobic interactions are the main factors that induce gelification, rather than pH value or ionic strength [210,162,170]. In any case, as the pH is lowered, ionization of few carboxylate groups in the PEC HM structure is suppressed, this favors the gelification process [163]. In HM-PEC, the acetic acid is slightly involved in protonation process of carboxylate groups and does not participate significantly in gelification of the polysaccharide. Therefore, the concentration of available H + ions was sufficient to preserve the PANI conductive state.

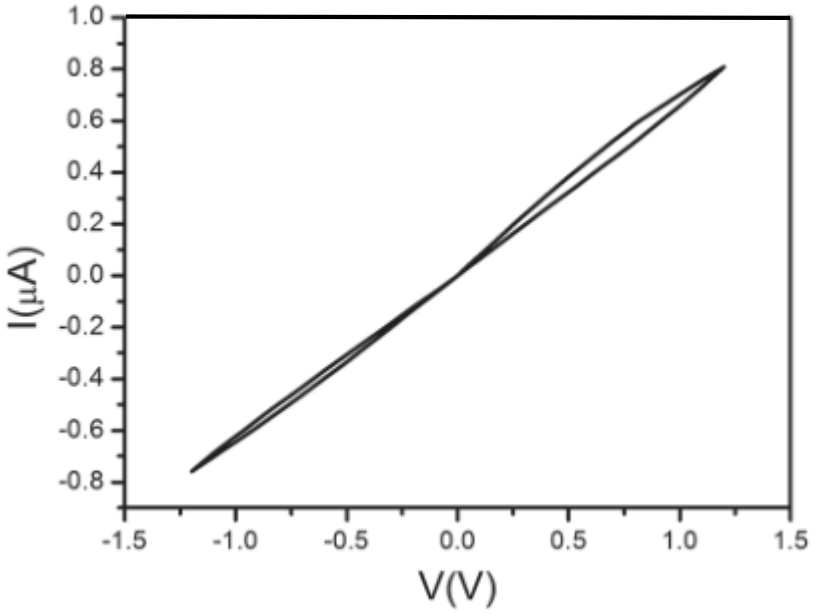

Figure 47 Cyclic voltage-current characteristic (electronic current) of device with solid polyelectrolyte stripe made of pectin-gel without addition of HCl.

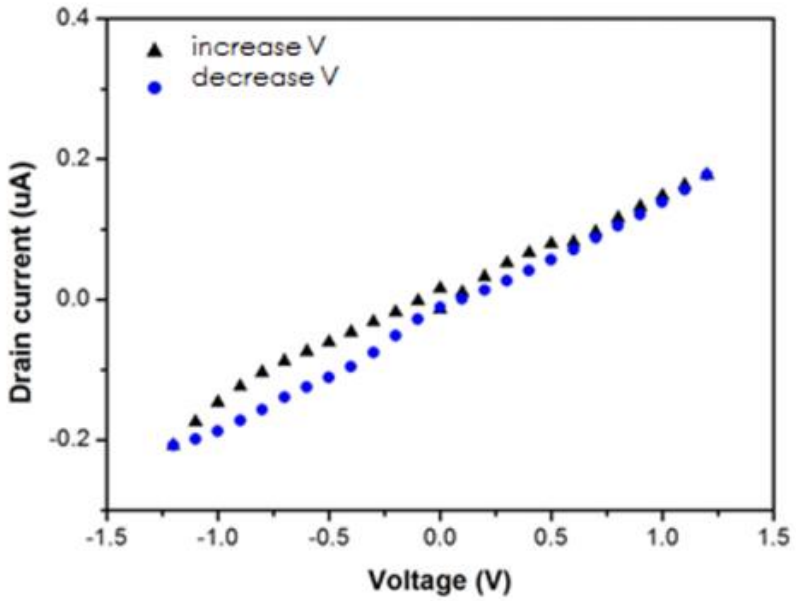

Figure 48 Cyclic voltage current characteristics measured for devices containing a layer of pectine (0.25% p/p) and succhrose (0.65% p/p) in acetic acid solution.

In addition, the different behavior of pectin- and chitosan-gels in contact with PANI layers could be explained on the basis of water uptake by their three-dimensional polymeric networks, which can be a possible cause of PANI de-doping.
The electrical properties of pectin- and chitosan-gels in contact with polyaniline were investigated. Only pectin, used at high degree of methylation, without strong acids and doped only by acetic acid (2% max), resulted suitable for the purpose. A qualitative explanation for the different behaviors of the two polyelectrolytes was suggested.

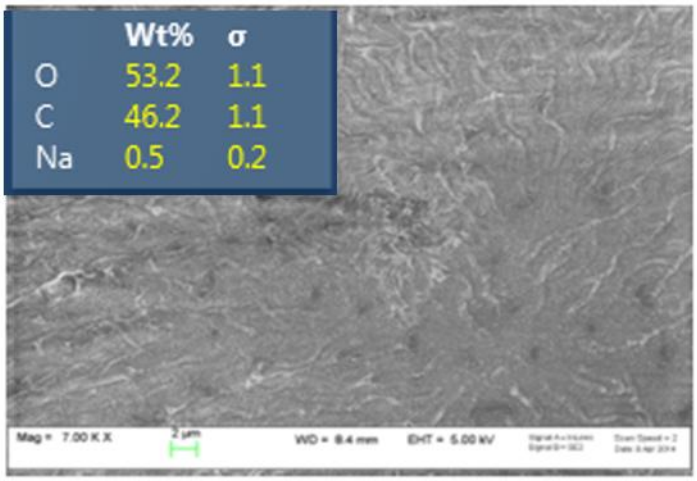

Figure 49 Morphology of pectin cast film.

I would like to underline that, even if the EDX analysis showed (figure 49) that some ions are present in commercial pectin (from apple, see par-3.3), they are not enough to support the ion conductivity in the device, and to operate, as consequence, the polyaniline switching.

4.6 Study of parameters affecting the memristive behaviour of ST-OMD.

In a previous section (par. 4.1) it is demonstrated that OMD with chitosan does not differ from a ST-OMD, although in this case the addition of a lithium salt into the organic polyelectrolyte was not done. Metal ions in chitosan casting films are not detectable by means of EDX analysis. Thus, the experimental data could indicate that the lithium salts are not necessary as doping agents in OMD. The second step was to check the operation of OMD with chitosan, when HCl was not introduced into the gel. It was found that it was impossible to register I-V characteristics of the device because PANI in the active zone became non-conductive due to dedoping effects. This transition of PANI to the insulating state is much slower with respect to the case of PEO, but, nevertheless, it takes place and the measuring of current-voltage characteristics is not possible due to the rupture of the conductive circuit. The addition of acetic acid up to its maximum concentration did not overcome the problem of dedoping of PANI.
Thus, the substitution of the PEO solid polyelectrolyte by a bio- polyelectrolyte chitosan in OMD is possible and memristor has good I-V characteristics, but only in the case when 0.1M HCl is present in the composition of the gel stripe. The introduction of Li^+ ions does not lead to any change in the behavior of the I-V characteristics. It turns out that the availability (presence) of HCl is necessary to have a memristivity of the device, while the presence or absence of metallic cations is not so important.

In addition, also the study of OMD with Pectin (par. 4.3 and 4.4.) opened many questions.
The experimental data confirm that the hydrochloric acid and chloride salts (differently from acetates) have a key role in PANI electrochemistry, not only for chemical doping (see chapter 3), but also in the redox processes that involve PANI. Note that in absence of HCl the electrical characteristics of devices with pectin is linear (Ohmic), even if the PANI film is in a conductive state.

This moment seemed to us worthy of attention and additional control studies have been carried out.
In this section, ST-OMD with PEO was characterized from the electrical point of view, changing the same parameters (material electrodes, delay times, doping agents) studied for OMD with pectin and chitosan.

4.6.1 Study of effect of electrode materials on memristive behavior of ST-OMD.

To understand the effect of the electrode material on the memristive device, we studied different combinations of source, drain and gate electrodes in standard organic devices.

The devices characterized in par. 4.2.1 were fabricated using doped-PEO as solid polyelectrolyte and $LiClO_4$ and HCl as doping agents. When platinum (Pt(0)) is used as source, drain and gate electrodes no memristive behavior is observed in V-I characteristic. The dependence of resistance as a function of the applied voltage for the device with all platinum electrodes confirms that electrochemical switching of PANI does not occur. There is not any variation due to the PANI transition into the conducting state (figure 50).

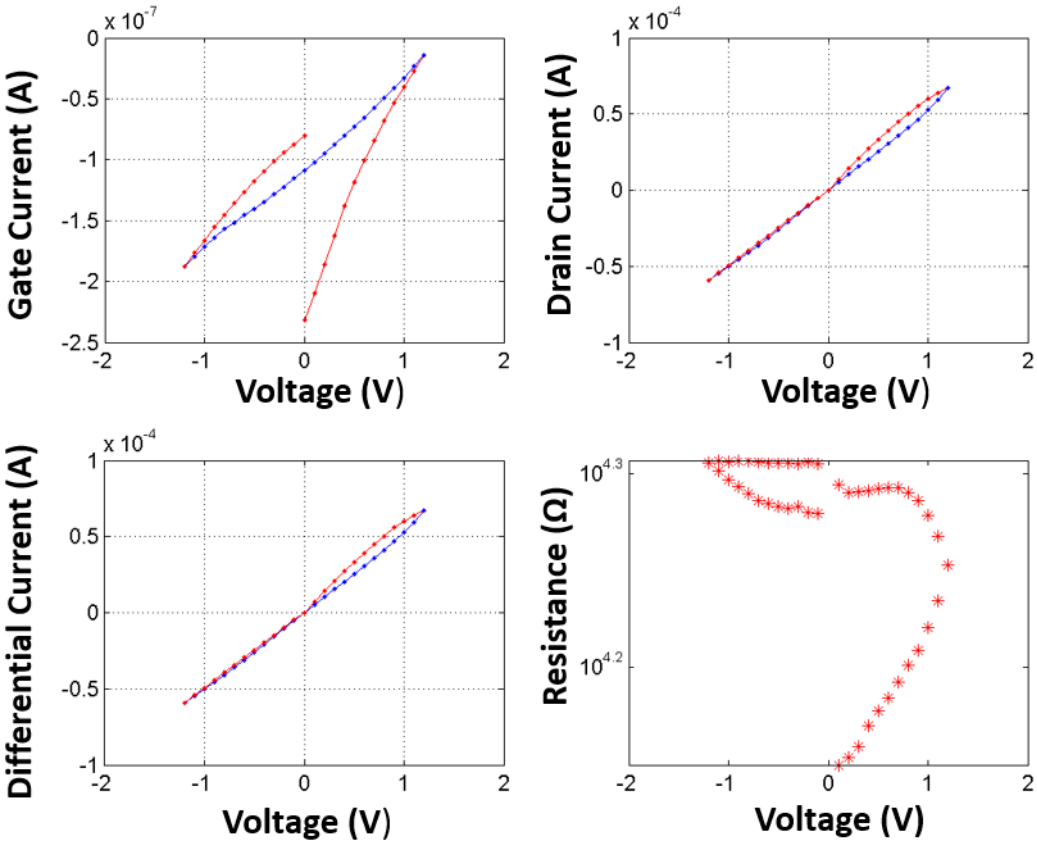

Figure 50 Cyclic V-I characteristics for the device with platinum S, D and G electrodes. PEO stripe, delay time is 60s. Direct sweep (red line); reverse sweep (blue line).

Differently from previous experiment, the memristive behavior is observed in V-I characteristic when platinum (Pt(0)) is used as source and drain electrodes and a silver (Ag(0)) wire as gate electrode. The drain and differential current shows a hysteresis loop at positive voltage and a rectifying behavior at negative voltage as in standard device (see figure 4, par. 4.1). The ionic current shows a couple of peaks due to oxidation and reduction of the PANI film. Finally, the resistance varies of about four orders of magnitude due to the PANI transition into the conducting state (figure 51).

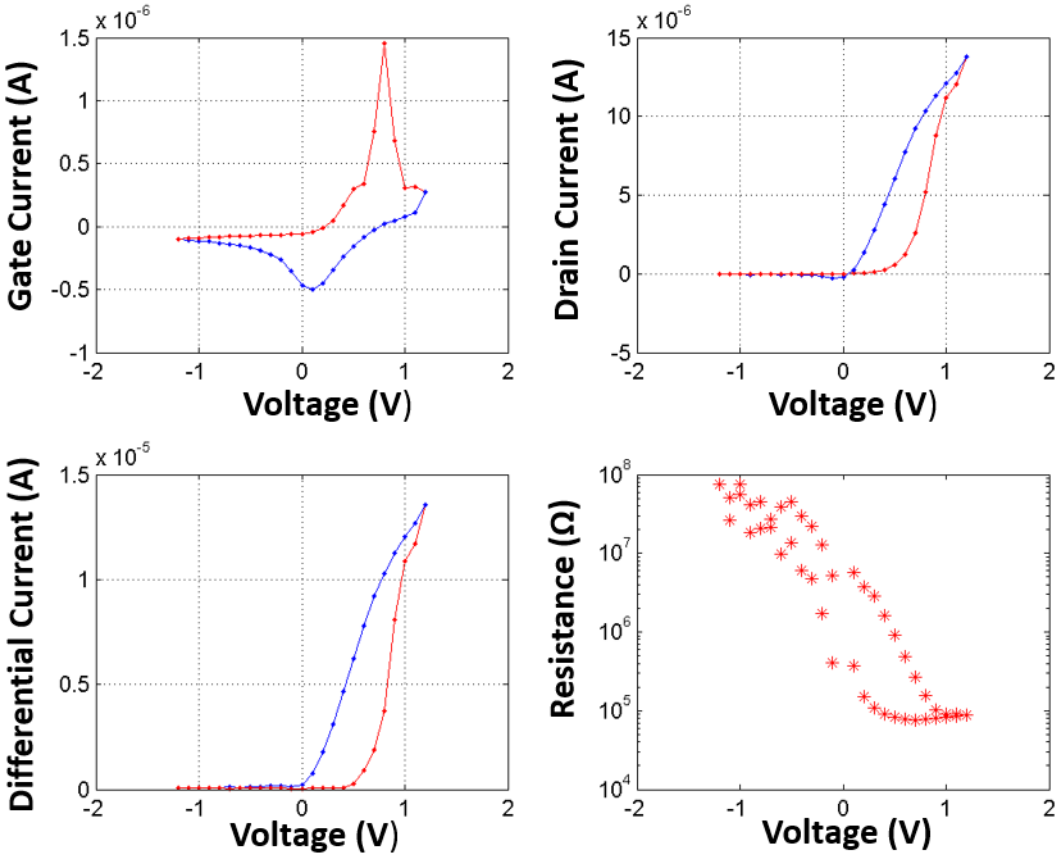

Figure 51 Cyclic V-I characteristics for the device with platinum (S and D) and silver (wire Ø50 µ) (G) electrodes. PEO stripe, delay time is 60s.

The experimental data shown in figure provide a strong indication that Ag wire used as gate electrode has a key role in the electrochemical mechanism at the basis of the memristive behavior.

The experimental data show that both platinum and chromium could be indifferently used as source and drain electrode while the material for the gate electrode has a great influence on memristive behavior. Results indicate that only silver can be used as gate electrodes in organic memristive element. Memristive behavior was not observed with platinum gate electrode, also in presence of hydrochloric acid.
The memristive behavior and the rectification of current in negative voltage branch were observed without any lithium salts in chitosan polyelectrolyte. Just hydrochloric acid and the acetic acid were added in gel formulation. There is a strong indication that lithium ions are not the key components in the mechanism of PANI switching in organic memristive elements.

4.6.2 Investigation of the effect of hydrochloric acid and lithium salts on the behavior of ST-OMD.

In this section is report the comparison between electrical behavior of devices in which $LiClO_4$ is used as doping agent (this is a standard device, see par. 2.3) and analog device in which $LiClO_4$ is missing in gel formulation; the hydrochloric acid HCl was added in both samples. The material electrodes is the same of a standard device (par. 2.3)

Both the voltage-current characteristics exhibit a pronounced rectifying behavior in the negative voltage branch and significant hysteresis of the conductivity in the positive voltage branch. The ionic current of both devices (doped and undoped by $LiClO_4$) show a couple of peaks due to redox processes in PANI. Figure 53b shows the dependence of resistance as a function of the applied voltage for salts-undoped sample (the HCl was added in any case). A variation of about four orders of magnitude due to the PANI transition from insulating into conducting state and vice versa.

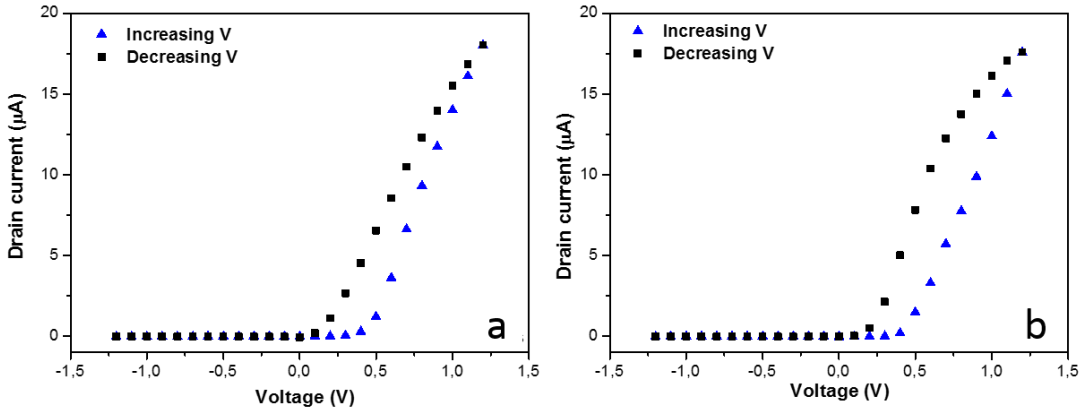

Figure 52 (a) Cyclic V-I characteristics for the drain current of the organic memristive device assembled with PEO doped by $LiClO_4$ and HCl (a) and only HCl (b). Time delay is 60 s.

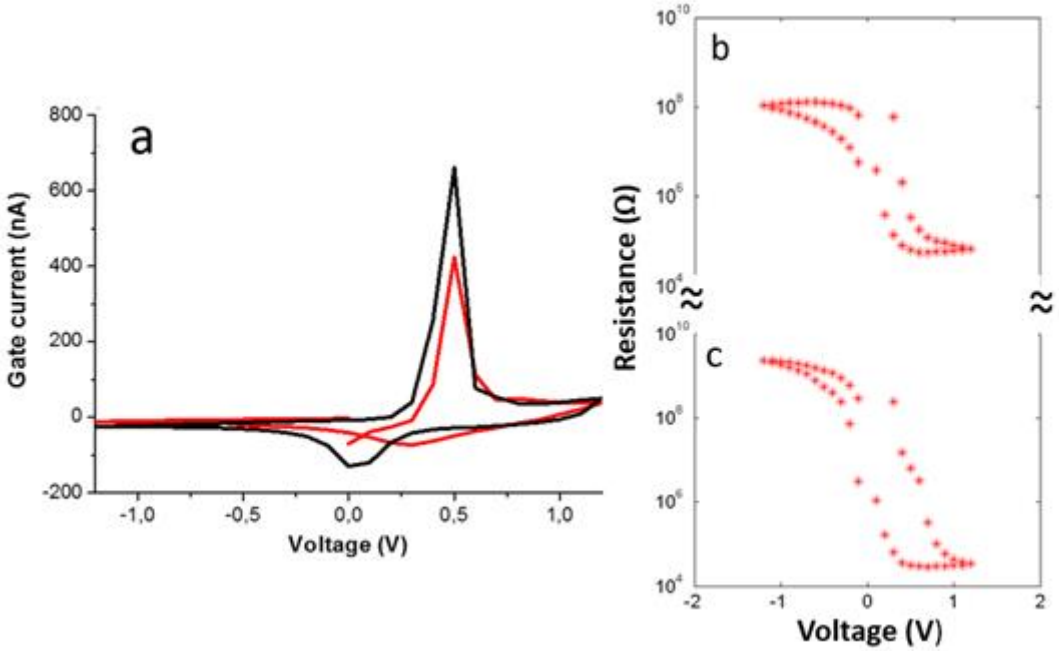

Figure 53. (a) Comparison between cyclic V-I characteristics for the ionic current of the organic memristive device assembled with PEO doped by $LiClO_4$ and HCl (black line) and only HCl (red line). The dependence of resistance for the memristor assembled with (b) HCl-doped PEO without salts addition; (c) PEO doped by $LiClO_4$ and HCl.

The experimental data prove that the elimination of lithium salt in PEO-gel formulation does not change significantly the memristive behavior. The hysteresis loops are not significantly different between them; and both curves show a suppression of current in negative sweep potential. The PANI

oxidation potential is observed at 0.3V for lithium salts free sample and at 0.5 V in memristor with both HCl and $LiClO_4$ as doping agents.
There is hence a strong indication that lithium ions are not the key components in the mechanism of PANI switching in organic memristive elements.

4.6.3 Kinetic study of ST-OMD.

As previously mentioned, the ionic conductivity ions in polymeric matrices tightly depends from different chemical-physical parameters of the ions involved (charge, ionic radius, hydration enthalpy). The rate of ion diffusion, in a polymeric matrix in a quasi-dried state, affects the electrochemical switching of PANI. Thus, the current trends would be depending upon the time delay between the voltage application and the readout of the current value.
There is a strong indication by previous studies that the alkali ions are the most mobile species in dried polyelectrolytes solid complex (PEC). Also in chloride-rich PEC, where Cl- ions should be the majority extrinsic charge carriers, residual alkali ions indeed provide the major contribution to the overall conductivity due to their much higher mobility.
Previous studies refer to the mobility of the ions along the chain of the polymer and not in the spaces inter-chains spaces, where the residual water (not bounded) controls the ion conduction. In addition, these models, for example, exclude the long-range transport and the conductivity due to anion-rich regions in a phase separated polymer-rich PEC.
In addition, the studies reported in previous literature describe processes that occur on a time scale very different from ours.
In this thesis, the kinetic study on ST-OMD in order to prove that exists a "limit-value" of delay-times to below which, it is no possible to have memristive behavior. In other words, the kinetic study on ST-OMD should prove that also for standard devices the ion diffusion occurs on a time scale compatible with anion migration with large size (such as Cl-ions) as suggested by experimental results reported above.
Electrical measurements of cyclic voltage-current (V-I) characteristics for standard organic element (see par 2. 3) (memristors with LiClO4 doped-PEO) were performed as described in paragraph 3.3.2, and different experiments have been carried out. At each voltage step, the delay of 5, 10, 20, 60 and 180 s was used to equilibrate the transient processes in the devices in each test.
Cyclic V-I characteristics for the delay time of 5, 20, 60 and 180 s are shown in figures 54, 55, 56, 57 respectively. Figures 54-57 (a) represent the dependences for the electronic current, while figures 54-57 (b) represent show the dependences for the ionic current. The electronic current is the difference between the total current of the device, measured in the drain circuit, and its ionic component, measured in the gate circuit.
The organic memristive devices reveal a variation of the hysteresis loop upon the frequency of the applied bias voltage due to not irreversibility of the redox process, not close enough to thermodynamic equilibrium. The on/off ratio of the conductivity increases to 700 times for the variation of time delay from 5 to 180 seconds.
It is interesting to compare the evolution of the cyclic V-I characteristics with the increase of the time of the delay. When the latter value is relatively small, we have observe a rather small difference in the conductivity for the positive and negative branches of the characteristics (figures 54). In this case The time delay was not enough neither for the completing on of the transition into the conducting state, nor for the transition to the reduced insulating state. For such small time delays, we can not observe both the important characteristics of the organic memristive device: the presence of a hysteresis and the rectifying behavior.
The cyclic V-I characteristics for the delay of 20 s is shown in figure 55. It demonstrates a very interesting behavior for the electronic conductivity. In the decreasing branch of the applied positive voltage, we can observe a feature, similar to negative differential resistance – the increase of the

conductivity for the decreasing of the applied bias voltage. Such behavior can be explained in the following way. The transformation of the PANI from the insulating to the conducting state occurs when the active zone is at a potential, higher than the oxidizing one. In addition, it demands requires some time for transferring change of the whole active area into the oxidized state. As the delay time was rather small also in this case, the transformation of PANI in the active zone is not yet completed when the maximum positive voltage was reached. Thus, the process is still continued proceeds even during the first part of the decreasing branch of the applied voltage. Thus, the maximum conductivity of the memristive device is registered at the applied voltage of about +0.7 V in the branch of the reduction of the applied voltage.

The cyclic V-I characteristics for the delay time of 60 s is shown in Figure 56. It appears that, this characteristic is different from both the previously reported ones: this time delay is practically enough for finishing completing the processes of oxidation and reduction of PANI in the active zone. Therefore, it exhibits a pronounced rectifying behavior and significant hysteresis of the conductivity in the positive voltage branch.

The cyclic V-I characteristics for the delay time of 180 s is shown in Figure 57. As it is possible to see it exhibits a pronounced rectifying behavior and hysteresis loop greater than for the 60 s of delay time in the positive voltage branch. A delay of 180s is enough hence long enough for fully finishing the processes of oxidation and reduction of PANI in the active zone. Indeed the current value reaches a plateau, which indicates that the conductivity of the PANI layer can not increase anymore for the oxidation reaction. This plateau condition should be avoided for a long time in order to avoid over-oxidation phenomena of the polymer.

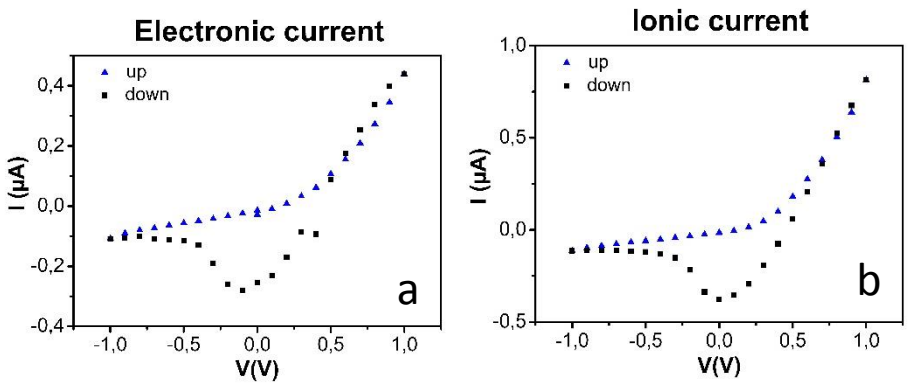

Figure 54 Cyclic V-I characteristics of the organic memristive device for the electronic (a) and ionic (b) currents. Time delay is 5 s.

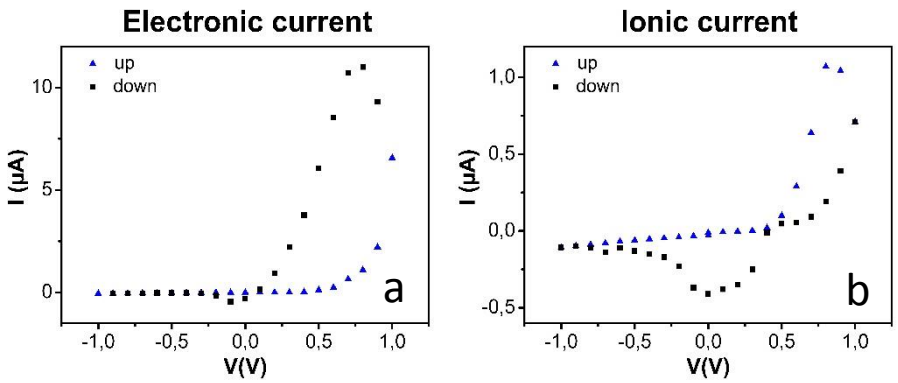

Figure 55 Cyclic V-I characteristics of the organic memristive device for the electronic (a) and ionic (b) currents. Time delay is 20 s.

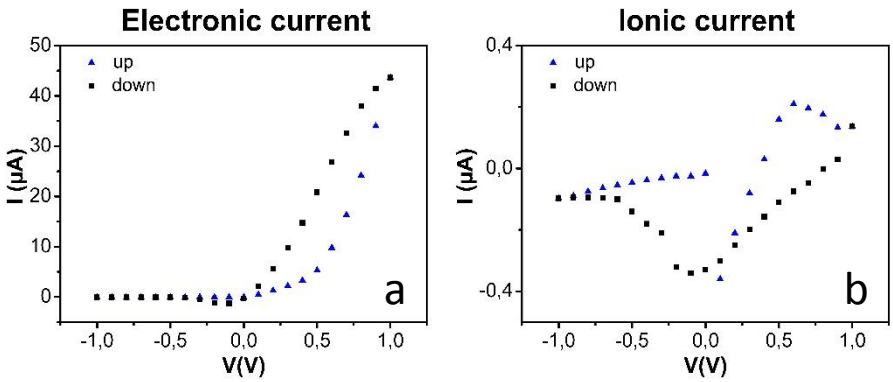

Figure 56 Cyclic V-I characteristics of the organic memristive device for the electronic (a) and ionic (b) currents. Time delay is 60 s.

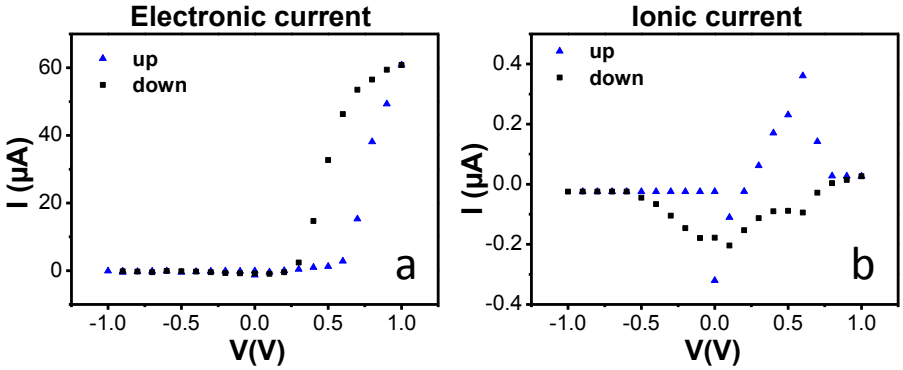

Figure 57 Cyclic V-I characteristics of the organic memristive device for the electronic (a) and ionic (b) currents. Time delay is 180s.

Summarizing, organic memristive devices have demonstrated a strong dependence of the hysteresis loop upon the time delay between the voltage application and the readout of the current value. For small delays, the element behaves as a usual resistor with practically linear characteristics that is due to rather slow processes, connected to ions diffusion, a rather high value of capacitance. This behaviour was due to redox processes not completed in the active zone. Slowing down the measurements results in the deviation of the curve from linearity (figure 55) and finally reaching the curve form with hysteresis loop, typical of memristive devices. We showed that the delay time of about 60s was enough for completing these processes (figure56).

Note that the kinetics of processes in organic devices are very slow. Cyclic V-I characteristics were usually recorded for organic memristive devices with long delay times, for each voltage step, in the range between 60s and 300s.
As proved by kinetic studies, for small delays, the element behaves as a usual resistor with practically linear characteristics that is due to rather slow processes, connected to ions diffusion. This result was confirmed by Gorshkov and Berzina (2011) [211]. The migration kinetic of the large size of the Cl- ions is compatible with the kinetic slow transitions that occur in our devices.
A preliminary supposition is that the Cl^- ions penetrate the polymeric matrix on application of a doping potential; even if , the rate to drifting Cl^- ions is slower than that of cations, as reported in PEDOT:PSS films [212]. More detailed and specific studies are required to confirm such a hypothesis.

It is now worth summarizing the major indications coming out from our experiments as discussed in paragraph 4.6 and that would require further studies to be fully understood:

-Ag wire used as gate electrode has a key role in the electrochemical mechanism at the basis of the memristive behavior;
- The memristive response and the current rectification in the negative voltage branch were observed without any lithium salts in chitosan polyelectrolyte
- The elimination of lithium salt in PEO-gel formulation does not change significantly the memristive behavior.
- Hydrochloric acid has a key role in PANI electrochemistry, not only for chemical doping (see chapter 3.3.1), but also in the redox processes that involve PANI: lithium ions appears not to be a key components in the mechanism of PANI switching in organic memristive elements.
-Cations have a marginal role in memristive switching of PANI in bio-based devices
-Pectin and chitosan (see par 4.1,4.3) in comparison to PEO show a slower kinetics for ion conduction processes in standard device.
These experimental results will be further discussed in paragraph 4.7.

4.7 Preliminary hypothesis on the electrochemical model of a polyaniline based organic memristive device.

In general, an OMD is an electrochemical cell with two electrodes, where a layer of polyaniline is the first electrode and a silver wire (figure 28) is another one. The solid-polyelectrolyte stripe is the supporting electrolyte. During the passage of ionic current through the cell PANI (depending on the applied bias) can act as an anode providing the oxidation reactions and, therefore, reinforcing the electronic conductivity (which is measured along the PANI channel, between electrodes D and S or as a cathode with reduction reactions on it.
The electrochemical model which is able to explain the device operation and its memristive properties should take into account all electrochemically active species such as ions, molecules, polymeric film and dissolved gases (Ag (0), the ions Ag^+ Cl^- and H+ and finally the PANI LS film).

4.7.1 Phenomena that occur at ground state potential in quasi-wet state

First, I describe the assembled system (figure 28) without the application of any potential difference. For the assembling of devices the Ag wire was chosen as "gate" electrode.

It is therefore reasonable to assume, that the chemical corrosion of silver and, consequently, the Ag dissolution (as Ag+) occurs in acid environment without that any potential difference is applied because the Ag wire is fully immersed in an aggressive electrolyte. The dissolution of metallic silver by direct chemical attack (etching), probably, with hydrogen evolution (H_2, gas) is due to formation of Ag complex or salts and the high protons (H^+) concentration. Furthermore, the chlorides are very aggressive and corrosive agents.
The oxidation of silver in chloride containing solution resulting in the formation of AgCl has been reported in a number of studies [213]. The reaction can be expressed as:

$$AgCl\ (s)^+ + e^- \rightarrow Ag(s) + Cl^-(aq) \qquad E^0\,(Ag+/Ag) = +0.222\ V \quad (3)$$

The Ag dissolution should be driven by silver chloride (AgCl) precipitation and by metal complexes in solution, that are probably the driving force of the process.
Precursor monolayer of AgCl was reported to be formed at potentials below the thermodynamic Ag/AgCl reversible potential [214-216]. The formation of the monolayer AgCl follows an adsorption-desorption mechanism. Ag wire is a sacrificial electrode as well as counter electrode. The net effect of reactions in acid solution is to consume H^+. They are able to establish a very small pH-gradient

with a high localized pH adjacent to the electrode surface, as shown in figure x1. The interesting and useful behavior of Ag/AgCl electrode is partly attributed to the high reversibility of Ag/Ag+ system in chloride environments [217-218].
The formation of silver oxide (Ag_2O) is not considered, because it is not thermodynamically favored reaction in acid medium.

4.7.2 Comparison between different electrode materials.

In all processes where hydrogen is involved, the hydrogen overvoltage should be taken into account: a higher value of voltage is required to develop hydrogen than the theoretical value which is based on the series of normal potential. This phenomenon occurs because there is a certain difficulty to win the "deconcentration" of H^+ ions which are discharged at the electrode, in other words, the electrodes are freed from hydrogen that is developed with a certain difficulty. Less noble metals than hydrogen, such as Sn, Zn, Pb, having very high hydrogen overvoltage values, in an acidic medium go into solution very slowly.
The hydrogen overvoltage of silver Ag^0, compared to other metals as Sn, Zn, Pb, is not high: its value is 0.47V at 25°C in 2N sulfuric acid solution [219].
In literature there are numerous studies describing phenomena of corrosion of different metals, e.g. tin Sn0, by direct chemical attack by acid solutions with the evolution of gaseous hydrogen (H_2), as well as without hydrogen evolution [220,221]. In conclusion, the studies concerning the corrosion and dissolution phenomena of metals are today quite controversial.
The devices with platinum (Pt) gate electrode do not exhibit memristive behavior, even if Pt has a lower hydrogen overvoltage than Ag, 0.024V and 0.47V at 25°C in 2N sulfuric acid respectively [219]. On the other end, Pt has a more positive potential in the series of normal potentials, E^0_{Pt} = +1.190V (Pt/Pt^{++}) compared to silver normal potential E^0_{Ag} = +0.222 V (Ag+/Ag). On the basis of these arguments a quite preliminary conclusion could be made, that even if Pt has a lower hydrogen overvoltage than Ag, and HCl concentration is high enough in the system (pH= 0-1), the presence of silver electrode is necessary to observe memristive I-V characteristic. Thus, not only HCl, but also Ag^0, Ag^+ and AgCl play a key role in the switching mechanism of PANI in memristive device. These conclusions are only very preliminary and require further experimental experiments to be validated because at this stage other possible mechanisms cannot be excluded. This is true also for the whole following discussion that represent a preliminary and somewhat tentative interpretation of the experimental evidences that I have found in my thorough experimental work. This is a contribution for future work more than an established understanding of the mechanisms involved.

4.7.3 Ionic conduction in solid polyelectrolytes.

Even if, the Ag oxidation is not thermodynamically favored because the standard reduction potential (E^0) is positive, the AgCl coating can be formed by an "HCl bath". At first, we do not apply any potential to the device, but strong acidic conditions are necessary to provide a high concentration of protons (from inorganic and/or organic acids) that are responsible for the conductivity of PANI layer. In other words, the formation of an Ag/AgCl electrode occurs immediately in situ simply by the contact of silver wire with PEO-gel containing hydrochloric acid in the concentration of 1M. As a result, an electrochemical system is realized and can be considered as pseudo reference electrode. We have an Ag/AgCl electrode in which the filling solution is substituted with a solid-state exchange support doped with chloride ions (Cl^- from HCl) required for the electrode equilibrium. In particular, as solid polyelectrolytes we use polyethyleneoxide or chitosan, or pectin gels saturated with HCl.
Typically, solid-state support limits or eliminates convective mixing-induced drifts, so this can be considered as a new approach to the creation of solid-state microfabricated reference electrodes [222].

In “a solid state electrochemical cell” developed in this thesis, the solid polyelectrolyte is considered in a simplified form as an inert medium, in analogy with other application such as fuel cells [132]. A more detailed approach to study of transport properties in solid polyelectrolytes will be described in the Appendix.

4.7.4 Phenomena occurring under polarization of the solid polyelectrolyte in the active zone of the memristor.

We discuss here the electrochemical reactions that involve the PANI layer in the active zone, as result of the applied voltage. The triangular waveform of voltage shown in figure 58 was applied to the working electrode (the PANI film).
The discussed experimental I-V curves (chapter 4) show redox activity of PANI as indicated by the electronic current increasing at positive potential due to oxidation of emeraldine salt of PANI.
According to the previous studies where Ag/AgCl reference electrode (G) has been used, we observe a redox current associated with the conversion of partially oxidized emeraldine to the fully oxidized pernigraniline form occurring between 0.6 V and 0.8 V vs. Ag/AgCl. In other words, the quinonoid/benzenoid ratio variation takes place in some parts of the polymer chain during oxidation. The reactions shown in figure 59 were proposed by Focke et al. [209, 89]. During the reverse potential sweep, the reduction of fully oxidized pernigraniline form into emeraldine form takes place. Moreover, the conversion between emeraldine and the fully reduced leucoemeraldine base form follows between 0 V and +0.25 V.

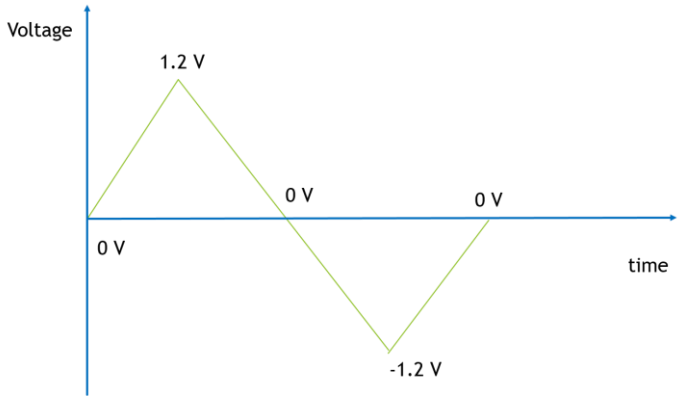

Figure 58 The waveform of voltage applied to the working electrode (the PANI film).

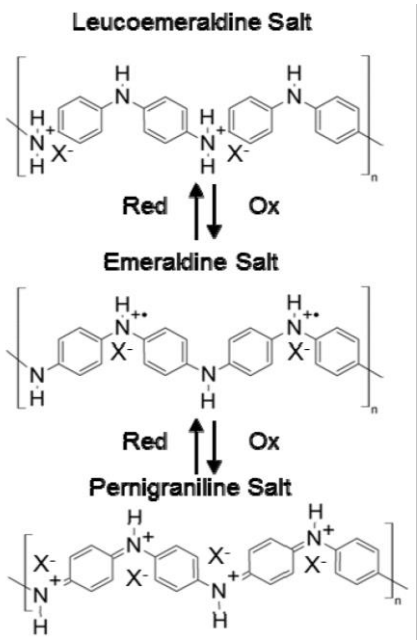

Figure 59 Redox processes in PANI.

Often the reactions (transitions) shown in the figure 59 are presented by other authors in a way different from the latter, because the proton tautomerism, proposed by Focke et al. [209], is not considered.

It is well known that relative basicities are strongly affected by solvation. Therefore, it is reasonable to assume that the relative basicities of amine and imine nitrogens may differ in the dry and wet states. The creation of defects due to proton tautomerism is proposed as shown in the figure 60. The positive charges remain in the same positions, but the proton migration occurs and a closed shell structure is formed in the dry state. By Focke et al. it is proposed as a possible defect structure, present in low concentrations, but not as the predominant form in the dry state [209].

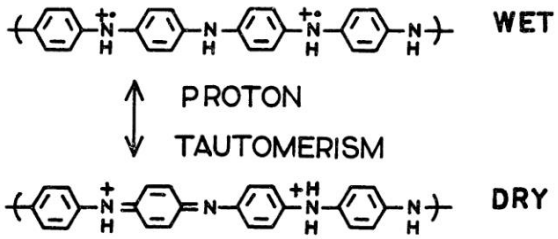

Figure 60 Defects induced by proton tautomerism in the dry state. This scheme is based on the assumption that the difference in basicity between amine and imine nitrogens is small in the dry state.

Generally, in previous studies the electrochemical processes described above are experimentally identified by the two pairs of anodic and cathodic current peaks between 0 and 0.25 V and 0.6 and 0.8 V vs. Ag/AgCl. The same behavior is observed in our I-V characteristics (figures 37,40). In other cases, for example replicating the potential cycles for the same devices, only one pair of redox peaks is recorded (figure 39).

The study that is discussed in this thesis differs in many aspects from the previous cyclic voltammetry studies of polyaniline. Usually redox mechanisms of polyaniline and other electroconductive polymers are established based on the thermodynamics of redox processes in homogeneous solutions**,** such as buffer solution and using fast scanning speed. Instead, our devices are more complex systems in solid state, which are usually characterized using a very slow scanning speed (at least 100 times

slower than in conventional electrochemical studies) from 60 sec to 300 sec for each potential step. Besides, the electrochemical behavior of polyaniline is dependent on many other parameters including the values of the applied potential, the choice of material and the surface area of the electrodes, composition of the electrolyte medium, temperature, etc. [86-109].

Some particular features of our I-V cycles can be easily explained. For example, the two pairs of redox peaks in the ionic current may not be well resolved, due to the scanning speed, the balance of protons exchanged, and the rearrangement of the polymeric chain. All these chemical processes necessarily complicate any electrochemical model. MacDiarmid (1987) found that PANI film has various intrinsic domains with different lengths of π -conjugated fragments. Each domain has an individual redox potential and they are distributed over a mean redox potential. Later these data were confirmed using potential-step chronocoulometry, and the mean redox potential of PANI, in different acidic solutions determined by measurement of doping level at different oxidation potentials, was +0.71 V and +0.16 V vs. Ag/AgCl for pernigraniline/ emeraldine base and emeraldine base/leucoemeraldine base, respectively [99].

The overlapping of oxidation peaks in PANI was observed also in other electrochemical studies of polyaniline [223]. The results from I-V technique exhibit two current peaks in the pH range of 2.0–3.5 at the voltage of 0.35 and 0.45 V, which correspond to oxidation of luecoemeraldine to emeraldine salt (ES) form and ES to Pernigraniline Salt (PS) form, respectively. However, during the further increasing of pH in the range of 4.0–5.0, the peaks become identically steeper as the two peaks overlap into one peak, which corresponds to transformation of Luecoemeraldine to PS form. Moreover, their current amplitudes become higher at the slightly lower voltage of about 0.35–0.4 V.

The electronic current graphs of devices with memristive behavior exhibit the hysteresis of the current at positive potential and the rectification of the current at negative potential that depends from polyaniline layer whose conductivity depends on the redox state (8 orders of magnitude ratio). Geniès et al. [224] demonstrated that the polymer is conductive in the oxidative state between -0.2V (versus Ag/ Ag + in acetonitrile) and 1.6 V, where degradation of the material starts.

Since the delocalized positively charged free radicals are the main source of conduction in polyaniline, it can be expected that maximum conductivity will be reached when the number of radical cations in the polymer chains is maximum. Our cycling I-V characteristics are in agreement with the fact that both leucoemeraldine and pernigraniline forms of PANI, neither of which have free radicals in their backbone structure, are insulating. The most conductive form of polyaniline is the fully protonated, half-oxidized emeraldine salt form, and the conductivity decreases as the oxidation state changes toward either a fully oxidized or a fully reduced state.

A positive hysteresis was observed because the current density (A/cm^2) of anodic reverse scan is larger than the current density of initial forward anodic scan. In other words, it was observed that the charge variation during the reverse cycle does not coincide with that observed during the forward sweep. This takes place because the redox process is not reversible, and is not close enough to thermodynamic equilibrium.

Some authors proposed the explanations for this abnormal behavior of electronic conducting polymer redox mechanisms as, for example, conformational change of polymeric chains [225] solvent and electrolyte movements [226], relaxation effects [227], phase transition [228] or inter-site interactions [229], and, more recently, dimerizable redox sites. [230].

The hysteresis phenomenon associated with the redox process of electronic conducting polymer were divided into two classes: dynamic and stationary hysteresis. Dynamic hysteresis may have a kinetic origin, and in this case, it is related to the rate of one of the steps of the redox mechanism, or it may display an ohmic origin, and therefore be caused by the presence of an electrical resistance in series with the system. Stationary hysteresis, in opposite to the other types of hysteresis, does not depend on current. It can be found in all systems that present several metastable states or significant interactions between electrochemical sites. A dynamic hysteresis was observed in cyclic voltammograms of polyaniline. For PANI, hysteresis does not depend on scanning velocity and the magnitude of the current [231]. This type of hysteresis can be characterized through the charge-

potential curves derived from cyclic voltammetry experiments performed on PANI due to surface redox reaction, if no mass transfer kinetically limits the transformation, this occurs for polymers on thin layer as the Langmuir-Shaefer films. According to previous studies, as the voltage-current cycles are carried out, we observed that the devices undergo a slow "death" due to formation of electrochemically inactive parts of the polymer chain, and a lower conductivity is observed. Focke et al. suggest an over-oxidation of polyaniline by applying potentials beyond +0.6 V vs. Ag/AgCl that causes the irreversible formation of quinonediimine structures which are electrochemically inactive [209]

Finally, it is necessary to couple two semireactions that occur at “gate” electrode and in PANI layer respectively.

The following scheme for PANI-HCl and Ag/AgCl redox reactions in acidic ambient is suggested. In the presence of high HCl content some monomer groups as the result of doping are protonated, resulting in formation of polarons [232, 89] In the presence of Ag+ the free radical form of the polymer is oxidized due to electrontransfer (figure 61).

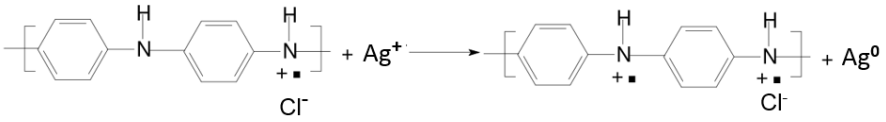

Figure 61 Redox processes in PANI.

It is known from volt-amperometric measurements that the standard reduction potential for the pair pernigraniline /emeraldine is ~0.71 V vs. Ag/AgCl in 1 M HCl, where pernigraniline and emeradine refer to fully oxidized and half oxidized form of PANI, respectively [89].

Cl^- anions are transported into the polymer matrix to compensate the excess of charges inside the film. This elementary step is followed by the release of two H^+ ions and Cl^- from the positively charged intermediate, and finally two imine groups are formed (figure y2). For this step of voltage-current cycle, Lei et al. suggested that if PANI is doped with HCl, the dopant anions can be released from polymer network during its oxidation and deprotonation process [233].

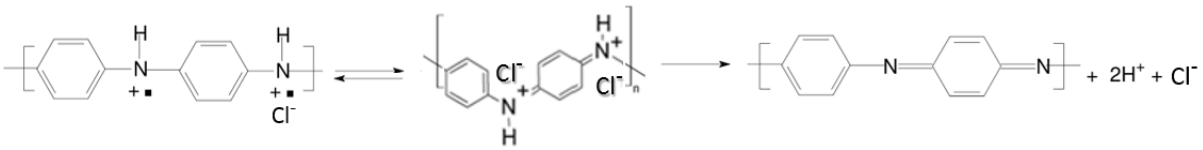

Figure 62 Rearrangements in PANI film.

The standard reduction potential (E^0) value for the couple redox $AgCl/Ag^+$ is +0.222 V. Based on these values it seems that PANI-HCl films should not be spontaneously oxidized by Ag+. This thermodynamic paradox can be resolved if we accept that the semi-reactions (oxidation of the polymer fragments and reduction of ions in the solution and vice-versa) are separated in space and have to be coupled via ion transport. A similar explanation was proposed by Zheng for the oxidation mechanism of PANI membrane by Fe^{3+} [234].

In any case the anion Cl^- concentration gradient across the polyaniline film/gel interface seems to play a fundamental role for the kinetic reaction. Otherwise, not compensated transport of electrons would generate an electrical potential due to charge separation and the process would immediately stop. For this reason, the transport of electrons in PANI is coupled with transport of chloride anion. Evidently, if we have high activity of anions in the solution and low activity of anions in the polymer, we should have a new driving factor for the redox process, which is simply the difference of electrochemical potentials for anions between the aqueous solution and the film.

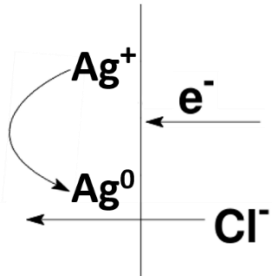

Figure 63 Semi-reaction at Ag wire coupled with Cl- ions transport.

The redox reactions of PANI are believed to be accompanied by ion migration into/out of the polymer film to maintain the local electroneutrality of the bulk polymer. It was demonstrated that transmembrane potential through doped PANI is a mixed potential due to both electron transport in redox processes and Cl^- ion transport [235].
It was suggested that two kinds of redox reactions in polyaniline occur [236]. One concerning proton addition/elimination reaction while the other reaction was related with the insertion of anions into PANI film during its oxidation (ionic radius of Cl^- ions is 184pm) and the transfer/elimination of anions during its reduction.

Polymer	Anion	D ($m^2\ s^{-1}$)
Polyaniline	Cl^-	2.0×10^{-13}
Polyaniline	ClO_4^-	1.8×10^{-14}

Table 4 Anion diffusion coefficients in polyaniline films.

We should note that direct transport of Ag+ in the film is negligibly small in accordance with the previous studies that confirms the presence of chloride near film surface after its oxidation in acidic environment [237]
The existence of covalent chlorine may be attributed to the concomitant ring chlorination at high oxidation level of PANI in the presence of HCl [96]. The figure 64 shows electron/Cl - coupled counter transport at the interface of PANI film.

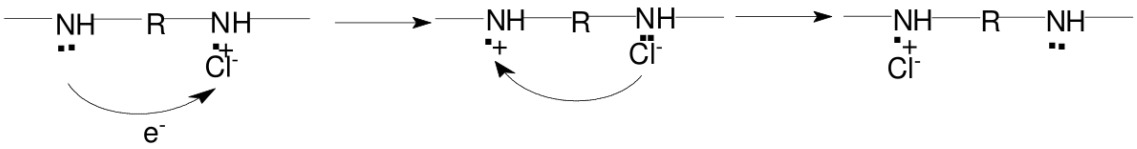

Figure 64 Scheme for electron transfer from amine nitrogen to its neighboring nitrogen.

The crucial role of Cl- in PANI electrochemistry is confirmed not only considering the work illustrated in this thesis but also in previous literature.
Kang et al. (1996) [237] observed a hysteresis effect for the protonation-deprotonation cycle involving HCl as the protonic acid. The hysteresis has been in part attributed to the secondary interactions, such as HCl covalently linked to the polymer backbone and the associated reduction in intrinsic oxidation state. Furthermore, the hysteresis effect involving HCl was not observed in the protonation-deprotonation cycle involving H_2S0_4.
In addition, hysteresis in the conductivity of the polymer as a function of the HCl protonic concentration during the protonation-deprotonation cycle has been observed. The changes in intrinsic oxidation state ([-N-] and [-NH-] content) and protonation level ($[N^+]/[N]$ ratio) of emeraldine (EM) base powders as a function of protonic acid loadings resulting from the protonation-deprotonation cycle have been assessed quantitatively by X-ray photoelectron spectroscopy. Thus, a hysteresis

effect in both intrinsic oxidation states and protonation levels was observed in the protonation-deprotonation cycle. This study [237] suggests the presence of ionic (Cl^-) species, and covalent (-Cl) chlorine. The anionic chloride species result from the charge transfer interactions between the halogen and the metal-like conducting state of the polymer chain, while the covalent bounded species result from structure alteration of the polymer due to the formation of C-Cl species. The presence of a high content of the covalently bonded chlorine (-Cl) species at high HCl concentrations is proposed. During the deprotonation cycle, the proportion of covalently bonded Cl species remains at a high level until a substantial degree of deprotonation has occurred. As a result, the intrinsic oxidation state of the polymer persists at relatively low level, as indicated by the high amine contents (>50%), during the deprotonation cycle [237].

In conclusion, the redox reactions occurring on both electrodes (PANI layer and Ag wire) can be described and summarized by the following equations:

$PANI^+Cl^-$ (emeraldine salt) + e^- $\rightleftarrows$ PANI (leucoemeraldine) + Cl^-,
Ag *(s)* + HCl $\rightleftarrows$ AgCl *(s)* + ½ H_2 *(g)*

Figure 65 shows the silver wire before and after a cyclic voltage- current measurements in standard conditions (see par.) The SEM images clearly show a degradation of silver wire after one measurement cycle.

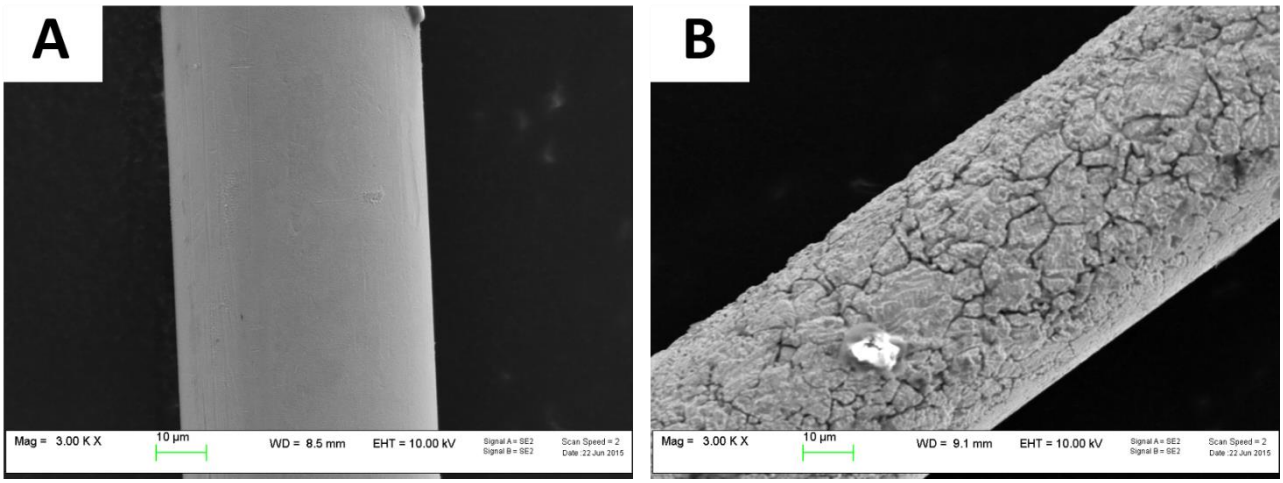

Figure 65 SEM images of a bare Ag wire Ø 50 µ (A) before the insertion in device, (B) after one cycle cyclic V-A measurement.

The EDX analysis (shown in figure 66) confirms the presence of chlorine on the surface of bare wire after a cyclic voltage-current measurements with standard device (see par. 2.3). The amount of oxygen is negligible in any EDX spectrum recorded.

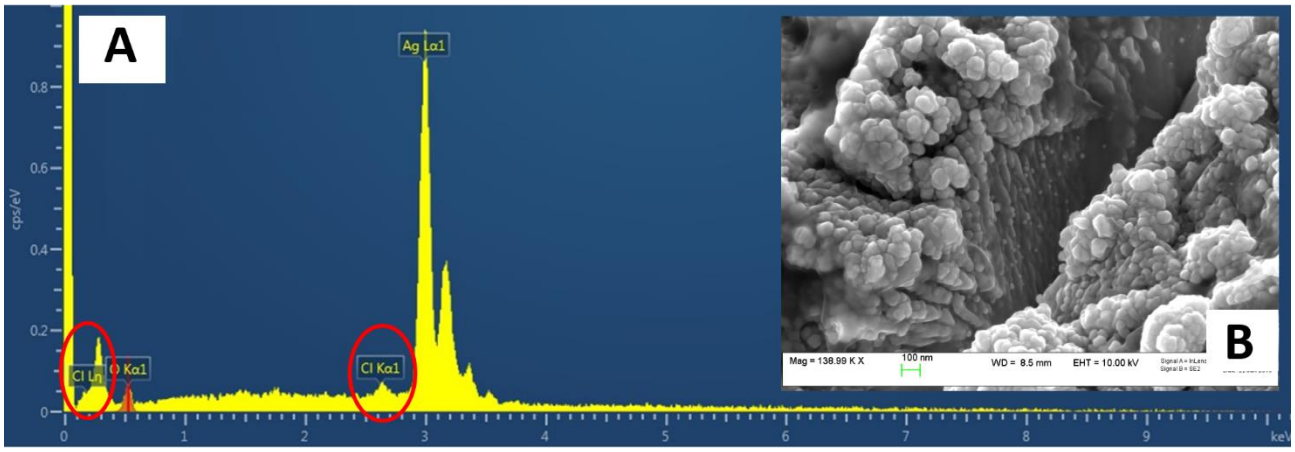

Figure 66 The EDX analysis carried out on silver wire after cycle V-A measurements**.**

Of course, all the charged species that are electrochemically active will move in the solid state polyelectrolyte due to the applied potential; but the studied presented in this thesis confirms that Cl^- ions and of Ag wire have a the key role in PANI electrochemistry. An asymmetric and memristive behavior was observed in organic solid-state device only in presence of chlorine ions and silver wire.

As already mentioned this preliminary interpretation of all our experimental data should be considered only as a tentative guideline for needed further studies where on one end to measure all the needed parameters to qualify further the different steps and then possibly develop a more detailed model of the whole process.

5. Towards Hybrid-Organic memristive elements.

One of the main interests in bioelectronics, besides the relevant expected impacts in bio-medicine and prosthetics, is driven by the aim to emulate abilities that, essentially present in living beings, can scarcely be reproduced with artificial man-made devices. Even the simplest living organisms, for example, learn from and adapt themselves to stimuli from the surrounding environment. A challenging perspective is the integration of these adaptive/learning behaviors into artificial systems, possibly interfacing them with existing devices and technologies. Even though the great efforts of the scientific community in this direction have brought enormous progress in interfacing living beings with electronic devices, currently artificial models can barely mimic the basic properties of the simplest living organism in an over-simplified way [238].
We report here on a novel hybrid bioelectronic organic electrochemical device based on a living being – the Physarum polycephalum cell.
The paragraphs 5.2.2 shows the characterization of hybrid-device in terms of memristive behavior.
First of all in the following section we illustrate the motivations that leads to choose the Physarum Polycephalum as “model organism” to realize a bio-organic prototype.
The so-called "double-layer solid polyelectrolyte" technology which was developed in this thesis (par. 4.5) will be fully validated within the bio-organic prototype.

6.1 Slime Mould.

Physarum polycephalum mould (PPM), belongs to one of the predominant groups in the world of eukaryotes: Amoebozoa [239] belonging to the family of myxomycetes, in the past defined as fungi, nowadays simply slime moulds, and consists of a multinuclear single-cell mass of protoplasm.
PPM lives in humid and dark environments. The studied form, in particular, is the plasmodium, PPM vegetative form; it looks like an amorphous yellow mass with networks of protoplasmic tubes branching towards nutrients. Its foraging behavior can be seen as a computation: data are represented by spatial configurations of attractants and repellents, and results by the structure of protoplasmic networks [240]
Physarum polycephalum's behavior has been the object of different studies belonging to different research fields, from biology to unconventional computing and from experimental to theoretical science. Therefore, PPM is widely studied for unconventional computing [241].The choice of PPC was based on its unique, recognized properties of "intelligence", "creativity" and "capacity of learning" that are being increasingly investigated [242]. For example, during its life cycle, and especially when it seeks food, PPM is able to remember already trodden paths, in order not to retrace them.
A recent example of Physarum's capability of designing optimized networks, allows the retracing of Canadian Highway Networks [243].
Its behavior can be resumed as: capability of optimizing shortest path [244], calculation of proximity and planar graphs [245], calculation of basic logical operation [246], motion control [247], self-adaptation [248], and self-reparation [249].
For this reason, PPM has recently been exploited as the main material in non-conventional computing, robot-Physarum and PPM-based network circuits [250]. In addition, it is rather easy to keep the PPM alive: it requires room temperature, dark conditions and humidity. The PPM colony needs to be fed with oat fakes and periodically replanted to fresh substrates. Therefore, given a little care and constant attention it is possible to grow PPM in its yellow plasmodial stage.

In this thesis are reported some experiments done to study the behavior of this organism under different conditions and stimuli. In particular, we analyzed not only spatial distribution of attractants/repellents (feed, water, solid polyelectrolytes, PANI films), but also the effect of external elements inserted and transported by Physarum polycephalum.
These unique properties could be employed to realize deterministic adaptive networks and spatial distribution of nanoscale and microscale materials.
Choosing, among transported materials, those able to change electrical, optical and, magnetic properties of the system it should be possible to enable information sensing and processing.
We loaded Physarum polycephalum slime mold with three kind of particles: polystyrene and $MnCO_3$ microparticles and Barium hexaferrite $BaFe_{12}O_{19}$ nanoparticles (see par.3.3). The performed experiments had, as an objective to verify the compatibility and the ability of the mold to transport micro and nanobjects, of different nature.
We studied two kinds of transport: first case we loaded Physarum with particles, by directly mixing the two elements together; in the second one, we observed what happened if Physarum had to cross a strip of particles. The latter study, however, was performed only with polystyrene microparticles. Moreover, it has to be distinguished two main transport mechanisms: in a first case, particles are transported on Physarum veins, in a second one, they are taken inside the body of the mold. The first case is typical of those substances that Physarum almost ignore; they are not dangerous, nor interesting for it. Thus, they are transported just because, during its motion, they sticked to its body, but they are not incorporated. Therefore, it is possible to find them only on the surface of mold's body, and not inside it. In the second case, particles are mistaken as food, so they are engulfed inside Physarum that picks them up and tries to absorb. The figures 68 shows the SEM measurements performed on the sclerotized Physarum veins charged with different particles.

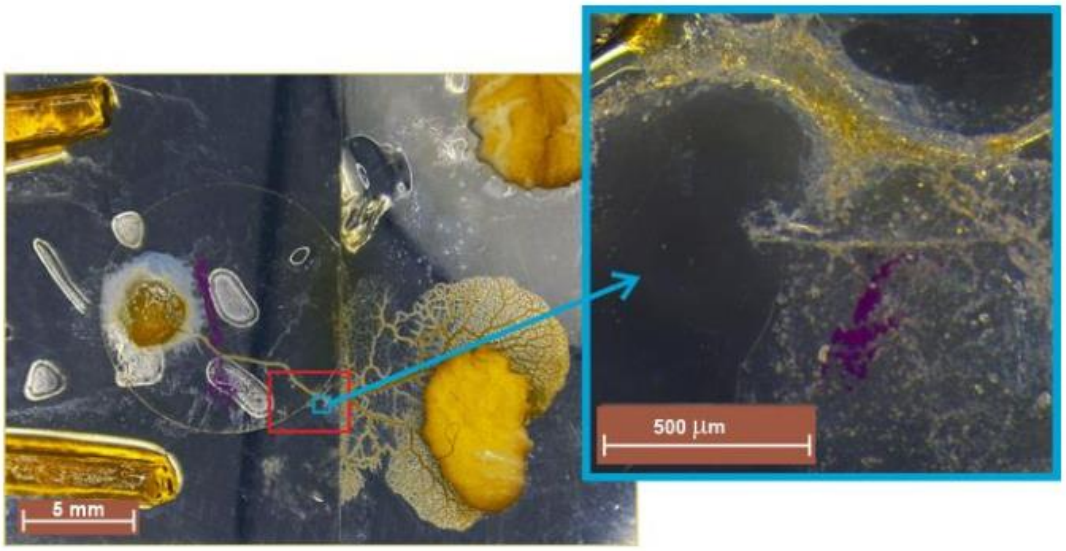

Figure 67 Optical microscopy photograph of one of the developed experiment with slime mold and red polystyrene microparticles.

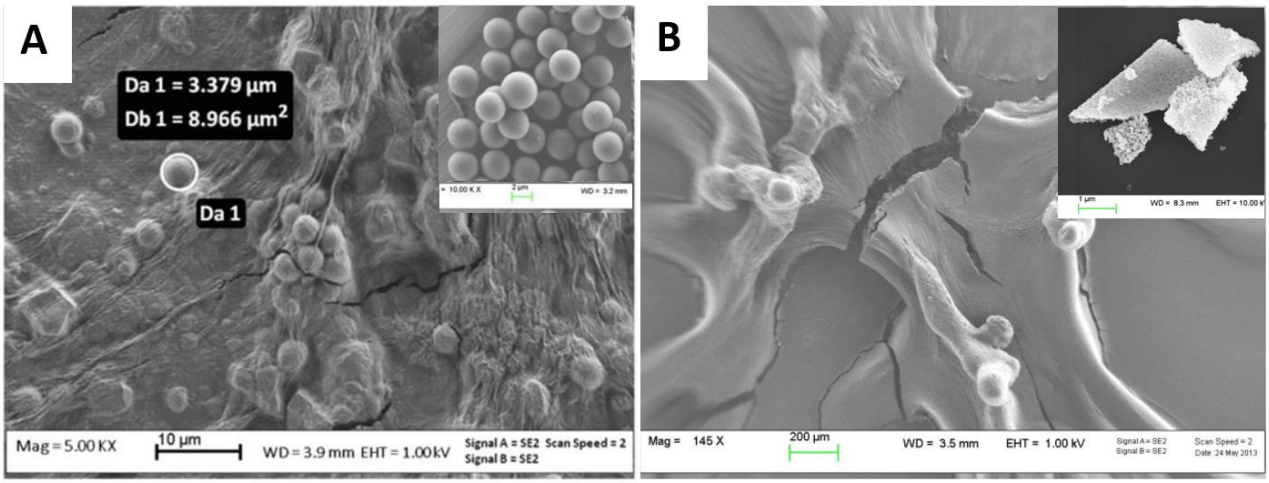

Figure 68 SEM images: (A) sclerotic PPM vein loaded with polystyrene microparticles by mechanically mixing method; insert: polystyrene microparticles. (B), 3D structures of sclerotized PPM vein loaded with magnetic nanoparticles $BaFe_{12}O_{19}$, insert: aggregates of hexaferrite nanoparticles $BaFe_{12}O_{19}$.

The results here reported can be useful for unconventional computing and bio-computing application devices. In such field, Physarum polycephalum's networks become the scaffolds of hybrid circuits at the micro and nano-scale. For the development of self-growing computational systems, we must consider and study the slime mold as a medium capable of integrating and redistributing foreign particles. Therefore, Physarum polycephalum acts as a programmable transport medium as showed in [251].

To evaluate how well Physarum propagates on surface of polymer employed in in bio-organic prototype (see par. 5.2.2), in other words to test their biocompatibility toward the mould, we conducted experiments with PANI, chitosan, pectin films. Typically, a slime mould was inoculated

in the middle of dish. The supports were kept in darkness in separated cylindrical containers, with shallow water on the bottom to keep the humidity very high. The boards with Physarum were not in direct contact with the water. The water generated chemoattractive fields to guide Physarum wires towards imaginary pins.

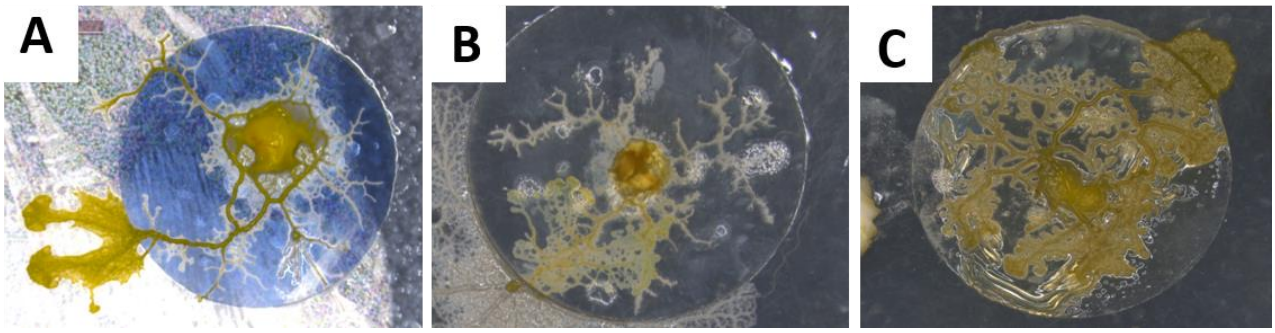

Figure 69 Optical microscope image of Physarum's network created on (A) PANI (HCl-free) deposited sample; (B) acetic acid- doped pectin layer; (C) acetic acid- doped chitosan layer. The pattern created by mold on the polymer surface is clearly visible.

The analysis carried out by optical microscope shows the full-compatibility between chitosan or pectin films and PPW. A different behavior was observed for PANI film: the mould forms an inhomogeneous and sparse network of veins both on undoped (emeraldine base) and doped HCl-PANI (emeraldine salts).
This study shows that the polysaccharides films are more suitable and "restful" for the mould.
This was the first step towards the realization of a full integrated bio-organic device.

6.2 Electrical properties of the Slime Mould.

The electrical properties of slime mould Physarum polycephalum (PPM) has been the object of different studies [252] even if are few or missing examples of PPM full integration in electrical circuits and devices.
Physarum responds to mechanical stimulation, twisting and stretching by unique patterns of oscillations of its membrane potential. It was reported that the electrical responses to stimuli may propagate along protoplasmic tubes for distances exceeding tens of centimeters, like impulses in neural pathways do [253].
In addition, the adaptive 'learning' behavior of PPM was described in terms of memristor model; [254, 255]. Gale et al. [256] occasionally observed that PPM protoplasmic tubes showed hysteretic current-voltage characteristics, consistent with those of the memristive systems.
A hybrid bio-organic electrochemical transistor was developed by interfacing an organic semiconductor, poly(3,4-ethylenedioxythiophene) doped with poly(styrene sulfonate), with the Physarum polycephalum cell. It was demonstrated that the electrolyte is efficiently replaced by the living cell in organic OECT device, where the PPM-OECT device response is quite sensitive to the presence of the PPM on the surface of PEDOT:PSS film.
Figure 70A shows a schematic of the hybrid PPC-OECT structure, where the yellow area represents the slime mould, while the black stripe between the source and drain electrodes represents the PEDOT:PSS film and the gate electrode is placed inside the PPC.
Figure 70B shows the typical kinetic curves, Ids(t), measured by switching the gate voltage in the range 0–1.6 V with steps of 0.2 V. The device response upon application of gate voltage steps is defined by the modulation ratio $\Delta I/I_0 = (I-I_0)/I_0$. The comparison among the typical current modulations is reported for the three different gate electrodes is reported in figure 70C. As expected

[257], the Ag gate, being redox-active, generates the highest current modulation over the whole voltage range investigated. On the other hand, Pt and Au, both without any significant redox reactivity, show lower current modulations. Figure 70C shows the progressive gate voltage shift towards lower gate voltages of the transfer curves depending on the material of the gate electrode (Au < Pt < Ag), indicating that the V_g^{eff} , that acts on the transistor channel increases progressively.

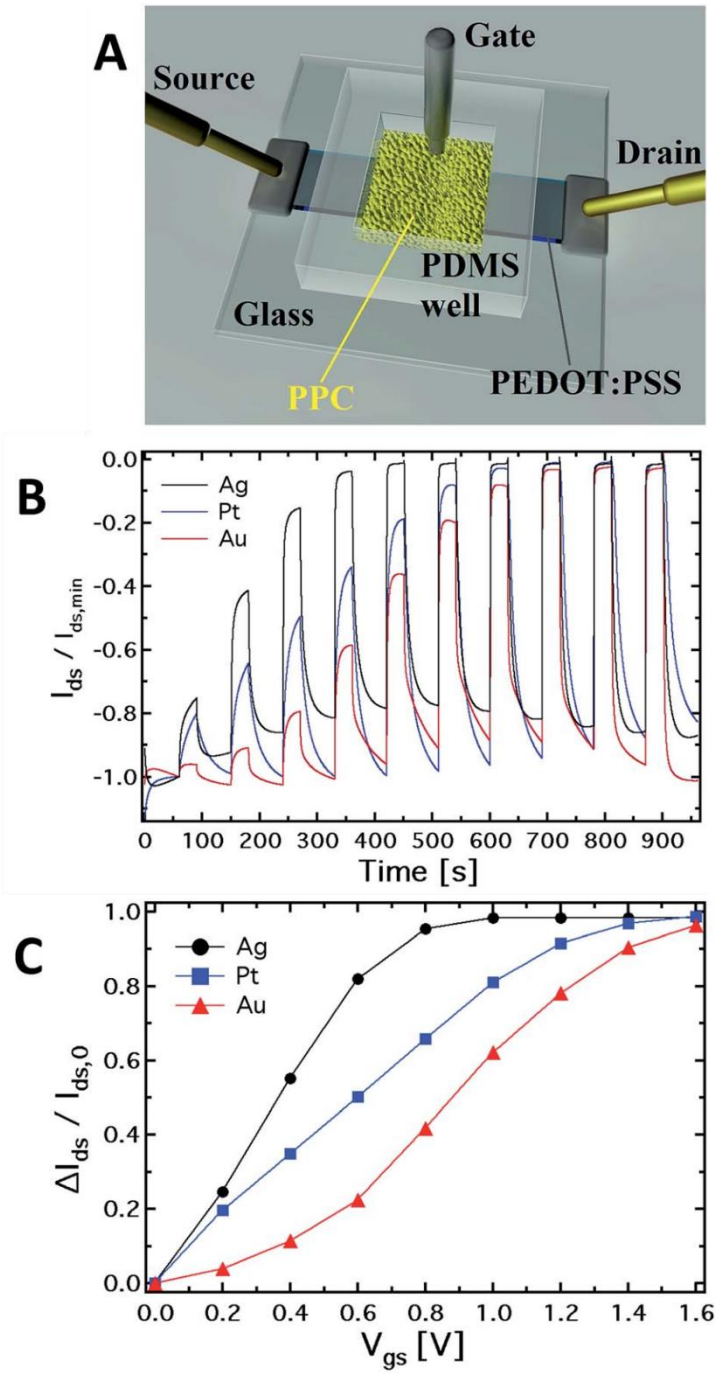

Figure 70 (A) Schematic diagram of the OECT based on PEDOT:PSS (the black stripe is the PEDOT:PSS film) where the gate electrode is immersed into the Physarum polycephalum cell (the yellow area in the figure). (B) Normalized kinetic curves (I ds /I ds,min vs. time) and corresponding (C) current modulation (DI/I 0): each step corresponds to an increment of 0.2 V of the gate voltage.

Moreover, I–V measurements were carried out using the device in a 2-terminal configuration: the OECT organic semiconducting layer works as the reference electrode and the metal gate plays the role of the working electrode. The transfer characteristics were recorded in a cyclic mode, i.e. using

a scan sweep with increasing gate voltage followed by a backward sweep. In particular, Vgs was varied between -2 to 2 V, starting from 0 V, with step voltages of 0.2 V, at different bias step durations, e.g. 2, 5 and 10 s.

Figure 71A–C report the typical PPC-OECT transfer characteristics (I ds vs. Vgs, Vds = -0.4 V) comparing once again the performance of Ag, Pt and Au gate electrodes. The hysteresis loops were investigated. In the positive range (0 < V gs < 2 V) the action of Vgs induces the incorporation of cations into the PEDOT:PSS, causing its de-doping. Hence we observe a decrease of the channel current up to a saturation of the curves that depends on the gate material. In the negative range of the gate bias (-2 < V gs < 0 V) we observe in all cases that a higher gate voltage is needed to establish the original doping level of the PEDOT:PSS channel, i.e. for the cations to desorb from the polymer backbone towards the PPC. In particular, in the case of an Ag-gate, the change of the backward current is quite small in the negative V gs range, while it saturates at -1.5V for the Pt-gate electrode and at about -2 Vfor the Au-gate electrode. Such behavior suggests that chemical processes occur at the gate/PPC interface.

A complementary observation concerns the area of the hysteresis curves, which have been found to be dependent on the gate material. In particular, the lowest area was found for the Ag-gate and the largest one for the Pt-gate electrode. In general, hysteresis arises from the competition between the dynamics of cation adsorption/desorption and the timescale with which the doping/de-doping occurs. [258, 259]. The increase of the hysteresis area is hence related to the different operating regimes under which the OECT works according to the material of the gate electrode. More specifically, as already mentioned, the Ag-OECT operating regime (with a saline electrolyte) is almost fully Faradaic, and is characterized by a negligible potential drop at the gate/electrolyte interface, [260, 261] while with Au and Pt gates, OECTs are expected to work mostly in a capacitive operation mode (non-Faradaic mode), above all at lower gate voltages. It is worth noting that for Pt and Au (inert electrode materials) the channel current I ds (in the range of mA) is much higher than the gate current I gs (in the range of mA). Instead, when Ag is the gate electrode, I gs is considerably higher (on average, by a factor of 5), this being the fingerprint of a Faradaic regime [262]. A similar consideration holds for the I ds steady-state level (saturation) in the positive range of Vgs. Figure71C shows that the Ag-gate gives a full-saturation level already at Vgs < +1 V, a value that is achieved at higher voltages with Au (about 1.8 V), while a real onset of saturation is not observed for Pt in the range studied. This behavior further indicates possible electrochemical reactions taking place at the PPC/Ag-gate electrode (as already indicated by the curves in figure 70.B). In fact, we expect that a Faradaic reaction at the Ag-gate electrode results in a higher modulation and a fast response of the device, that is in faster channel current decrease (de-doping phase) and enhancement (desorption of cations from the channel). These are exactly the trends observed in the data of figure 70 B.

The cyclic current–voltage measurements (I–V), by give insight into the memory capabilities of the mould, showing a “memristive-like” response as well as a hysteresis loop ascribable to the cell membrane properties.

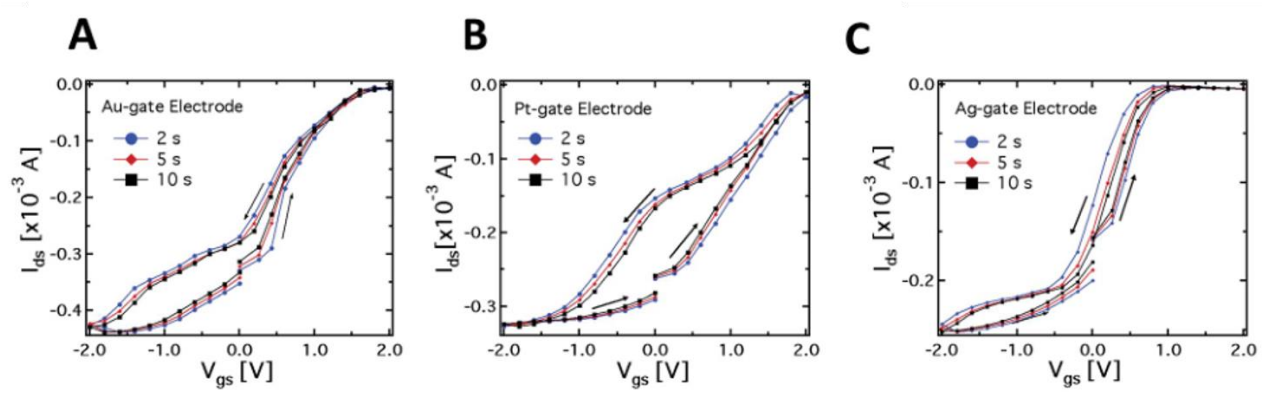

Figure 71 transfer characteristics (I ds vs. Vgs) of the PPC-OECT device recorded by using for Au, Pt and Ag gate electrodes (Vds 0.4 V) are reported in panels D, E and F, respectively.

Even if an attempt to realize a bio-organic memristive element was reported [31], this research topic is still innovative and unexplored.
In particular, our issue is to obtain a bio-integrated device with not only memristive but also synaptic electrical features. Concretely, the electrical features of the bio-organic device should not show only a hysteresis loop (ascribed to memristive behavior) but also a current rectification in another potential range (ascribed to "synaptic-like" behavior).
The polyaniline can be switched between two redox states in which it presents a very different conductivity (~ 6 magnitude orders). The current rectification probably is due to slow kinetic PANI reduction process that occurs in solid state (see chapter 4)
The main aim of this thesis consists in developing of a synergy between the polyaniline electrochemistry and the biological object. This thesis proposes a bio-organic element exploiting both peculiar electrochemical feature of PANI and the PPW.
The electrical property of the mould are characterized by means voltage-current measurements. Cyclic I-V characteristics were carried out in darkness a relative humidity of 80 -90%, respecting the required conditions for the mold life using the chamber shown in figure 72. This section reports several experiments carried out both with simple electrode array and with multi-layer structure, in which a living Physarum wire or plasmodium portion was incorporated.

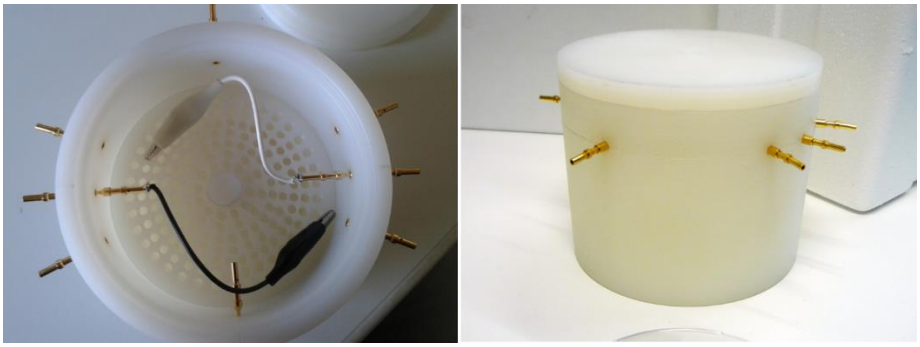

Figure 72 Set-up for electrical characterization of slime mould-integrated devices and arrays.

5.2.1 Non-linear Bioelectronic Element: Schottky Effect and Electrochemistry.

A first approach to the study of slime mould electrical properties is dedicated to the realization of a non-linear electronic elements with properties, depending also on the slime mold.
One of the simple ways of realization of non-linear elements is the formation of asymmetric structures. In particular the plasmodium of PPM is placed between two electrodes, realized from the metals with a significant difference in the work functions. In this case, a system, similar to the Schottky diode can be realized. Similar approach has been already successfully applied for the realization of threshold elements in systems [263-265] based on organic memristive devices [81, 266, 267].
We have used gold and indium for the electrodes of the asymmetric structure as they have a significant difference in their work functions [263]. An image of the system under the measurements is shown

in figure 73. After the growth in the direction of the attractor (food, left side of the image), the formed channel of the slime mold was contacted by the freshly cleaned indium material and gold wire. Cyclic voltage-current characteristics were measured in the following way. Measurements were started at 0 V bias voltage. Readouts of the current were performed after the 0.1 V increment of the applied voltage, with the time delay for the equilibration in the range 1-60 seconds. At least 20 samples in the configuration, similar to that shown in figure 73 were prepared and investigated. Of course, the length, width and thickness of the slime mold channels were different for each experimental set up, as the system was in the living state during the experiments.

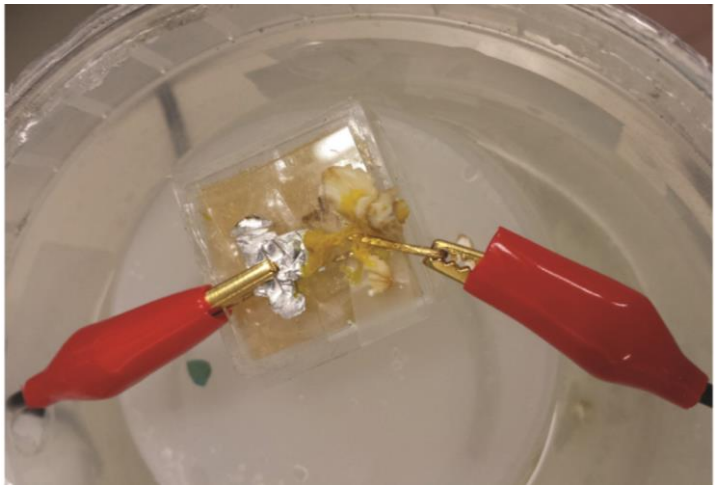

Figure 73 An image of the experimental setup for the study of cyclic voltage-current characteristics of the slime mold placed between asymmetric metal junctions (yellow substance in the center is a Physarum polycephalum).

Typical cyclic voltage-current characteristic of the system, shown in figure 73, is presented in figure 74 for the time delay of 1 second. All the investigated samples have revealed similar qualitative behavior: of course, the absolute values of the measured currents were different due to the difference in the length, width and thickness of the slime mold channels, as it was mentioned above. Analysis of the characteristics, shown in figure 74 reveals the presence of some features, that we expected to realize – suppression of the conductivity for low voltage values of the characteristics in the direction of the positive bias and, in general, rectification features, that, as it must be, are more pronounced for the low values of the bias voltage. However, the characteristics, shown in figure 74 has also one important feature, that is impossible for a simple Schottky junction – the presence of the hysteresis. First explanation of these features regards RC of the system. However, simple estimations of the observed values give a 0.02 mF for the capacity of the junction that, considering the length between the electrodes (about 5 mm) seems hardly possible. However, in order to be sure that the presence of the hysteresis cannot be attributed only to the RC of the system, the measurements with the increased delay between the voltage increment application and the current readout were performed.

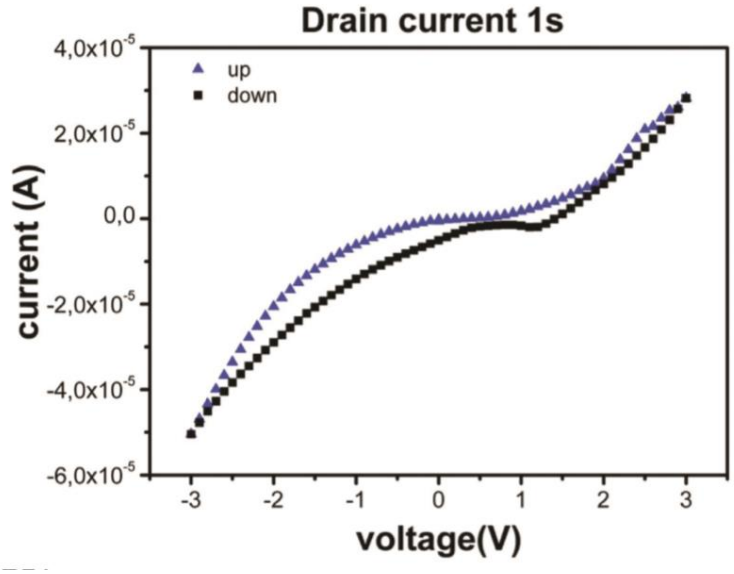

Figure 74 Cyclic voltage-current characteristics measured on the structure, shown in figure 73 with the time delay of 1 second between the application of the voltage increment and readout of the current value.

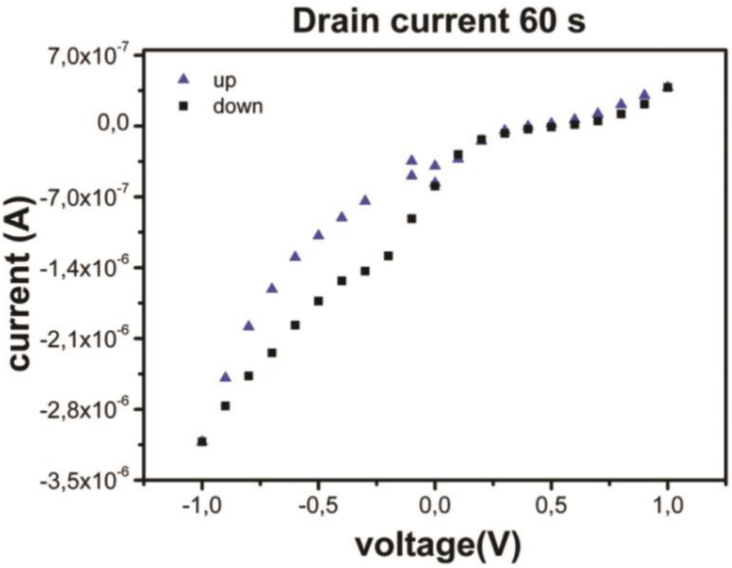

Figure 75 Cyclic voltage-current characteristics measured on the structure, shown in figure 73 with the time delay of 60 second between the application of the voltage increment and readout of the current value.

Typical cyclic voltage-current characteristics with the delay of 60 seconds is shown in figure 75. Disregarding the difference in the absolute values of the current, due to the above discussed reasons, the characteristics presents also suppression of the conductivity in the positive applied voltage branch and rectification. However, there is a difference with respect to the characteristics, shown in figure 74: the hysteresis in the positive branch is practically suppressed, while it is practically unchanged in the negative branch of the applied bias voltages. Therefore, the presence of the hysteresis in the realized and studied structures is very likely connected to the internal electrochemical processes, occurring in the slime mold. The last statement is also confirmed by the comparison of figure 74 and figure 75– the most of biological electrochemical processes occur at negative potentials. Thus, increase of the delay time can result in reaching of the equilibrium in the positive bias voltage branch, while it cannot affect the internal activity of the living system, resulting in the preservation of the hysteresis in the negative bias voltage branch.

And thus, we have realized a non-linear bioelectronic element with properties, that are a superposition of the features of the asymmetric junction with those, resulted from the internal electrochemical activity of the slime mold. Such behavior can establish a basis for the bio-computational systems, where memorizing of the event is an essential part of the computation. The presence of the hysteresis, as in the case of memristive devices, will vary at different time scale the connectivity within the system, allowing learning and decision making. It seems very challenging to develop the work in order to make a comparison of features of the completely artificial systems with threshold elements with slime mold based system, where natural attractors and repellents can be inserted

5.2.2 Bio-integrated devices: polyaniline as conductive polymeric film.

The ability of the pectin-gel to act as buffer layer in the device was tested by introducing the PPM as a model living organism. A multi-layer structure was assembled, depositing the living organism onto a dried pectin layer in the contact zone with PANI channel.
Two types of configurations are tested: a flipped structure "sandwich"-like and a standard configuration. The electrical circuit was the same as for the standard organic memristive devices.
A new architecture of organic memristive device is proposed with a double-layered polyelectrolyte, one of which is a biological system.
In the device the Physarum polycephalum was used as living organism, the polyaniline as conducting polymer for the source-drain channel. The key choice for the device functioning was the interposition of a biocompatible solid layer between polyaniline and living organism, that must result both electrochemically inert and able to preserve a good electrical conductivity of the polyaniline, not withstanding the alkaline pH environment required for the surviving of living being, by avoiding strong acids. Two biopolymers were investigated, chitosan and pectin.
In the first step of the study (described in par.4.5), we achieved the best conditions to preserve high conductivity of polyaniline at neutral pH and to assure linear electrical characteristics of the device by a polymeric interface.

Hybrid multi-layer structure: "sandwich" configuration

First of all we have modified the geometry of the standard device, in particular we flipped the standard structure and we develop a sandwich structure shown in figure 76.
The Teflon support that was used has a cavity, in which the determined and fixed volume of plasmodium of Physarum can be placed. A groove with a depth corresponding to the silver wire diameter (0.05 mm) was formed in the other solid support also made of Teflon (figure 76). The reference wire was fixed at the bottom of the groove and a portion of P. polycephalum plasmodium was placed over it. The volume of plasmodium was determined by volumetric capacity of groove. After drying for 30 min of polymeric gel, these two supports with formed structures were put in contact mechanically to form the device as shown in figure 76. The PANI area under the plasmodium is the active zone with the width of about 2 mm, where the oxidation and reduction of PANI layer take place (see par.2.3). Electrical measurements were performed as before described (par 3.3.2.)

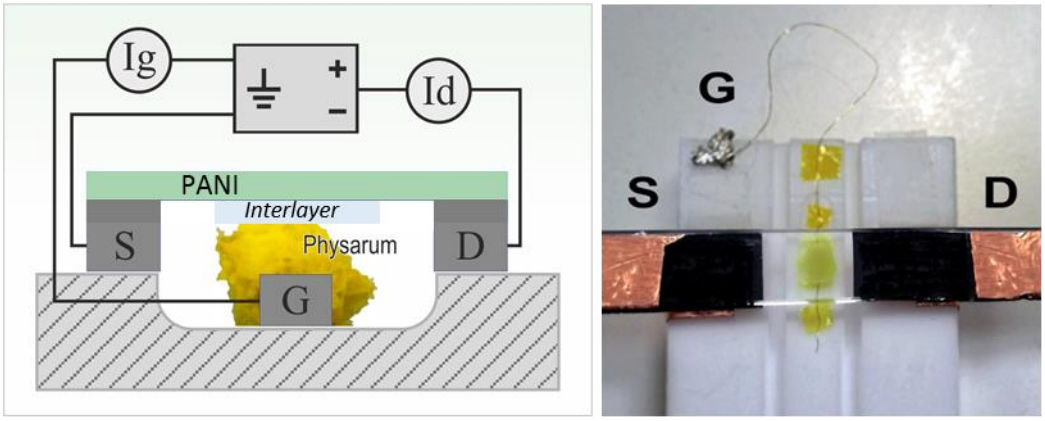

Figure 76 Cross-section of the element with sandwich structure (left) and photo of device with sandwich structure with Physarum polycephalum's yellow plasmodium in the chamber and Source (S), Drain (D) and Gate (G) electrodes.

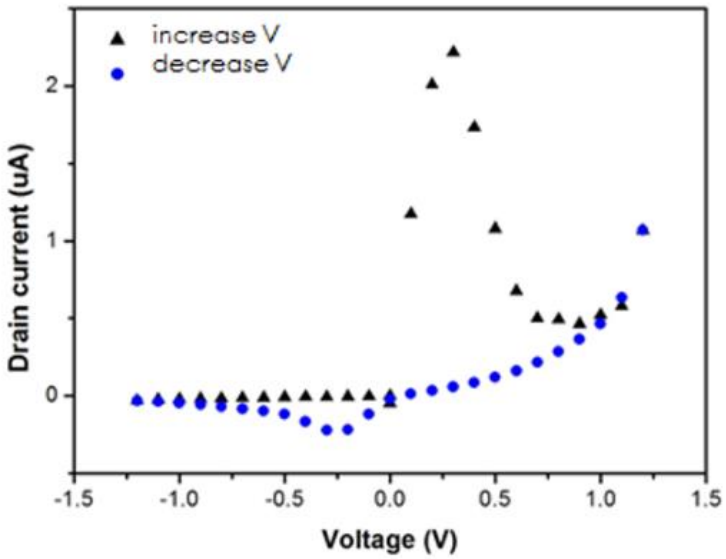

Figure 77 Cyclic voltage current characteristics measured for devices containing a layer of pectine (0.25% w/w) and succhrose (0.65% w/w) in acetic acid solution.

Resultant cyclic voltage-current characteristic measured when only sublayer was used between PANI and reference electrode is shown in figure 48. While the cyclic voltage-current characteristic measured when slime mold was placed between these layers are shown in figure 77.

As it is clear from cyclic voltage current characteristics of interlayer, shown in figures 47-48, the use of sublayer does not allow to realized organic memristive device : the characteristics is practically linear, what can be connected to the lack of ions necessary for the carrying out redox reactions, responsible for the conductivity switching.
The addition of the slime mold varies significantly the current trend that shows a rectificant behavior, a pronounced hysteresis and the presence of two peaks in current (one positive and one negative) figure 77. Such characteristics were never observed for a standard organic memristive device configuration. All the tested devices of such type revealed similar characteristics during the measurement of the first cycle. During next cycles both peaks disappeared, with preserved rectification behavior. Thus, the observed characteristics can be attributed to processes at the PANI-slime mold interface, even their nature will be discuss in following section.
It was realized a system that couple an organic memristive device with a living being – slime mold in a flipped geometry "sandwich"-like. The use of Physarum demanded the modification of the

standard device that consists of a biocompatible sublayer. The measured cyclic voltage-current characteristics revealed unusual behavior (presence of strong peaks) that can be explained by electrochemical processes at the interface between slime mold and other materials.

Hybrid multi-layer structure: standard geometry

The ability of the pectin-solid electrolyte to act as buffer layer in the device was tested by introducing the PPM in the device structure. A multi-layer structure was assembled, depositing the living organism onto a dried pectin layer in the contact zone with PANI channel. The geometry of device is the same the standard devices. As indicated from figure 78, the Physarum Policephalum, integrated in the device, is able to induce a hysteretic-rectifying trend, typical of memristive devices.
The interaction between electronic device based on conductive polyaniline and living organism Physarum polycephalum can be understood by taking into account the ionic species of the mould protoplasm, which drive the membrane potential variations.
It is known that changes in the membrane potential of the Physarum Polycephalum take place in motor cells, which control the slow movements of the plasmodia. Plasmodia movements occur as a result of strands of endoplasm that is squeezed by alternating contractions of Ca^{2+}sensitive actomyosin fibers [268, 269]. The relationship between cytoplasmic streaming and associated electrical activity is now already discuss [270], and the role of propagating electrical signals (action potentials) in plant movements (including those of carnivorous traps, leaves, floral parts, root tips, cytoplasmic streaming, cilia and flagella) was extensively reviewed [270]. If the mould is induced to move by a stimulus into the surrounding environment, like the presence of polysaccharides beneath it, the motor cell permeability to K^+ and Cl^- increases, while the Ca^{2+} ions alter the membrane properties, triggering large fluxes of K^+ and Cl^-. Moreover, the passage of water inside or outside the motor cell changes the motor cell turgor and promotes the ionic exchanges.
The image of PPM after three successive cycles of I-V measurements is shown in figure 78. The brilliant yellow color of Plasmodium assures that the organism remained alive. In fact, the mould resulted to survive a series of at least three cycles of voltage-current measurements carried out in sequence. Anyway, we would like to note that the factors limiting the device lifetime concern mostly the experimental conditions necessary for the survival of the living organism, such as humidity and feeding, rather than current compliance or voltage value. When the mould switches in its sclerotic phase, after making the experimental conditions unfavorable for the life of the mold, it darkens and the current-voltage characteristic loses the memristive features, becoming simply linear, although the PANI layer retains its conductivity. Figure 5a also shows that the PPM plasmodium is able to grow and develop on the layer of pectin, thus demonstrating the biocompatibility of the interface layer.

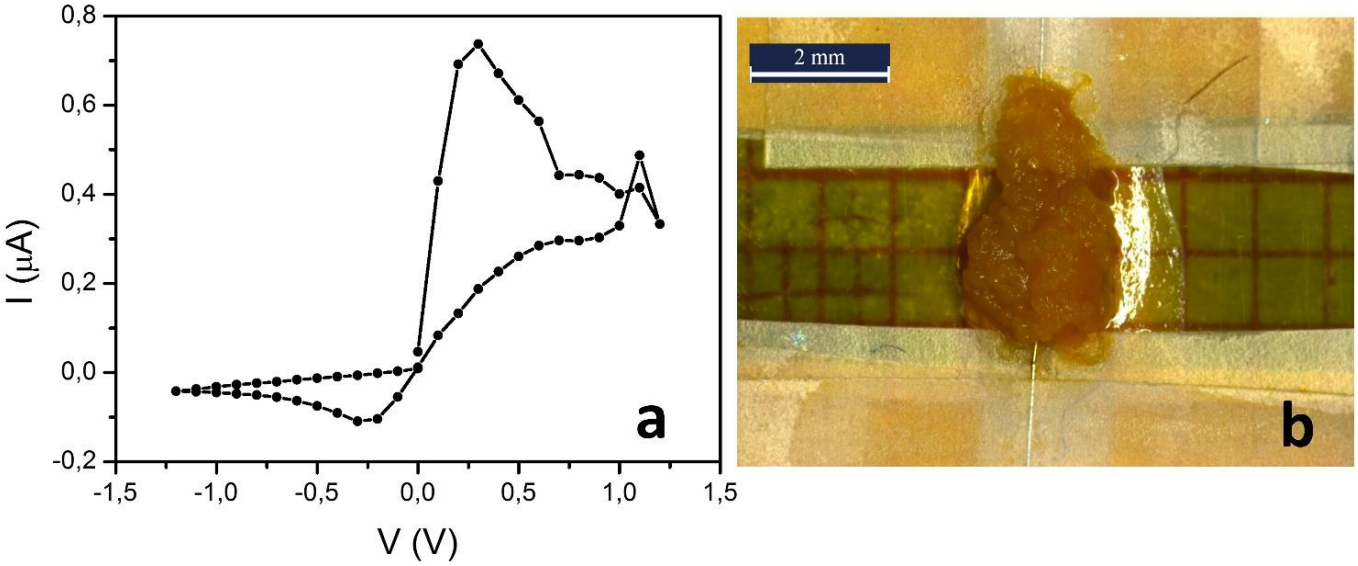

Figure 78. (a) Cyclic voltage-current characteristic of electronic current in a hybrid organic memristive device with PPM as electrolyte over interfacing layer of pectin-gel; (b) Optical microscope photograph of PPM over the interface layer of pectin-gel after three cycles of V-I measurements.

A new architecture of organic memristive device is proposed with a double-layered polyelectrolyte, one of which is a biological system that alone drives the memristive behavior. It was demonstrated that only when the living organism was integrated in the device, the current-voltage characteristics showed the hysteretic rectifying trends typical of the memristive devices, which however disappeared if the Physarum Polycephalum switched to its sclerotic state.
We demonstrate that this hybrid “living” device operates reproducibly as a memristive device, and its peculiar features pave the way to novel strategies based on the integration of organic bioelectronics with memristive approaches.

6. Conclusions.

The research work of this thesis explores and demonstrates the feasibility of interfacing organic memristive devices, considered as basic neuromorphic elements and natural biologic systems, starting from cells. In this framework we had to face some basic limits inherent in the materials presently used that are at the basis of present methods that use PANI/PEO materials and interfaces. One of the major questions is the low pH regimes needed for such materials to be memristive functional. The approach adopted is to use a polysaccharide-based interface layers, in particular Pectin and Chitosan, which are ideally suitable materials among others. We demonstrate that such solutions are viable. We disclosed a large variety of responses depending on different treatments that we have explored.

A wide variety of device behavior was found during the research work, that paved the way for the study of very interesting phenomena, such as ion kinetics and kinetics of electrochemical processes that have led us to new discoveries in some very interesting questions about the mechanisms involved and the dynamics of the processes that were previously not even considered.

An innovative multilayer architecture is proposed in this thesis; it is able to avoid the de-doping process of polyaniline (PANI) at neutral pH, which is a necessary requirement for bio-systems. The key idea consists in use of polyelectrolytes of natural origin as protective films at the interface between biologic element and polyaniline layer.

In order to improve the biocompatibility of the system, biopolymers, materials never used before in organic memristive element, are tested in combination with LS PANI films in standard configuration. It is proved that Pectin and Chitosan could be used as solid polyelectrolytes in organic memristive element (OMD); even if the kinetics of ion migration processes in the different tested polymers affect the performance of devices. A certain selectivity degree for monovalent and divalent cations is identified in pectin-based systems. These particular sensing properties are explained from a qualitative point of view, considering the different stability of chloride salts, the chain-to-chain or chain-ion interactions, as well as ion pairs formation.

Then, the chemical species and components in OMD responsible for the electrochemical switching of PANI are identified by several trials reported in this thesis. This preliminary study is carried out in order develop the "double-layer solid polyelectrolyte" technology: the polyelectrolyte in solid state and as well as additives in its formulation should not produce the electrochemical switching of PANI, this is one of the main requirements to the interface. It was found that chloride salts and hydrochloric acid could be the key elements in the electrochemical response of PANI, while acetates are not useful as doping agents in OMD. A preliminary hypothesis on the electrochemical model able to explain these experimental results is proposed.

Therefore, the suitable formulation of pectin and chitosan gels for intermediate films in bio-organic hybrid systems is successfully identified. The films of chitosan and pectin are tested in combination with PANI LS-film.

Only pectin, used at high degree of methylation, without strong acids and doped only by acetic acid (2% max), resulted suitable for the purpose. A qualitative preliminary explanation for the different behaviors of the two polyelectrolytes has been proposed and discussed.

The interface layer based on pectin (in combination with components mentioned above) is a “solid buffer” able to retain the PANI conductivity at neutral pH value without inducing its oxidation or reduction. For these reasons films based on pectin are electrochemically “inert”, thus they should not interfere with the ion exchange in more complex structures, they are good candidates for making an intermediate layer in bio-organic multilayers structures.

Verification and validation proof of "double-layer solid polyelectrolyte" technology for OMD was carried out by the integration of Physarum Policephalum (PPM) in this organic architecture. PPM was chosen as model living organism in this multilayer architecture for its peculiar properties that are fully characterized in this work. This thesis demonstrated that this hybrid “living” device operates reproducibly as a memristive device. A hysteretic-rectifying trend, typical of memristive devices,

appeared in current-voltage characteristic, what is happening because of the ion exchange through the living mould.

In a broader perspective, the device proposed here can be classified as a Bio-Organic /Memristive Device (BOMD), where the dual functionality allows merging of the sensing and memory properties, paving the way to new and unexplored opportunities in bioelectronics. In fact, the integration of biological elements with organic devices could in principle allow the direct monitoring of the internal cellular bioactivities, including cell metabolism and the reactions/interactions with environmental changes. The electrical transduction of such processes and the control of the mentioned “smart” functions that PPM for example is capable of to permit, pave the way to hybrid devices to implement new neuromorphic systems.

The present work is a starting point for the interfacing and integration of living organism with an electronic device based on polyaniline. The bio-organic prototype validates the so-called "double-layer solid polyelectrolyte" technology, which that was developed in this thesis, and that can be extended to other materials, opening and opens the possibility to assemble novel organic bio-integrated devices.

In addition, this thesis expands the knowledge of the working mechanisms and OMDs function. This study is useful to have a deeper understanding and control memristive properties of organic elements. As the result the "double-layer solid polyelectrolyte" technology is successfully developed.

Further efforts will be directed to the particular realization of more complex devices by through the integration of other biological elements such as proteins, some cells and, finally, neurons.

Appendix

A.1 Conductivity characterization: electrochemical impedance spectroscopy (EIS).

Impedance spectroscopy is a commonly used technique to determine electrical properties of polymer electrolytes. The use of alternating current (AC) techniques are preferred to direct current (DC) measurements because the data obtained by AC measurements contains information about long range migration of ionic species and polarization phenomena.

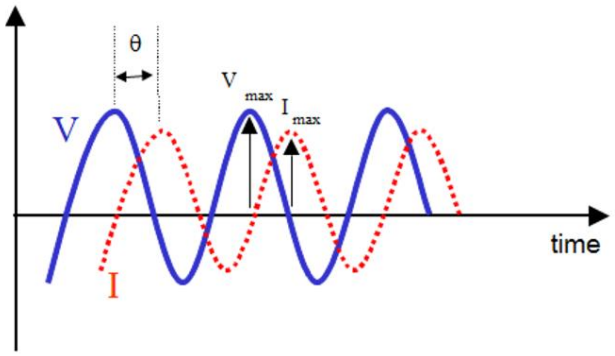

Figure A.1 Representation of applied sinusoidal voltage, resulting current and phase angle.

In an AC experiment, when a sinusoidal potential is applied to a cell, the resulting sinusoidal current passing through the cell is measured, with a focus on the phase difference between the two signals. I can have, in fact, a phase shift of the measured current (I) with respect to the applied AC potential (V) (see figure A.1, as example). The phase difference between V and I is called "phase angle" θ. Unlike in DC techniques, where I is related to V by one parameter, the resistance R, obeying a proportionality relation (eq. A.1), in AC measurements, therefore, I is related to V by two parameters, the resistance R, representing the "opposition" to the flow of charge, and the phase angle, θ. R and θ together define the impedance Z of the cell, which is a complex number (eq. A.2). In eq. A2(a), the symbol i is the imaginary unity. The relationship between radial frequency ω (radians/sec) and frequency f (Hertz=1/sec) is given in eq. A.3. Both the magnitude of the impedance Z and the phase angle θ depend on the radial frequency, ω. eq. A.4 give additional relations between, on one side, amplitude of the electrical signals and their phase shift with, on the other side, the magnitude of the impedance and their real and imaginary parts. Thus, AC measurements imply the measure of the complex impedance Z over a wide frequency range of the applied voltage signal [271].

$$V = IR \qquad \textit{Eq. A1}$$

$$Z^* = Z' - iZ'' \qquad \textit{Eq. A2(a)}$$

$$i = \sqrt{-1} \qquad \textit{Eq. A2(b)}$$

$$Z' = |Z|cos\theta \qquad \textit{Eq. A2(c)}$$

$$Z'' = |Z|sin\theta \qquad \textit{Eq. A2(d)}$$

Z‟ is the real component of complex number Z*.
Z" is the imaginary component of complex number Z*

$$\omega = 2\pi f \qquad \textit{Eq. A.3}$$

$$|z(\omega)| = \frac{V_{max}}{I_{max}} \qquad \textit{Eq. A4(a)}$$

$$tg(\theta)=Z''/Z' \qquad \textit{Eq. A.4(b)}$$

Generally speaking, real and imaginary parts of complex impedances can be plotted as distinct curves dependent on frequency; alternatively the data can be plotted in the (Z', Z") plane, resulting in the so called Nyquist plot; also the Bode plots (|Z| vs. frequency and θ vs. frequency) are used.

As the interpretation of measured complex impedance is difficult, the AC experiment results can be interpreted by constructing different equivalent circuits, depending on the physical system, and by determining which model better fits the data. In the present case, the model is an electrical circuit consisting of resistors and capacitors. For a purely resistive system, the applied voltage is in phase with the current, θ = 0 and |Z| = R and the impedance is frequency independent. In a complex impedance plot, i.e. a plot of Z'' vs. Z', this behavior is represented by a single point on the real axis Z', at a distance R from the origin (see figure A.2a). For a purely capacitive system, the voltage lags behind the current by 90°, θ = -π/2 and |Z| = 1/ωC, where C is the capacitance (figure A.2b). Here, |Z| is frequency dependent. In a complex impedance plot, this result is represented by series of points on the imaginary axis Z".

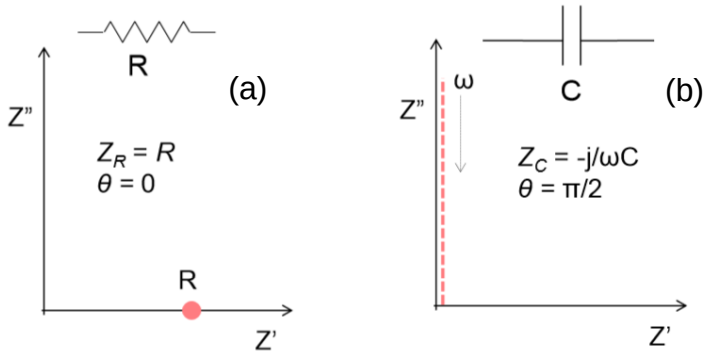

Figure A.2 Graphical representation of a resistor R (a) and capacitor C (b) and their behavior in the complex impedance plane.

A.2 Conductivity characterization of solid polyelectrolytes.

The circuit model generally used to describe the AC response of polymer electrolytes [272, 273] is shown in figure A.3. The electrical circuit consists of a parallel combination of a resistor R_b and a capacitor C_b, which is connected in series with another capacitor C_e. The resistance R_b accounts for the migration of ions in a polymer electrolyte, while the dielectric polarization of the polymer is related to the capacitive response (capacitance C_b) of the layer. By supposing a parallel-plate configuration, the dielectric constant ε of the polymer is related to C_b by eq. A.5.

$$C_b = \frac{\varepsilon\varepsilon_0\Sigma}{d} \qquad \textit{Eq. A.5}$$

where ε_o ($\varepsilon_0 = 8.8541\times10^{-12}$ F/m) is the vacuum permittivity, Σ is the electrode area and d is the separation between two electrodes. When an AC current is applied, ions migrate back and forth in the polymer matrix and, at the same time, the polymer chains become polarized. Thus, ion migration and polarization are two processes coexisting in the same space region (along the thickness of the electrolyte) and therefore C_b and R_b are connected in parallel. C_e represents, instead, processes of charge accumulation occurring at the interface between electrode and electrolyte, whose details depend on the geometry of the electrodes. In the figure below (Fig. A.3), two "contact capacitances" are considered, one for each electrode; in this geometry, each capacitance can be assumed as an additional parallel-plate capacitor.

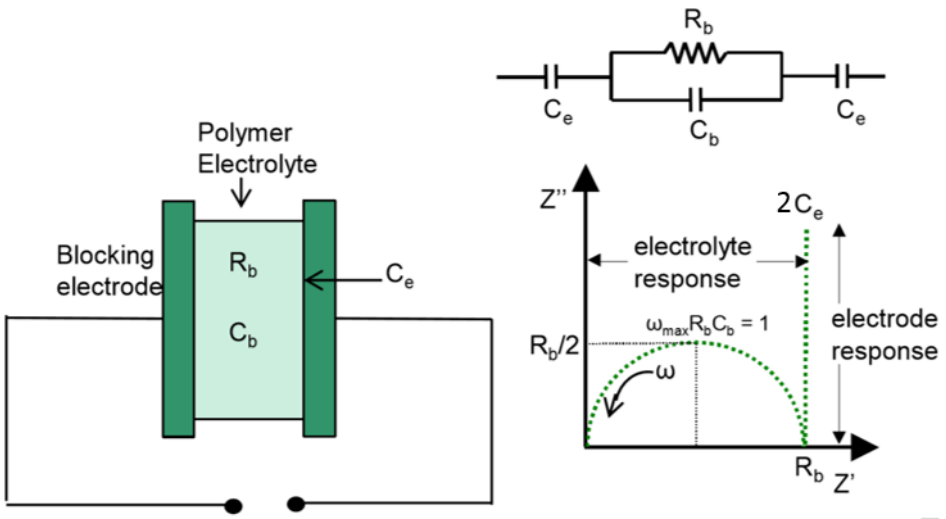

Figure A.3 To the right: sketch of cell for a polymer electrolyte sandwiched between two blocking electrodes. To the left: the equivalent circuit of the cell, and below an example of Nyquist plot.

The complex impedance response Z* for the circuit shown in figure A.3 is calculated below. C_e includes a factor 2 in the following equation.

$$Z^* = \left[\frac{1}{\left(\frac{1}{R_b} - \frac{\omega C_b}{i}\right)}\right] + \frac{-2i}{\omega C_e}$$

$$= \left[\left(\frac{R_b}{1 + i\omega C_b R_b}\right) \cdot \left(\frac{1 - i\omega C_b R_b}{1 - i\omega C_b R_b}\right)\right] - \frac{2i}{\omega C_e}$$

$$= \frac{R_b}{1 + \omega^2 C_b^2 R_b^2} - \frac{i\omega C_b R_b^2}{1 + \omega^2 C_b^2 R_b^2} - \frac{2i}{\omega C_e}$$

$$Z^* = R_b\left[\frac{1}{1 + (\omega R_b C_b)^2}\right] - i\left(R_b\left[\frac{\omega R_b C_b}{1 + (\omega R_b C_b)^2}\right] + \frac{2}{\omega C_e}\right) \qquad Eq.A.6$$

In figure A.3, the semicircular part of the Nyquist plot could give information, e.g., charge transfer processes in the polymer electrolyte. To the minimum imaginary response, on the side of the low frequencies, the capacitive contribution of the polymer becomes negligible and eq. A.6 reduces to $Z^*=R_b$, giving the bulk resistance of polymer electrolyte; which, it is related to the DC conductance. In intermediate frequency region, at the highest point of semicircle, occurring at a radial frequency named ω_{max}, bulk resistance and capacitance contribute equally to the impedance, so that $R_b=1/\omega_{max}C_b$. The product $R_bC_b=1/2\pi f$ has the dimension of a time, and has the meaning of a relaxation time, characterizing the relaxation processes occurring on the polyelectrolytes solutions. The capacitance of the electrolyte can be calculated from this relation, knowing R_b and ω_{max}. The low-frequency conductivity, σ_l, of the polymer electrolyte is determined from the eq. A.7, considering the polymer as a layer of uniform thickness, length t and section Σ. In this geometry, Σ is also the area of the sample in contact with the electrodes.

$$\sigma_l = \frac{t}{R_b \Sigma} \qquad Eq.A.7$$

A.3 Materials and Methods.

An experimental set up for an impedance spectroscopy investigation in polymeric material has been assembled and tested, by employing a prototypal electrochemical cell. Different alternative geometries were tested. The complete method of analysis of the data was developed, by properly taking into account the cell constants and including the effects of contact polarization with the aim to remove spurious effects from the acquired data.
All the impedance spectroscopy experiments reported in this thesis were performed using a 4284 LCR-meter fully interfaced and remotely controlled by a LabVIEW script working in the frequency range 50Hz-1MHz, although an intermediate frequency range was chosen for data analysis. The voltage amplitude of the oscillation level (applied alternating field) at RT was 500 mV. The measurements were performed at ambient room temperature (RT).
During the work, however, difficulties arisen due to uncontrolled deterioration effects of the metallic electrodes in the cell, so that the measurements remained at an initial stage of testing. A preliminary calibration of the cell was anyway performed using the sample holder shown in figure A.4.
It was designed to hold a small sample in a fixed geometry and stable and reproducible position during the measurement. The polymer was housed in a cavity of cylindrical shape, whose basic areas must function as electrodes; therefore the latter were made of alluminum or stainless steel coated with gold by sputtering. Length and cross-sectional area of the cell were precisely measured, although uncertaintly in the contact area of a poorly wetted electrode may be a source of error.
The structure, in Teflon, provides electrical insulation and assures the interlocking of the electrodes in appropriate holes, for the electrical connection. The top fixture is adjustable and its vertical motion is governed by screw mechanism.
Such an electrochemical cell was employed to perform some test-measurement on polyelectrolytes in gel phase, i.e. PEO, chitosan, pectin.

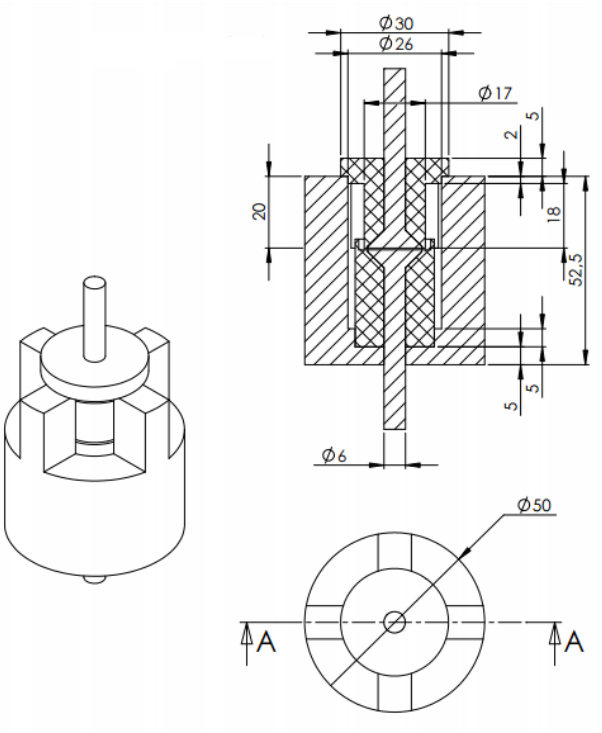

Figure A.4 Design of the sample holder used in measurements.

A calculation has been developed to fit the data, using MATHEMATICA©, a nonlinear regression fitting module of the Levenberg-Marquardt-algorithm. The routine was then tested by analyzing data taken from the literature, by reproducing the fitting of the curves, included the evaluation of the effects of the contacts.

A.4 Results and Discussion.

In order to develop a method of measurement of impedance spectra and to study of the ionic transport properties of polyelectrolytes, the preliminary determination of the dielectric constant of known materials was considered an essential step of the work, to verify the control of parasitic impedance contributions and/or systematic error in the measurement. In particular, the first goal was the measure of the dielectric constant of the commercial polymers interesting for this research (chitosan, pectin, PEO).
The dielectric constant and the dielectric loss are real ($Re(\varepsilon^*) = \varepsilon'$) and imaginary ($Im(\varepsilon^*) = \varepsilon''$) part of the dielectric response of a material, again a complex number, ε^*. Such a response can be derived assuming an equivalent circuit similar to that one shown by Fig. A.3, with a resistance (ECR) and a capacitance (C) in parallel configuration, so that the admittance Y^* of the circuit, rather than the impedance, is directly measured. The admittance is $Y^*=1/Z^*=G(\omega)+i\omega C(\omega))$, where G is the conductance (G=1/ECR) and C the capacitance. The connection between these parameters and the dielectric response is expressed by the relations: $C = \varepsilon_0\varepsilon' \Sigma/t$; $G = \omega\varepsilon_0\varepsilon'' \Sigma/t$, where Σ and t have yet the meaning of thickness and section of the conductive channel,. Note that the dielectric response is only dependent on the material, not on the geometry. Conductance and capacitance, instead, depend on the geometry of the experiment.
As concerns the dielectric constant, it is particularly significant for ion-conducting polymers, because it plays a fundamental role in the ability of a polymer to dissolve salts. In fact, it represents how well a material screens an external electric field, therefore it is a measure of the reduction of Coulomb interactions. A high dielectric constant reduces the ion-ion interactions. [274]. An operative definition of dielectric constant is given by the ratio of the capacitance C of a parallel-plate capacitor including a dielectric material over the capacitance C_0 of the same capacitor with vacuum (air) in between the plate electrodes [275].

The microscopic origin of the dielectric response can be described in terms of simple dipoles that attempt to align themselves to the electric field, as sketched in Fig. A.4. When an alternating electric field is applied, supposed uniform in direction and in instant value throughout the volume of the dielectric material, the permanent and induced dipoles try to follow the variations of the field. Several mechanisms of polarization in a dielectric material have been proposed, including electronic polarization, distortion polarization and orientation polarization [276].
A complete model, however, has also to include the polarization effects occurring at the electrodes [131].

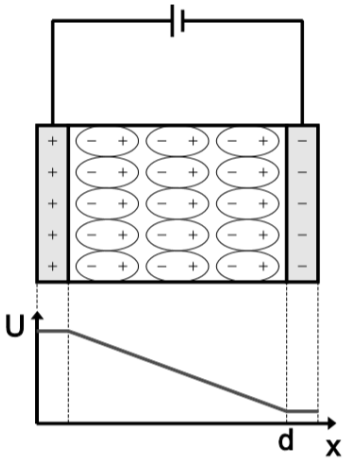

Figure A.4 Illustration of the polarization of a parallel-plate capacitor sandwiching a dielectric material and the electric potential profile across the capacitor.

In polar polymers, the dipoles require a certain time (>0.1 ns) to align themselves with the applied electric field [277]. Thus, the dielectric constant of a polar polymer is usually frequency-dependent with respect to the applied electric field. At very high frequencies (e.g. $>10^{10}$ Hz) the polar polymer does not have sufficient time to align completely with the applied electric field before it has again varied its direction, so that the dielectric constant resulted low. Oppositely, if the applied electric field alternates at low frequencies, the dipoles in the polymer have enough time to align with the electric field before it changes its direction. Polar polymers have higher dielectric constant at low frequencies. As the dipoles try to align themselves with an alternating electric field, they always slightly 'lag' behind the electric field, which is described as the phase angle (ϕ), and energy is thus absorbed by the friction caused by rotational motion of dipoles. The absorbed energy in molecular polarizations is measured by the dielectric loss. The amount of dielectric loss in a capacitor can be characterized quantitatively by the dissipation factor (tan(δ)).

$$tan(\delta) = Im(\varepsilon^*)/Re(\varepsilon^*) = \omega C \cdot ESR \quad Eq.\ A.8$$

where δ[°] is called the loss angle, which equals 90°- ϕ; ω[rad/s] is the angular frequency; C [F] is the capacitance and ESR [Ω] is the equivalent parallel resistance in the capacitor.
For polar polymers, the energy dissipation is low when the applied electric field has both very high ($>10^{10}$ Hz) and very low frequencies ($<<10^{10}$ Hz). But, at intermediate frequencies the dielectric loss is large due to "lag" of polarization [131].

A.4.1 Determination of the cell constant and the stray capacitance.

Before to perform any capacity measurement of polyelectrolytes, it is necessary to measure the cell constants, depending on the geometric characteristics of the cell [278].
I considered the model of Chun-Yan et al. [278] requires the determination of the cell constant C_l and the stray capacitance C_r by using two standard liquids (pure water, ethanol) and air,
The figure A.5 reports the experimental curves. The trend of capacity versus the frequency is reported in range between $4 \cdot 10^3 - 4 \cdot 10^5$ Hz.

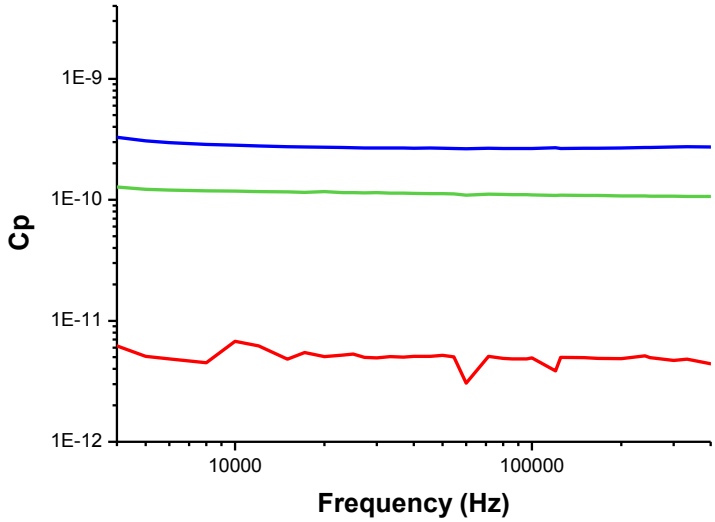

Figure A.5 Plot of capacity (Cp, measured in parallel configuration) versus the frequency for the H_2O (blue line); EtOH (green line) and air (red line).

The measured capacity presents constant values only in the range between $4 \cdot 10^3$ Hz and $4 \cdot 10^5$ Hz. The experimental capacity values for the two standard liquids (water and ethanol) are $(2.492 \pm 0.005) \cdot 10^{-10}$ F ($C^{H2\,O}$) and $(7.60 \pm 0.02) \times 10^{-11}$ F (C^{EtOH}) respectively.
By solving the following system of equations $A9$a, it is possible to obtain the equations A9 (b-d).
Known the values of dielectric permittivity of pure water (80.4) and ethanol (24.3) it is possible to determine the cell constant C_l and the stray capacitance C_r. The cell constant C_l and the stray capacitance C_r were determined by using the standard liquids are 3.1pF and 0.67 pF, respectively.

$$\begin{cases} \varepsilon_{EtOH} = \dfrac{C^{EtOH} - C_r}{C_l} \\ \varepsilon_{H_2O} = \dfrac{C^{H2\,O} - C_r}{C_l} \end{cases} \qquad Eq.A9(a)$$

$$C_r = C^{EtOH} - C_l \varepsilon_{EtOH} \qquad Eq.A9(b)$$

$$C_l = \frac{C^{H2\,O} - C^{EtOH}}{\varepsilon_{H_2O} - \varepsilon_{EtOH}} \qquad Eq.A9(c)$$

$$C_r = C^{EtOH} - \varepsilon_{EtOH} \frac{C^{H2\,O} - C^{EtOH}}{\varepsilon_{H_2O} - \varepsilon_{EtOH}} \qquad Eq.A9(d)$$

In order to obtain true conductance and capacitance of a sample, all the raw data were subjected to proper corrections for the errors due to stray capacitance C_r and the cell constant C_l. The raw data of conductance G and capacitance C at each frequency were converted to the corresponding dielectric permittivity ε and conductivity σ according to the following equations: $\varepsilon = (C - C_r)/C_l$ and $\sigma = G\varepsilon_0/C_l$
Also the residual inductance L_r due to the terminal leads affects the measured conductance G and capacitance C value. The values of C and G measured directly were subjected to modification by the following equations [279]:

$$C_s = \frac{C_x\left(1+\omega^2 L_r C_x\right)+ L_r G_x^2}{(1+ \omega^2 L_r C_x)^2+(\omega L_r G_x)^2} - C_r \qquad Eq.A10$$

$$G_s = \frac{G_x}{(1+ \omega^2 L_r C_x)^2+(\omega L_r G_x)^2} \qquad Eq.A11$$

where the subscript *x* and *s* denote the directly measured and modified values, respectively.
The value of the residual inductance L_r should be determined by use of standard KCl solutions with different concentration by the relation $C=L_rG^2$. But, in the study proposed in this Appendix the determination of residual inductance L_r was not performed because several experimental difficulties were found associated with an uncontrolled and progressive deterioration of the metal electrodes in subsequent measurements. Thus, the measured conductance G and capacitance C values were not reproducible. In any case, the data of the preliminary calibration of the cell reported in this paragraph refer to the undamaged cell, designed to perform capacitance measurements.
For these reasons, the work was continued by focusing on the analysis of data taken from the literature, in order to complete the routine for the analysis of the data.

A.4.2 Correction of the data for contact polarization.

Independently of the mentioned difficulties in the experiments, all the data relative to the polyelectrolyte investigated presented an exponential increase of the capacitance by decreasing the frequency. As example, the frequency dependence of capacitance of PEO (30 mg/mL in pure water solution, see par. 3.3) is reported in figure A.6. This behavior is known in the literature [280] and is attributed to electrode polarization effect. It is a spurious contribution superimposed to the true dielectric response of the polymer and it is not eliminable through the constant-cell correction. However, it can be removed "a posteriori" from the raw data by software. Thus, the first step of my data analysis was the develop of the calculation routine to perform such a correction. The method was applied to experimental data taken from the literature relative to dielectric permittivity of chitosan solutions. These data are reported in figure A.7 as a function of the frequency, for different concentrations of 0.01, 0.08, 0.4, 0.8, 1.6, 2.4 mg/mL^{-1}, at 25 °C [278].

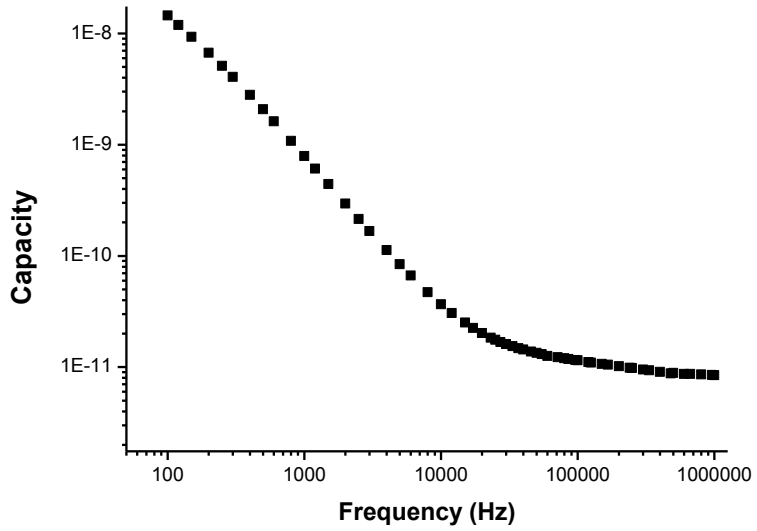

Figure A.6 Frequency dependence of capacitance of PEO (30mg/mL in H_2O milli-Q), 500 mV oscillation level.

The calculation was based on the following theory. Under an applied electric field, the dielectric properties of a polyelectrolyte aqueous solution can be characterized by the complex permittivity ε* which is defined as: [281, 282]

$$\varepsilon^* = \varepsilon - \frac{i\sigma}{\omega\varepsilon_0} = \varepsilon - i\left(\varepsilon'' - \frac{\sigma_l}{\omega\varepsilon_0}\right) \qquad Eq.A12$$

where ε and σ is the permittivity and conductivity of the system as mentioned above, ε'' is the dielectric loss, σ_l is the low-frequency limit of conductivity, and i = $(-1)^{1/2}$. The measured dielectric loss $\sigma/(\varepsilon_0\omega)$ consists of two parts, one part is the contribution of DC electric conductivity $\sigma_l/(\varepsilon_0\omega)$, and another is the dielectric loss, ε''[278].

The high ionic electrical conductivity of polyelectrolyte solutions o gels (about $9\cdot10^{-3}$- 5.4 S m^{-1}) causes a giant frequency-dependent electrode polarization, which masks the relaxation behavior at low-frequency range [281]. In order to remove the electrode polarization, the method of Mitsumata et al. [283]. By fitting the experimental data with the Cole-Cole equation, i.e. *eq. A13*, which includes electrode polarization term $A\omega^{-m}$, to the experimental data, both the dielectric parameters and $A\omega^{-m}$ were determined by according to [283-285]. Then, the corrected data were obtained by subtracting the $A\omega^{-m}$ contribution from the experimental data. In this contest, *A* and *m* are adjustable parameters.

$$\varepsilon^* = \varepsilon_h + \frac{\Delta\varepsilon_l}{1+(i\omega\tau_l)^{\beta_l}} + \frac{\Delta\varepsilon_h}{1+(i\omega\tau_h)^{\beta_h}} + A\omega^{-m} \qquad Eq.A13$$

where $\Delta\varepsilon_l(=\varepsilon_l - \varepsilon_m)$ and $\Delta\varepsilon_h(=\varepsilon_m - \varepsilon_h)$ are low and high frequency dielectric increment, respectively, τ ($\tau = 1/2\pi f_0$) is the characteristic relaxation time, f_0 is the characteristic relaxation frequency, β is the Cole-Cole parameter ($0 < \beta \leq 1$, $\beta = 1$ is the Debye relaxation) denoting the width of the distribution of relaxation times. The subscripts *l*, *m*, and *h* denote the low, medium, and high frequency limit values, respectively.

At last, the dielectric relaxation parameters are obtained by fitting the eq. $A14$ to the corrected data.

$$\varepsilon^* = \varepsilon_h + \frac{\Delta\varepsilon_l}{1+(i\omega\tau_l)^{\beta_l}} + \frac{\Delta\varepsilon_h}{1+(i\omega\tau_h)^{\beta_h}} \qquad Eq.A14$$

In order to obtain the ε''- f curve, it is necessary to calculate ε'' from the σ_l with eqn. $A15$. The k_l can be obtained through the σ''– σ plot. The imaginary part σ''of the conductivity can be calculated from the obtained dielectric parameters ε_h, with eq. $A16$.

$\varepsilon'' = (\sigma - \sigma_l)/\omega\varepsilon_0$ $\qquad A15$

$\sigma'' = \omega\varepsilon_0\ (=\varepsilon - \varepsilon_h)$ $\qquad A16$

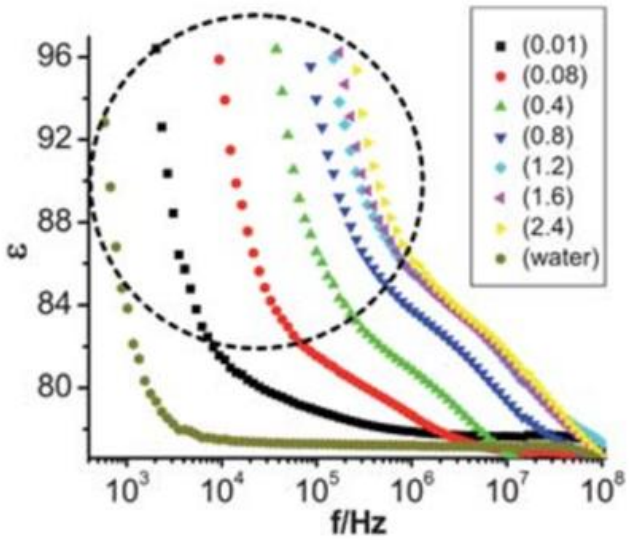

Figure A.7 Frequency dependence of dielectric permittivity of chitosan solutions with different concentrations of 0.01, 0.08, 0.4, 0.8, 1.6, 2.4 mg/mL^{-1}, at 25 °C [278].

The first step of this analysis consisted in the digitalization of the curve reported by Liu et al. [278] (figure A.7, black points). It is the frequency dependence of dielectric permittivity of chitosan solution (0.8 mg/mL^{-1}), at 25 °C

The dielectric data were fit by utilizing a program that incorporated the MATHEMATICA© nonlinear regression fitting module of the Levenberg-Marquardt-type.

The data obtained from digitalization routine carried out by Origin software is reported below.

```
data =
{{95964,94},{81632,96},{112811,93},{129024,91},{147566,90},{168773
,89},{198403,89},{226916,88},{253267,87},{289664,87},{331293,86},{
389455,86},{457828,85},{632693,85},{723618,84},{805189,84},{946549
,84},{1.2^6,84},{1^6,83},{1.4^6,83},{1.6^6,83},{1.8^6,83},{1.9^6,8
3},{2.2^6,82},{2.4^6,82}{2.9^6,82},{3.3^6,82},{3.7^6,81},{4.3^6,81
},{4.9^6,81},{5.9^6,80},{765699,84},{851474,84},{1000000,84},{1.2^
6,83},{1.3^6,83},{1.5^6,83},{1.7^6,834},{2^6,83},{2.2^6,82},{2.5^6
,82}};
model=A*x^-m
fit = FindFit[data,model,{A,m},x,Method -> "LevenbergMarquardt",
MaxIterations -> 100,PrecisionGoal-> 1,AccuracyGoal-> 1]
modelf= Function[{x},Evaluate [model/.fit]]
Plot[modelf[x],{x,95500,2.5^6},Epilog -> Map[Point,data]]
Plot[data//Evaluate,{x,95500,2.5^6}]
```

$$Ax^{-m}$$

$$\{A \to 1.057071489575624, m \to 0.8307994295595047\}$$

$$\text{Function}[\{x\}, \frac{1.057071489575624}{x^{0.8307994295595047}}]$$

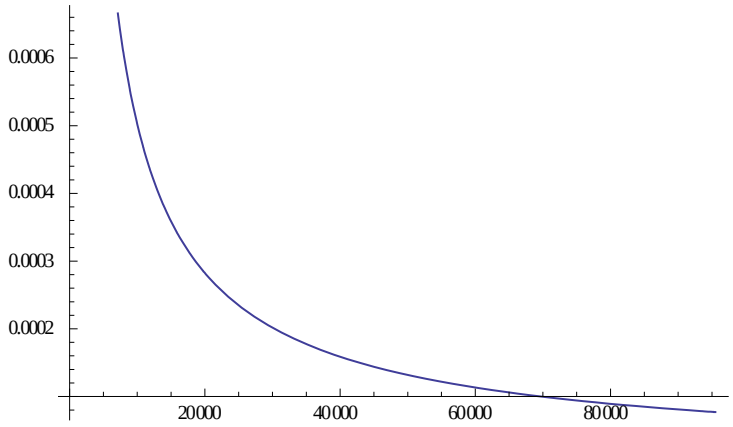

Figure A.8 Fitting of data using the model $A\omega^{-m}$.

The figure A.8 shows the curve obtained by evaluating the contribution $A\omega^{-m}$, using the parameters obtained by fitting of data.

Then, I compered the fitting obtained by the contribution $A\omega^{-m}$ with another model, in order to confirm the validity of the approach.

Klein et al. [286] proposed a simplified version of equation A13, where the electrode polarization (EP) is found to be represented by a simple Debye relaxation, considering only a relaxation time τ_l :

$$\varepsilon^*_{EP} = \varepsilon_R + \frac{\Delta\varepsilon_{EP}}{1 + i\omega\tau_{EP}} \qquad A17$$

$$\varepsilon_R = \text{dielectric permittivity (indipendent from EP)}$$
$$\Delta\varepsilon_{EP} = \varepsilon_{R,EP} - \varepsilon_R$$

The real part of the equation is:

$$\varepsilon'_{EP} = \varepsilon_R + \frac{\Delta\varepsilon_{EP}}{i\omega^2\tau^2_{EP}} \qquad A18$$

The digitized data were fitted by the model reported below (eq. *A19*).

$$e + Ax^{-m} + \frac{d}{1 + c^2x^2} \qquad A19$$

```
data =
{{95964,94},{81632,96},{112811,93},{129024,91},{147566,90},{168773
,89},{198403,89},{226916,88},{253267,87},{289664,87},{331293,86},{
389455,86},{457828,85},{632693,85},{723618,84},{805189,84},{946549
,84},{1.2^6,84},{1^6,83},{1.4^6,83},{1.6^6,83},{1.8^6,83},{1.9^6,8
3},{2.2^6,82},{2.4^6,82}{2.9^6,82},{3.3^6,82},{3.7^6,81},{4.3^6,81
},{4.9^6,81},{5.9^6,80},{765699,84},{851474,84},{1000000,84},{1.2^
6,83},{1.3^6,83},{1.5^6,83},{1.7^6,834},{2^6,83},{2.2^6,82},{2.5^6
,82}};
model=(A*(x^-m))+e+(d/(1+(x^2*c^2)))
```

```
fit = FindFit[data,model,{A, m,e,d,c},x,Method ->
"LevenbergMarquardt", MaxIterations -> 1000,PrecisionGoal->
1,AccuracyGoal-> 1]
modelf= Function[{x},Evaluate [model/.fit]]
Plot[modelf[x],{x,95500,2.5^6},Epilog -> Map[Point,data]]
```

$$e + Ax^{-m} + \frac{d}{1 + c^2x^2}$$

$$\{A \to 1.0650393219330534, m \to 0.806073522545129, e \to 1.1047414656330097, d \to 1.0914597919809605, c \to 0.8987505000161475\}$$

$$\text{Function}[\{x\}, 1.1047414656330097 + \frac{1.0650393219330534}{x^{0.806073522545129}} + \frac{1.0914597919809605}{1 + 0.8077524612792752x^2}]$$

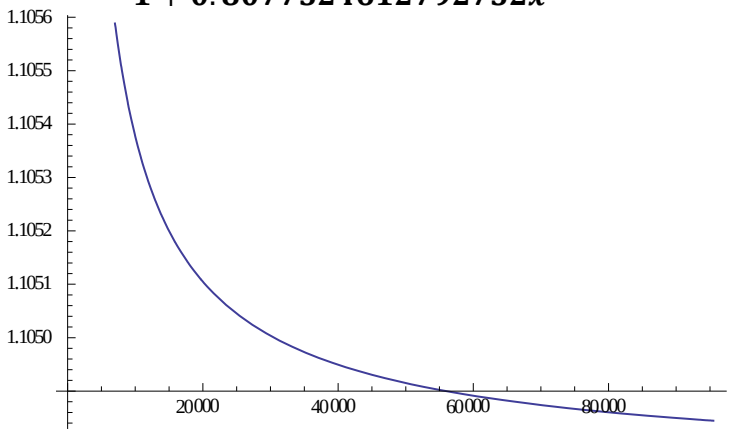

Figure A.9 Fitting of the low frequency data using the model: $e + Ax^{-m} + \frac{d}{1+c^2x^2}$.

Note that the same parameters were found by using both model ($A\omega^{-m}$,) and ($e + Ax^{-m} + \frac{d}{1+c^2x^2}$).

The function

$$Ax^{-m}$$

$$\{A \to 1.057071489575624, m \to 0.8307994295595047\}$$

was evaluated in the frequency range 10^2 – 10^6 Hz. In this way, the curve that represents the "effect of electrode polarization" is obtained.

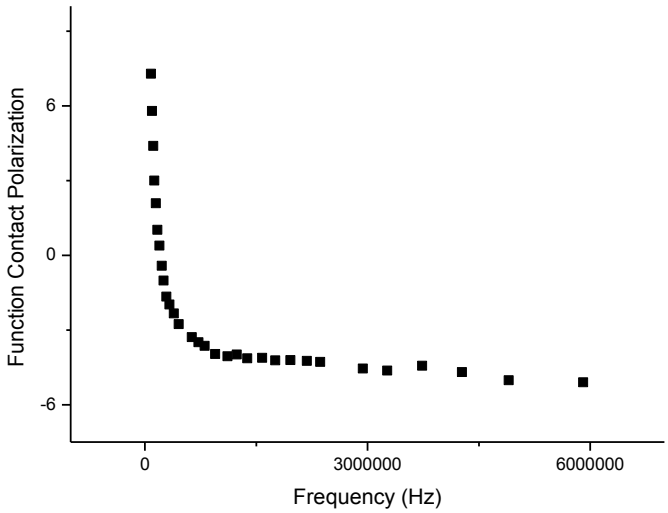

Figure A.10 Function that represents the "effect of electrode polarization".

Then, the contribution of exponential function ("function of effect of electrode polarization") was subtracted from the digitized curve. Finally, the curve that represents the frequency dependence of dielectric permittivity without the electrode polarization (EP) contribution was obtained.

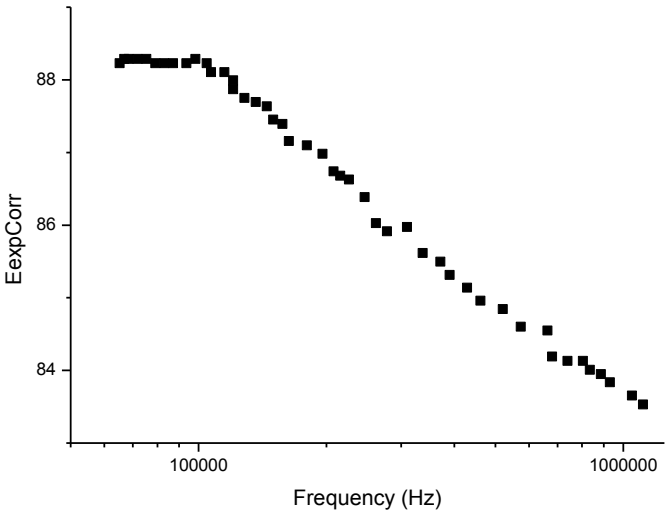

Figure A.11 Frequency dependence of dielectric permittivity without the EP contribution.

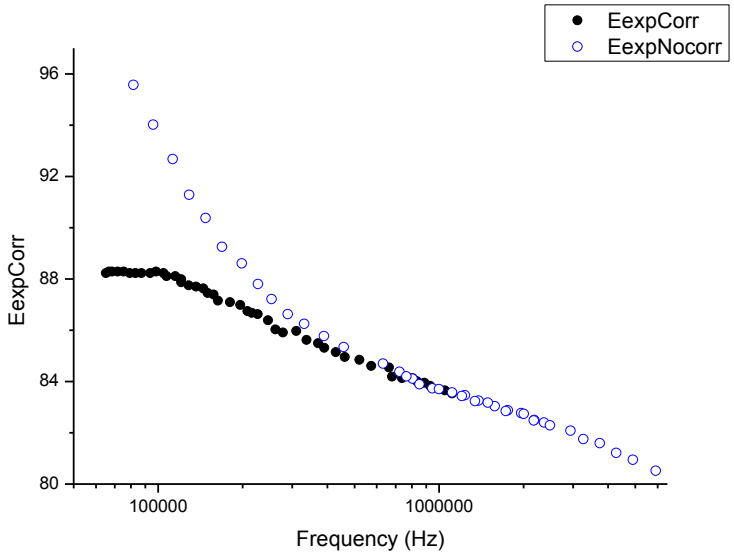

Figure A.12 Comparison between (the frequency dependence of dielectric permittivity with EP contribution (the digitized curve, blue symbols) and the frequency dependence of dielectric permittivity without the EP contribution (black symbols).

It is possible to conclude that a suitable method for the analysis of the frequency dependence of dielectric permittivity of polyelectrolyte solutions or gels was identified. The method for data analysis takes into account the strong contribution of electrode polarization that affects the experimental data. The correction described in the Appendix of this thesis is necessary for all systems with a high water content as well as for polyelectrolytes in a quasi-dried state.

Bibliography

[1] N.F. Lepora, P. Verschure, T.J. Prescott, *Bioinspir. Biomim.* (2013) **8**, 013001. doi:10.1088/1748-31828/1/013001

[2] N. Huebsch, D.J. Mooney, *Nature* (2009) **462**, 426. doi:10.1038/nature08601.

[3] M.A. McEvoy, N. Correll,. *Science* (2015) **347**, 1261689. doi: 10.1126/science.1261689.

[4] D. Kuzum, S.M. Yu, Wong, H.S.P. *Nanotech.* (2013) **24**, 382001.

[5] J. Grollier, Julie. "From Spin Torque Nano-Oscillators to Memristors: Multi-Functional Nanodevices for Advanced Computing." arXiv preprint arXiv:1407.1494 (2014).

[6] W. Xu, S.-Y. Min, H. Hwangand, T.-W. Lee, *Sci. Adv.* (2016) **2**, e1501326. doi:10.1126/sciadv.1501326

[7] V. Erokhin, M.P. Fontana, *J. Comput. Theor. Nanosci.* (2011) **8**, 313.

[8] S. M. Yu, Y. Wu, R. Jeyasingh, D.G. Kuzum, H.S.P. Wong, IEEE *Trans. Electron Devices* (2011) **58**, 2729.

[9] Q. Lai, L. Zhang, Z. Li, W.F. Stickle, R.S. Williams, Y. Chen, *Adv. Mater.* (2010) **22**, 2448.

[10] L. Q. Zhu, C. J. Wan, L. Q. Guo, S. Yi, Q. Wan, *Nat. Commun.* (2014) **5**, 3158.

[11] K. Kim, C. L. Chen, Q. Truong, A. M. Shen, Y. A Chen, *Adv. Mater.* (2013) **25**, 1693.

[12] N. Locatelli, V. Cros, J. Grollier. *Nature materials* (2014) **13**, 11.

[13] Z. Q. Wang, H. Y. Xu, X. H. Li, H. Yu, Y. C. Liu, X. J. Zhu, *Adv. Funct. Mater.* (2012) **22**, 2759.

[14] J. Grollier, D. Querlioz, M.D. Stiles. "Spintronic Nanodevices for Bioinspired Computing."*Proceedings of the IEEE* (2016) **104**, 2024.

[15] Z. Wang, S. Joshi, S. E. Savel'ev, H. Jiang, R. Midya, P. Lin, M. Hu, N. Ge, J.P. Strachan, Z. Li, Q. Wu, M. Barnell, G.-L. Li, H. L. Xin, R. S. Williams, Q.Xia, J. J. Yang, *Nature Materials* (2016) **16**, 101. doi: 10.1038/nmat4756.

[16] A. Richter-Dahlfors, K. Svennersten, K. C. Larsson and M. Berggren, *Biochim. Biophys. Acta*, (2011) **1810**, 276.

[17] J. Rivnay, P. Leleux, M. Ferro, M. Sessolo, A. Williamson, D. A. Koutsouras, D. Khodagholy, M. Ramuz, X. Strakosas, R. M. Owens, C. Benar, J.M. Badier, C. Bernard, G. G. Malliaras, S*cience Advances* (2015) **1**, e1400251.

[18] G. G. Malliaras, *Biochim. Biophys. Acta* (2013) 1830, 4286.

[19] M. Zanetti, D. Maniglio, C. Fasoli, M. Pola, E. Borga, C. Corradi, M. Dalla Serra, S. Iannotta, A. Motta, T. Toccoli, *Electroanalysis* (2014) **26**, 1653.

[20] J.J. Park, X. Luo, H. Yi, T.M. Valentine, G.F. Payne, W.E. Bentley, R. Ghodssi, G.W. Rubloff, *Lab Chip* (2006) **6**, 1315.

[21] W.E. Bentley, G.F. Payne, G.W. Rubloff, R.A. Ghodssi, *Lab Chip* (2005) **5**, 583.

[22] E. Kim, Y. Xiong, Y. Cheng, H.-C. Wu, Y. Liu, B.H. Morrow, H. Ben-Yoav, R. Ghodssi, G.W. Rubloff, J. Shen, W. E. Bentley, X. Shi, G.F. Payne. *Polymers* (2015) **7**, 1.

[23] L.Wang, J. Yoshida, N.Ogata, *Chem. Mater.* (2001) **13**, 1273.

[24] J.A. Hagen, W. Li, A.J. Steckl, J.G. Grote, *Appl. Phys. Lett.* (2006) **88**, 171109.

[25]©Source: SRI Consulting Business Intelligence (SRIC-BC; Menio Park, CA, USA) https://ir.nctu.edu.tw/bitstream/11536/79881/1/251001.pdf

[26] Y. Liu, E. Kim, R. Ghodssi, G.W. Rubloff, J.N. Culver, W.E. Bentley, G.F. Payne. *Biofabrication* (2010) **2**, 022002.

[27] T. Gordonov, E. Kim, Y. Cheng, H. Ben-Yoav, R. Ghodssi, G. Rubloff, J.J.Yin, G.F. Payne, W.E. Bentley, *Nat. Nanotechnol.* (2014) **9**, 605.

[28] Z. T. Zhu, J. T. Mabeck, C. Zhu, N. C. Cady, C. A. Batt, G. G. Malliaras, *Chem. Commun*., 2004, 1556.

[29] D. Nilsson, M. Chen, T. Kugler, T. Remonen, M. Armgarth, M. Berggren, *Adv. Mater.* (2002) **14**, 51.

[30] G. Cellot, P. Lagonegro, G. Tarabella, D. Scaini, F. Fabbri, S. Iannotta, M. Prato, G. Salviati, L. Ballerini, *Front Neurosci.* (2015) **9**, 521.

[31] G. Tarabella, P. D'Angelo, A. Cifarelli, A. Dimonte, A. Romeo, T. Berzina, V. Erokhin, S. Iannotta, *Chem. Sci*, (2015) **6**, 2859.
[32] L.E.P. Dietrich, T.K. Teal, A. Price-Whelan, D.K. Newman, *Science* (2008) **321**, 1203.
[33] D. Koley, M.M. Ramsey, A.J. Bard, M. Whiteley, *Proc. Natl. Acad. Sci. USA* (2011) **108**, 19996.
[34] G.W. Lau, D.J. Hassett, H. Ran, F. Kong, *Trends Mol. Med*. (2004) **10**, 599.
[35] D.A. Recinos, M.D. Sekedat, A. Hernandez, T.S. Cohen, H. Sakhtah, A.S. Prince, A. Price-Whelan, L.E.P. Dietrich, *Proc. Natl. Acad. Sci. USA* (2012) **109**, 19420.
[36] I. Willner, *Science* (2002) **298**, 2407.
[37] B.D. Ratner, S.J. Bryant, *Annu. Rev. Biomed. Eng.* (2004) **6**, 41.
[38] D. D. Ordinario, L. Phan, W. G. Walkup, J.-M. Jocson, E.Karshalev, N. Hüsken, A. A. Gorodetsky, *Nat. Chem.* (2014) **6**, 597.
[39] C.Y. Lee, J.-C. Hwanga, Y.-L. Chueha, T.-H. Changa, Y.-Y. Chengb, P.-C. Lyub, *Org. Electron* (2013) **14**, 2645.
[40] H. Wang, F. Meng, Y. Cai, L. Zheng, Y. Li, Y. Liu, Y. Jiang, X. Wang, X. Chen *Adv. Mater.* (2013) **25**, 5498.
[41] H. Wang, F. Meng, B.Zhu, W.R. Leow, Y. Liu, X. Chen, *Adv. Mater*. (2015) **27**, 7670.
[42] Y.C. Chen, C.Y. Huang, S.L. Wu, Y.K.Su, *Scientific Reports* (2015) **5**, 10022.
[43] W-P Su, J.R. Schrieffer, A.J. Heeger, *Phys. Rev. Lett.* (1979) **42**, 1698.
[44] A. G. MacDiarmid, "The Polyaniline: A Novel Class of Conducting Polymers. In Conjugated Polymers and Related Materials", W. R. Salaneck, I. Lundstrom, B. Ranby (Eds.), Oxford Science Publication. New York (1993) 73-98.
[45] A. J. Heeger, *Rev. Mod. Phys.* (2001) **73**, 681.
[46] C. K. Chiang, C. R. Fincher, Y. W. Park, A. J. Heeger, H. Shirakawa, E. J. Luis, S. C. Gau, A. J. MacDiarmid, *Phys. Rev. Lett.* (1977) **1098**, 1098.
[47] G. M. Silva, *Synth. Met.* (2001) **119**, 225.
[48] J. Brédas, R. Chance, R. Silbey, *Phys. Rev. B* (1982) **26**, 5843.
[49] L. Miller, Q. X. Zhou, *Synth. Met.* (1987) **20**, 1594.
[50] J. L Wojkiewicz, S. Fauveaux, N. Redon, *Int. J. Appl. Electrom. Mechanics*, (2004) **19**, 203.
[51] B.*Ong*, Y. Wu, L. Jiang, P. Liu, K. Murti, *Synth. Met.* (2004) **142**, 49.
[52] L. Chua, Memristor, *IEEE Trans. Circuit Theory* (1971) **18**, 507519.
[53] D.B. Strukov, G.S. Snider, D.R. Stewart, R.S. Williams, *Nature* (2008) **453**, 80.
[54] R.M. Fano, L.J. Chu, R.B. Adler, *Am. J. Phys*. (1961) **29**, 562.
[55] L. Chua, M. Hasler, G.S. Moschytz, J. Neirynck, IEEE Trans. Circuits Syst. I, Fundam. Theory. (1995) **42**, 559.
[56] K. Cai, J. Sun, B. Li, J. Zhoua, *ECS J. Solid State Sci. Tech*. (2013) **2**, 6.
[57] F.A. Buot, A.K. Rajagopal, *J. Appl. Phys.* (1994) **76**, 5552.
[58] J.H. Krieger, S.V. Trubin, S.B. Vaschenko, N.F. Yudanov, *Synth. Met.* (2001) **122**, 199.
[59] G.S. Snider, *Nanotechnology* (2007) **18**, 365202.
[60] G.S. Snider, *Appl. Phys.* A. (2005) **80**, 1165.
[61] P.J. Kuekes, G.S. Snider, R.S. Williams, *Sci. Am.* (2005) **293**, 72.
[62] D.B. Strukov, G.S. Snider, D.R. Stewart, R.S. Williams, Nature (1971) **453**, 80.
[63] T. Prodromakis, K. Michelakis, C. Toumazou, *Phys. Rev*. (2010) **2,** 1520.
[64] N. Gergel-Hackett, B. Hamadani, B. Dunlap, J. Suehle, C. Richter, C. Hacker, *IEEE Electr. Device L.* (2009) **30**, 706–708.
[65] N.C. Cady, M. Bergkvist, N.M. Fahrenkopf, P.Z. Rice, J.V. Nostrand, "Biologically self-assembled memristive circuit elements". In: Circuits and Systems (ISCAS), Proceedings of IEEE (2010) 1959-1962.
[66] T. Driscoll, J. Quinn, S. Klein, H.-T. Kim, B.J. Kim, Y.V. Pershin, *Appl. Phys. Lett.* (2010) **97**, 093502.
[67] T. Driscoll, H.-T. Kim, B.-G. Chae, M. Di Ventra, D.N. Basov, *Appl. Phys. Lett.* (2009) **95**, 043503.
[68] T. Driscoll, H.-T. Kim, B.-G. Chae, B.-J. Kim, Y.-W. Lee, N.M. Jokerst, *Science* (2009) **325**, 1518.

[69] R. Muenstermann, T. Menke, R. Dittmann, R. Waser, *Adv. Mater.* (2010) **22**, 4819.
[70] A.A. Zakhidov, B. Jung, J.D. Slinker, H.D. Abruña, G.G. Malliaras, *Org. Electron.* (2010) **11**, 150.
[71] D. Sacchetto, M.H. Ben-Jamaa, S. Carrara, G. De Micheli, Y. Leblebici, *Infoscience.epfl.ch*. (2010) 9.
[72] E. Lehtonen, J.H. Poikonen, M. Laiho, *Electronics Letters.* (2010) **46**, 230.
[73] D. Conti, A. Lamberti, S. Porro, P. Rivolo, A. Chiolerio, C. Pirri, C. Ricciardi Nanotechnology, (2016) **27**, 485208.
[74] S. Porro, A. Jasmin, K. Bejtka, D. Conti, D. Perrone, S. Guastella, C. Pirri, A. Chiolerio, C. Ricciardi, *J. Vac. Sci. Technol.* (2016) **34**, 01A147.
[75] T. Driscoll, H.-T. Kim, B.-G. Chae, B.-J. Kim, Y.-W. Lee, N.M. Jokerst, *Science* (2009) **325**, 1518.
[76] V. Erokhin, T. Berzina, K. Gorshkov, P. Camorani, A. Pucci, L. Ricci, G. Ruggeri, R. Sigalad, A. Schuz, *J. Mater. Chem.* (2012) **22**, 22881.
[77] V. Erokhin, T. Berzina, P. Camorani, M. P. Fontana, *BioNanoSci.* (2011) **1**, 24. doi: 10.1007/s12668-011-0004-7.
[78] S.H. Jo, K.H. Kim, T. Chang, S. Gaba, W. Lu, Si "Memristive devices applied to memory and neuromorphic circuits", in: Circuits and Systems (ISCAS), Proceedings of IEEE (2010) 13–16.
[79] G.S. Snider, *Nanotechnology* (2007) **18**, 365202.
[80] V. Erokhin, T. Berzina, M.P. Fonatana, *J. Appl.Phys.* (2005) **97**, 064501.
[81] T. Berzina, V. Erokhin, M.P. Fontana M.P., *J. Appl.Phys* (2007) **101**, 024501.
[82] G. Roberts, "Langmuir-Blodgett Films" Plenum Press, New York. (1990) 93.
[83] K. Roßberg, G. Paasch, L. Dunsch, S. Ludwig, *J. Electroanal. Chem*. (1998) **443**, 49.
[84] D.O. Hebb "Distinctive features of learning in the higher animal". In "Brain Mechanisms and Learning", J. F. Delafresnaye (Ed.), Oxford University Press, London (1961).
[85] J. Reddinger, J. Reynolds, "Molecular Engineering of π-Conjugated Polymers". In "Advances in Polymer Science" Springer: Berlin, Heidelberg, Germany (1999) 145, 57–122.
[86] A.A. Syed, M.K. Dinesan, *Talanta* (1991) **8**, 815.
[87] J. Gong, R.-N. Hua1, Z.-W. Xie1, S.-G. Wang, L.-Y. Qu, *Polym. J.* (2001) **33**, 377.
[88]doi:10.1295/polymj.33.377 E.M. Geniès, A. Boyle, M. Lapkowski, C. Tsintavis, *Synth. Met.* (1990) **36**, 139.
[89] W.-S. Huang, B.D. Humphrey, A.G. MacDiarmid, *J. Chem. Soc. Faraday Trans. 1* (1986) **82**, 2385.
[90] S. Bhadra, D. Khastgir, N.K. Singha, J.H. Lee, *Prog. Polym. Sci.* (2009) **34**, 783.
[91] A. J. Epstein, J.M. Ginder, F. Zuo, R.W. Bigelow, *Synth. Met.* (1987) **18**, 303.
[92] D. Ofer, R.M. Crooks, M.S. Wrighton, *J. Am. Chem. Soc.* (1990) **112**, 7869.
[93] M. Nechtschein, F. Genoud, C. Menardo, K. Mizoguchi, J.P. Travers, B. Villeret, *Synth. Met.* (1989) **29**, 211.
[94] H. He, J. Zhu, N.J. Tao, L.A. Nagahara, I. Amlani, R. Tsui, *J. Am. Chem. Soc.* (2001) **123**, 7730.
[95] D. Zhang, Y. Wang, *Mater. Sci. Eng. B* (2006) **134**, 9.
[96] J.G. Masters, Y. Sun, A.G. MacDiarmid, A.J. Epstein, *Synth. Met.* (1991) **41**, 715.
[97] A.G. MacDiarmid, J.C. Chiang, A.F. Richter, A.J. Epstein, *Synth. Met.* (1987) **18**, 285.
[98] J.C. Chiang, A.G. MacDiarmid, *Synth. Met.* (1986) **13**, 193.
[99] J.Yano, M. Kobayashi, S. Yamasaki, Y. Harima, K. Yamashita, *Synth. Met*. (2001) **119**, 315.
[100] V. Gupta, N. Miura, *Electrochem. Commun.* (2005) **7**, 995.
[101] S. Dong, Z. Sun, Z. Lu, *J. Chem. Soc.* (1988) 10, 993.
[102] Zh. A. Boeva, V. G. Sergeyev, *Polym. Sci. C* (2014) **56**, 153.
[103] Kh. Ghanbari, M. F. Mousavi, M. Shamsipur, *Electrochim. Acta* (2006) **52**, 1514.
[104] M. Lira-Cantu, P. Gomez-romero, *Int. J. Inorg. Mater*. (1999) **1**, 111.
[105] K. Zhang, L. L. Zhang, X. S. Zhao, J. Wu, *Chem. Mater.* (2010) **22**, 1392.
[106] P.J. Hung, K.H. Chang, Y.F. Lee, C.C. Hu, K.M. Lin, *Electrochim. Acta* (2010) **55**, 6015.
[107] T.C. Girija, M. V. Sangaranarayanan, *Synth. Met.* (2006) **156**, 244.
[108] M. Malta, E. R. Gonzalez, R. M. Torresi, *Polymer* (2002) **43**, 5895.

[109] Y. Bardavid, I. Goykhman, D. Nozaki, G. Cuniberti, S. J. Yitzchaik, *Phys. Chem.* C (2011) **115** , 3123.
[110] S. Jussila, M. Puustinen, T. Hassinen, J. Olkkonen, H. G. O. Sandberg, K. Solehmainen, *Org. Electron.* (2012) **13**, 1308.
[111] W. Wang, X. Lu, Z. Li, J. Lei, X. Liu, Z. Wang, H. Zhang, C. Wang, Adv. Mater. (2011) **23**, 5109.
[112] M.R. Choi, T.H. Han, K.G. Lim, S.H. Woo, D.H. Huh, T.W. Lee, *Angew. Chem*. (2011) **50**, 6274.
[113] D. H. Huh, M. Chae, W.J. Bae, W.H. Jo, T.W. Lee, *Polymer* (2007) **48**, 7236.
[114] H. Bejbouj, L. Vignau, J. L. Miane, T. Olinga, G. Wantz, A. Mouhsen, E. M. Oualim, M. Harmouchi, Mater. *Sci. Eng. B* (2010) **166**, 185.
[115] W. Wang, Z. Li, X. Xu, B. Dong, H. Zhang, Z. Wang, C. Wang, R.H. Baughman, S. Fang, Small (2011) **7**, 597.
[116] M.I. Vladu, N. Marjanovic, A.Vlad, A. M. Ramil, G. Hernandez-Sosa, R. Schwoodiauer, S. Bauer, N.S. Sariciftci, *Adv. Mater.* (2008) **20**, 3887.
[117] M.R. Choi, T.H. Han, K.G. Lim, S.H. Woo, D. H. Huh, T.W. Lee, *Angew. Chem.* (2011) **50**, 6274.
[118] A.W. Marsman, C.M. Hart, G.H. Gelinck, T.C.T. Geuns, D.M. De Leeuw, *J. Mater. Res*. (2004) **19**, 2057.
[119] Z. Li, B. Ye, X. Hu, X. Ma, X. Zhang, Y. Deng, *Electrochem. Commun*. (2009) **11**, 1768.
[120] H. Sun, Y. Luo, Y. Zhang, D. Li, Z. Yu, K. Li, Q. Meng, *J. Phys. Chem.* (2010) **114**, 11673.
[121] M. Zhiani, H. Gharibi, K. Kakaei, *J. Power Sources* (2012) **210**, 42.
[122] M.R. Anderson, B.R. Mattes, H. Reiss, R.B. Kaner, *Science* (1991) **252**, 1412.
[123] C.-H.Chang, T.-C. Huang, C.-W Peng, T.-C. Yeh, H.-I. Lu, W.-I. Hung, C.-J. Weng, T.-I. Yang, J.-M.Yeh, *Carbon* (2012) **50**, 5044.
[124] L.F. Lux, *Polymer* (1994) **35**, 2915.
[125] A. G. MacDiarmid, A. J. Epstein, *Faraday Discuss. Chem. Soc*. (1989) **88**, 317.
[126] W. Lei, N. M. Kocherginsky, *React. Funct. Polym.* (2000) **45**, 65-77.
[127] M.J. Panzer, C.D. Frisbie, *J. Am. Chem. Soc.* (2007) **129**, 6599. doi: 10.1021/ja0708767.
[128] F. Bordi, C. Cametti, R.H. Colby, *J. Phys. Condens. Matter*. (2004) **16**, R1423.
[129] G. Casalbore-Micelia, M.J. Yangb, Y. Lib, A. Zanellia, A. Martellia, S. Chenb, Y. Sheb, N. Camaionia, *Sensors Actuat. B: Chem*. (2006) **114**, 584–590.
[130] S.-W. Joo, M.-S. Gong, *Sensors Actuat. B: Chem*. (2005) **105**, 150.
[131] X.Wang. PhD thesis "Controlling ion transport in organic devices" , Linkoping University Electronic Press (2013).
[132] K. Murata, *Electrochim. Acta* (2000) **45**, 1501.
[133] A. M.Stephan, *Eur. Polym. J*. (2005) **42**, 21.
[134] J. Song, *J. Power Sources* (1999) **77**, 183.
[135] C. Berthier, W. Gorecki, M. Minier, M.B. Armand, J.M. Chabagno, *Solid State Ion.* (1983) **11**, 91.
[136] B. Martin, A. Wagner, H. Kliem, *J. Phys. D: Appl. Phys.* (2003) **36**, 343.
[137] R.F.T. Stepto, "Polymer networks: principles of their formation, structure and properties", Blackie Academic & Professional London (1998).
[138] L.H. Sperling, "Introduction to physical polymer science", Wiley Online Library (1986).
[139] J.R. MacCallum, C.A. Vincent, "Polymer electrolyte reviews", Springer (1989).
[140] D.W. Murphy, J. Broadhead, B.C.H. Steele "Materials for advanced batteries", Plenum Press (1980).
[141] Y-W. Cho, J. Jang, C.R. Park, S-W. Ko. *Biomacromolecules* (2000) **1**, 609.
[142] M. Rinaudo, G. Pavlov, J. Desbrieres, *Polymer* (1999) **40**, 7029.
[143] K.M. Kim, J.H. Son, S-K. Kim, C.L. Weller, M.A. Hanna, *J. Food Sci.* (2006) **71**, E119.
[144] Kurita K., *Polym. Degrad. Stabil*. (1995) **59**, 117.
[145] S. Mima, M. Miya, R. Iwamoto, S.Yoshikawa. *J. Appl. Polym. Sci*. (1983) **28**, 1909.
[146] M. Rinaudo, G. Pavlov, J. Desbrieres, *Int. J. Polym. Anal. Charact.* (1999) **5**, 267.
[147] A. Domard, *Int. J. Biol. Macromol*. (1987) **9**, 98.
[148] S. Popa-Nita, P. Alcouffe, C. Rochas, L. David, A. Domard, *Biomacromolecules* (2010) **11**, 6.

[149] L. Rami, S. Malaise, S. Delmond, J.C. Fricain, R. Siadous, S. Schlaubitz, E. Laurichesse, J. Amedee, A. Montembault, L. David, *J. Biomed. Mater. Res. A* (2014) **102**, 3666.
[150] Y. Maki, K. Furusawa, S.Yasuraoka, H. Okamura, N. Hosoya, M. Sunaga, T. Dobashi, Y. Sugimoto, K. Wakabayashi. *Carbohydr. Polym.* (2014) **108**, 118.
[151] S. T. Koev, P. H. Dykstra, X. Luo, G. W. Rubloff, W. E. Bentley, G. F. Payneb, R. Ghodssi, *Lab Chip* (2010) **10**, 3026. doi: 10.1039/c0lc00047g.
[152] S. T. Koev, M. A. Powers, H. Yi, L.-Q. Wu, W. E. Bentley, G. W. Rubloff, G. F. Payne, R. Ghodssi, *Lab Chip* (2007) **7**, 103.
[153] G. Crini, *Prog. Polym. Sci.* (2005) **30**, 38.
[154] W.Y. Won, F.X. Feng, D. Lawless, *J. Membr. Sci*. (2002) **209**, 493.
[155] I. Arvanitoyannis, *J. Macromol. Sci*. (1999) **C39**, 205.
[156] I. Arvanitoyannis, A. Nakayama, S. Aiba, *Carbohydr. Polym*. (1998) **37**, 371.
[157] D. Sahoo, S.Sahoo, P. Mohanty, S. Sasmal, P. L. Nayak, *Des. Monomers Polym.* (2009) **12**, 377.
[158] J.S. Mao, L.G. Zhao, Y.J. Yin, *Biomaterials* (2003) **24**, 1067.
[159] K.G. Li, Y.Wang, Z.C. Miao, *Biotechnol. Lett.* (2004) **26**, 879.
[160] R.L.Whistler, J.N. BeMiller, "Carbohydrate Chemistry for Food Scientists", M. G. Lindhauer (1997). doi: 10.1002/star.19970490718.
[161] C. Rolin, J. de VriesIn, "Food Gel", P. Harris (Ed.), Elsevier Applied Science, Barking, U.K. (1990).
[162] D. Oakenfull, A. Scott, "New approaches to the investigation of food gels, in Gum and Stabilizers for the Food Industry", G. O. Philip, D. J.Wedlock, P. A.Williams (Eds.), Elsevier, London (1986).
[163] B. R. Thakur, R. K. Singh, A. K. Handa, *Crit. Rev. Food Sci. Nutr.* (1997) **37**, 47.
[164] G. A. Towel, O. Christensen, "Pectin, in Industrial Gums—Polysaccharides and their Derivatives", R.L.Whistler, J. N. BeMiller, (Eds.), Academic Press, New York (1959) 377.
[165] I. Braccini, S. Pérez, *Biomacromolecules* (2001) **2**, 1089. doi: 10.1021/bm010008g.
[166] H. Lotzkar, T. H. Schultz, H. S. Owens, W. D. MacLay, *J. Phys. Chem*. (1946) **50**, 200.
[167] J. Pagán, A. Ibarz, M. Llorca, L. Coll, *J. Food Sci. Agr.* (1999) **79,** 1038.
[168] G. Zsivanovits, A.J. MacDougall, A.C. Smith , S.G. Ring .*Carbohydr Res.* (2004) **339**, 1317.
[169] R. C. Jordan, D. A. Brant, *Biopolymers* (1978) **17**, 2885.
[170] D. G.Okenfull,"The chemistry of high methoxyl pectins". In "The Chemistry and Technology of Pectin", R.H.Walter (Ed.), Academic Press, New York, (1991) 87.
[171] S. Nakai, E.Li-Chan, "Hydrophobic Interactions in Food Systems", CRC Press, Boca Raton, FL, (1988).
[172] W.G.T Willats, J. P. Knoxb, J. D. Mikkelsen, Trends Food Sci.Technol. (2006) **17**, 97.
[173] F. Licci, S. Rinaldi, and T. Besagni, U.S. Patent 622,159 (1986).
[174] M. Ram, *Synthetic Metals.* (1999) **100**, 249.
[175] A. Riul Jr, L. Mattoso, G. Telles, P. Herrmann, L. Colnage, N. Parizotto, *Thin Solid Films* (1996) **284**, 177.
[176] J. Cheung, M. Rubner, *Thin Solid Films* (1994) **244,** 990.
[177] "Langmuir-Blodgett Films" G. Roberts (Ed.), Plenum Press, New York (1990) 93-132.
[178] V. Troitsky, T. Berzina, M.P. Fontana, *Synthetic Metals.* (2002) **129**, 39.
[179] G. Hummer, L.R. Pratt, A.E. Garcı´a, *J. Phys. Chem.* (1996) **100**, 1206.
[180] S.Forsen, J. Kordel, *Bioinorganic chemistry* (1994) 107.
[181] Y. Zhou. PhD thesis "Exploring the Role of Calcium Ions in Biological Systems by Computational Prediction and Protein Engineering" (2007).
[182] E. Neher, T. Sakaba, *Neuron* (2008) 59, 861. doi: http://dx.doi.org/10.1016/j.neuron.2008.08.019,
[183] "Polyelectrolyte Complexes in the Dispersed and Solid State I Principles and Theory" Müller, Martin (Eds.), Springer (2014).
[184] J.L. Green, C.A. Angell, *J. Phys. Chem.* (1989) **93**, 2880.
[185] A.M. Massari, I.J. Finkelstein, B.L.McClain, A.Goj, X. Wen, K.L Bren, R.F. Loring, M.D. J. Fayer, *Am.Chem.Soc.* (2005)**127**, 14279.

[186] Lovorka Peri´C-Hassler. PhD thesis "Computer simulations of carbohydrates" (2009).
[187] A.S. Kamisan, T.I.T. Kudin, A.M.M. Ali, M.Z.A.Yahya, *Electrochim. Acta* (2011) **57**, 207.
[188] S.Z.Z. Abidin, M.F.M. Taib, T.I.T. Kudin, A.M.M. Ali, O.H. Hassan, M.Z.A. Yahya, *Int. J. Electroactive Mater.* (2013) **1**, 36.
[189] Y.K. Mahipal. PhD thesis "Solid state ionics: a brief overview" (2012).
[190] D. Golodnitskya, E.Strauss, E. Peled, S. Greenbaum, *J. Electrochem. Soc*. (2015) **162**, A2551. doi: 10.1149/2.0161514jes.
[191] R. C. Agrawal, D.K. Sahu, Y. K. Mahipal, R. Ashrafi, "Electrical and Electrochemical Properties of New Mg^{2+}-Ion Conducting Polymer Electrolyte Membranes". In "Solid State Ionics"K.Junichi (Ed.) World Scientific Publishing Co. Pte. Ltd., (2013), 144-151.
[192] D. V. Radziuk, H. Möhwald, *Polym.* (2011) **3**, 674. doi:10.3390/polym3020674 1.
[193] X. Zhang, "Advanced Organic and Inorganic Materials for Electrochemical Power Sources", N.J. Pennington (Ed.) The Electrochemical Society (2010).
[194] K.S. Ngai, S. Ramesh, K. Ramesh, J.C.Juan, Ionics (2016) **22**, 1259.
[195] G.G.Cameron, M.D. Ingram, "Polymer Electrolyte Reviews", J. R. MacCallum, C. A. Vincent (Eds), Elsevier, London (1989) p.l57.
[196] T. Ren, X.B. Huang, X. Zhao, X.Z. Tang, *Acta Polym. Sin.* (2003) **3**, 361.
[197] S. Malhotra, P.K. Varshney, *NCASH-2015* (2015) **4**, 8179.
[198] M.F. Shukur, R. Ithnin, M.F.Z. Kadir, *Electrochim. Acta* (2014) **136** 204.
[199] R. Mancinelli, A. Botti, F. Bruni, M. A. Ricci, A. K. Soper, *J. Phys. Chem. B* (2007) **111**, 13570.
[200] J. Mähler, I. Persson. *Inorganic Chemistry* (2011) **51**, 425.
[201] W.R. Fawcett, "Liquids, solutions and interfaces". Oxford Univ. Press, Oxford, U.K. (2004).
[202] S. Beladjine, M. Amrani, A. Zanoun, A. Belaidi, G. Vergoten, *Computational & Theoretical Chemistry* (2011) **977,** 97. doi: 10.1016/j.comptc.2011.09.010
[203] M.C. Jarvis, D.C. Apperley, *Carbohydr. Res.* (1995) **275**, 131.
[204] E.D.T. Atkins, H.H. Nieduszynski, W. Mackie, K.D. Parker, E.E. Smolko, *Biopolym.* (1973) **12** 1879.
[205] C.S. Pereira, D. Kony, R. Baron, M. Müller, W.F.van Gunsteren, P.H.Hünenberger, *Biophys. J.* (2006) **90**, 4337.
[206] R. P. McCall, *Phys. Rev. B* (1990) **41**, 5202.
[207] U. Rana, K. Chakrabarti and S. Malik, *J. Mater. Chem*. (2012) **22**, 15665.
[208] H. Yi, L.Q. Wu, W. E. Bentley, R. Ghodssi, G. W. Rubloff, J. N. Culver, G. F. Payne, *Biomacromolecules* (2005) **6**, 2881.
[209] W. W. Focke, G. E. Wnek,Y. Wei, *J. Phys. Chem.* (1987) **91**, 5813.
[210] S. Nakai, E. Li-Chan, "Hydrophobic Interactions in Food Systems", CRC Press, Boca Raton, FL, (1988).
[211] K.Gorshkov, T.Berzina, *BioNanoSci.* (2011) **1**, 198.
[212] A. Giovannittia, D.T. Sbirceaa, S. Inalb,C. B. Nielsena, E. Bandielloe, D.A. Hanifif , M.Sessoloe , G. G. Malliaras, I.McCullocha, J. Rivnay, *Proc. Natl. Acad. Sci. U S A* (2016) **113**, 12017.
[213] H. Haa, J. Payer, *Electrochim. Acta*. (2011) **56**, 2781. doi:10.1016/j.electacta.2010.12.050.]6,10-17
[214] V.I. Birss, C.K. Smith, *Electrochim. Acta*. (1987) **32**, 259.
[215] S. Jaya, T.P. Rao, G.P. Rao, *J. Appl. Electrochem*. (1987) **17**, 635.
[216] B.M. Jovic, V.D. Jovic, D.M. Drazic. *J. Electroanal. Chem.* (1995) **399**, 197.
[217] P.Bro, N. Marincic N., *J.* Electrochem. Soc. (1969) **116**, 1338.
[218] C. Cachet, *J. Electroanal. Chem.* (1979) **100**, 745.
[219] H.Cheftel, J. Monvoisin. "La corrosion des boites de Fer Blanc dans l'Industri des Conserves-Carnaud et Forges Basse Indre" (1954).
[220] R.M. El-Sherif, W.A. Badawy, *Int. J. Electrochem. Sci.* (2011) **6**, 6469.
[221] B.F. Gannetti, P.T. Sumodjo, T. Rabockai, A. Souza, J. Barboza, *Electrochim. Acta* (1992) **37**, 143.
[222] H. Suzuki, H. Shiroishi, S. Sasaki, I. Karube, *Anal. Chem.* (1999) **71**, 5069–5075. doi: 10.1021/ac990437t.

[223] W.Kit-Anan, A. Olarnwanich, C. Sriprachuabwong, C. Karuwan , A.Tuantranont, A. Wisitsoraat, W. Srituravanich , A. Pimpin, *J. Electroanal. Chem.* (2012) **685,** 72–78.
[224] E. M. Genies, S. Tsintavis, *J. Electroanal. Chem. Interracial Electrochem.* (1985) **195**, 109.
[225] G. Inzelt, M. Pineri, J.W.Schultze, M. A. Vorotyntsev, *Electrochim. Acta* (2000) **45**, 2403.
[226] H.Yang, J.Kwak, *J. Phys. Chem. B* (1997) **101**, 774.
[227] G. Inzelt, *Electrochim. Acta* (2000) **45**, 2403.
[228] P. Poks, M. Grzeszczuk, *Synth. Met.* (1997) **89**, 237.
[229] J.M. Pernaut, E.M. Genies, M. Nechtschein, E.Vieil, F. Genoud, F. Devreux, *Synth. Met.* (1986) **15**, 59.
[230] Vorotyntsev, M.A.; Heinze, J.; Electrochim. Acta 2001, 46, 3309.
[231] T. Matencio, J. M. Pernaut, E. J. Vieilb, *Braz. Chem. Soc.* (2003) **14**, 90.
[232] E, M. Houze, A. Nechtschein, *Synth. Met.* (1997) **84**, 981-982.
[233] W. Lei, N. M. Kocherginsky, *React. Funct. Polym*. (2000) **45**, 65.
[234] W. Zheng, "Redox reactions and charge transport through polyaniline membranes", PhD Thesis, National University of Singapore (2006).
[235] N. M. Kocherginsky, W. Lei, Z. Wang, *J. Phys. Chem*. (2005) **109**, 4010.
[236] Kobayashi, T., H. Yoneyama, H. Tamura, *J. Electroanal. Chem.* (1984) **177**, 293.
[237] E. T. Kang, K. G. Neoh, K. L. Tan, *Polymer* (1996) **37**, 925.
[238] A. Adamatzky, M. Komosinski, "Artificial Models in Hardware", A. A**damatzky**, M. **Komosinski**, Maciej (Eds.), Springer, London (2009). doi:10.1007/978-1-84882-530-7
[239] R. F. Watkins, M. W. Gray, *Protist*. (2008) **159**, 269.
[240] W. Baumgarten, M. J. B. Hauser, *Interdiscip. Sci.: Comput. Life Sci*. (2010) **1**, 24123.
[241] A. Dussutour, T. Latty, M. Beekman, S. J. Simpson, *Proc. Natl. Acad. Sci. U. S. A.* (2010) **107**, 4607.
[242] J. G. H. Whiting, B. P. J. de Lacy Costello, A. Adamatzky, *Sens. Actuators, B* (2014) **191**, 844.
[243] A. Adamatzky, S. G. Akl, *ArXiv:1105.5084v1 [nlin.PS]* (2011), 1.
[244] T. Nakagaki, H. Yamada, M. Hara, *Biophys. Chem*. (2004) **107**, 1.
[245] A. Adamatzky, *Parallel Process. Lett.* (2009) **19**, 105.
[246] M. Aono, S.-J. Kim, M. Hara, T. Munakata, *Biosyst*. (2014) **117**, 1.
[247] A. Tero, R. Kobayashi, and T. Nakagaki, *Phys. A: Statistical Mechanics and its Applications*, (2000) **363**,115.
[248] T. Saigusa, A. Tero, T. Nakagaki, Y. Kuramoto, *Phys. Rev. Lett.* (2008)**100**, 018101.
[249] W. Marwan, *Science* (2010) **327**, 419.
[250] S. Tsuda, M. Aono and Y.-P. Gunji, *Biosyst*, (2004) **73**, 45–55.
[251] A. Adamatzky, *Mat. Sci. and Eng. C* (2010) **30**, 1211.
[252] X. A. Walter, I. Horsfield, R. Mayne, I. A. Ieropoulos, A. Adamatzky, Sci Rep. (2016) **6**, 23924. doi: 10.1038/srep23924
[253] A. Adamatzky, "Slime mould gates, roads and sensors". In "Atlas of Physarum Computing". A. Adamatzky (Ed.) World Scientific Publishing Co. Pte. Ltd., pp. 1-34, (2015). doi:10.1142/9789814675321_0001.
[254] Y.V.Pershin, S. LaFontaine, M. DiVentra, *Phys.Rev.* (2009) **E80**, 021926.
[255] K.Alim, G.Amselem, F.Peaudecerf, M.P.Brenner, A.Pringle, *Proc. Natl. Acad. Sci.* (2013) **110**, 13306.
[256] E. Gale, A. Adamatzky, and B. de Lacy Costello, *J. BioNanoScience* (2015) **5**, 1–8.
[257] F. Lin and M. C. Lonergan, *Appl. Phys. Lett.*, (2006) 88, 133507.
[258] G. Tarabella, A. G. Balducci, N. Copped` e, S. Marasso, P. D'Angelo, S. Barbieri, M. Cocuzza, P. Colombo, F. Sonvico, R. Mosca and S. Iannotta, *Biochim. Biophys. Acta* (2013) **1830**, 4374.
[259] O. Larsson, A. Laiho, W. Schmickler, M. Berggren and X. Crispin, *Adv. Mater.* (2011) **23**, 4764.
[260] D. A. Bernards, D. J. Macaya, M. Nikolou, J. A. DeFranco, S. Takamatsu, G. G. Malliaras, *J. Mater. Chem*. (2008)**18**, 116.
[261] F. Cicoira, M. Sessolo, O. Yaghmazadeh, J. A. DeFranco, S.Y.Yang, G. G. Malliaras, *Adv. Mater.* (2010) **22**, 1012.

[262] G. Tarabella, C. Santato, S. Y. Yang, S. Iannotta, G. G. Malliaras, F. Cicoira, *Appl. Phys. Lett.*, (2010) **97**,123303.
[263] V. Erokhin, "Polymer-based adaptive networks", in "The New Frontiers of Organic and Composite Nanotechnologies", V. Erokhin, M.K. Ram, and O. Yavuz (eds.), Elsevier, Oxford, Amsterdam, pp. 287-353 (2008).
[264] T. Berzina, A. Pucci, G. Ruggieri, V. Erokhin, and M.P. Fontana, *Synth. Met.* (2011) **161**, 1408.
[265] V. Erokhin, T. Berzina, K. Gorshkov, P. Camorani, A. Pucci, L. Ricci, G. Ruggeri, R. Sigala, A. Schuz, *J. Mater. Chem.* (2012) **22**, 22881.
[266] V. Erokhin, T. Berzina, and M.P. Fontana, *J. Appl. Phys.* (2005) **97**, 064501.
[267] T. Berzina, S. Erokhina, P. Camorani, O. Konovalov, V. Erokhin, M.P. Fontana, *ACS Appl. Mater. Interfaces* (2009) **1**, 2115.
[268] V. T.Nachmias, A. Ash, *Biochem*. (1976) **15**, 4273.
[269] K. E.Wohlfarth-Bettermann, M. Fleischer, *Cell. Tissue Res.* (1976) **165**, 327.
[270] N. Kamiya, Rev. *Plant. Physiol.* (1981) **32**, 205.
[271] B. Macdonald, "Impedance Spectroscopy: Theory, Experiment, and Applications", E. Barsoukov, J. R. Macdonald (Ed.), Wiley-Interscience, New Jersey (2005).
[272] D. R. Rueda, F. Martinez, *Colloid Polym. Sci.* (1997) **275**, 419.
[273] P. G. Bruce, "Polymer Electrolyte Reviews", Elsevier Applied Science, New York (1987).
[274] M.C. Wintersgill, J.J. Fontanella, "Low-frequency dielectric properties of polyether electrolytes", in "Polymer Electrolyte Reviews", Elsevier Applied Science, New York (1987).
[275] C. Nordling, J. Österman, "Physics Handbook for Science and Engineering"(8th ed) Studentlitteratur, Lund, Sweden, (2006).
[276] P. Atkinsand, J.d. Paula, "Atkins' Phyical Chemistry" Oxford University Press, Oxford, UK (2010).
[277] F. Bueche, *J. Polym. Sci*. (1961) **54**, 597-602.
[278] C.-Y. Liu, K.-S. Zhao, *Soft Matter* (2010) **6**, 2742.
[279] K. Asami, A. Irimajiri, T. Hanai, N. Koizumi, *Bull. Inst. Chem. Res. Kyoto Univ*. (1973) **51**, 231.
[280] A. Nogales, T. A. Ezquerra, D. R. Rueda, F. Martinez, J. Retuert, *Colloid Polym. Sci*. (1997) **275**, 419.
[281] F. Bordi, C. Cametti and R. H. Colby, *J. Phys. Condens. Matter* (2004) **16**, 1423.
[282] L. K. H. Van Beek, "Dielectric behaviour of heterogeneous systems", in "Progress in Dielectrics", J. B. Birks (Ed.), Heywood Books, London (1967).
[283] T. Mitsumata, J. P. Gong, K. Ikeda, Y. Osada, *J. Phys. Chem. B* (1998) **102**, 5246.
[284] K. Asami, Langmuir (2005) **21**, 9032.
[285] M. T. Shaw, J. Chem. Phys. (1942) **10**, 609.
[286] R.J. Klein, S.Zhang, S. Dou, B.H. Jones, R.H. Colby, J. Runt, *J. Chem. Phys*. (2006) **124**, 144903.

Acknowledge

I would like to express my special thanks to my advisor Dr. Salvatore Iannotta. It has been an honor to be his Ph.D. student.
I appreciate all the opportunities that my tutor Victor Erokhin gave me, his scientific approach was able to open my mind.
Words cannot express how grateful I am to my tutors Dr. Tatiana Berzina and Prof. Antonella Parisini. They supported me in the work, teaching me a rigorous scientific approach. They incited me to strive towards my goal even during tough times in the Ph.D.

I am also thankful for the excellent example they have provided as successful physicists and professors. All their contributions of time, ideas, and funding made my Ph.D. experience productive and stimulating. The joy and enthusiasm they have for their research was contagious and motivational for me, I will never forget their teachings.

This work has been financially supported by: European project FP7-ICT-2011-8 "PhyChip-Physarum Chip: Growing Computers from Slime Mould" Grant Agreement no. 316366.

Publications

1. A. Cifarelli, A. Dimonte, T. Berzina, V. Erokhin. – On the Loading of Slime Mold Physarum Polycephalum with Microparticles for Unconventional Computing Application. – *BioNanoSci.*, **4** (2014) 92–96, doi: 10.1007/s12668-013-0124-3

2. A. Cifarelli, A. Dimonte, T. Berzina, V. Erokhin. - Non-linear bioelectronic element: Schottky effect and electrochemistry. - *International Journal of Unconventional Computing*, **10** (2014) 375-379
https://www.scopus.com/inward/record.uri?eid=2-s2.0-84907046276&partnerID=40&md5=ec006160fa6dfa1d12a9a38b9775f560

3. Tarabella, G., D'Angelo, P., Cifarelli, A., Dimonte, A., Romeo, A., T. Berzina, V. Erokhin, S. Iannotta. - A hybrid living/organic electrochemical transistor based on the Physarum polycephalum cell endowed with both sensing and memristive properties. - *Chemical Science*, **6** (2015) 2859-2868.
doi: 10.1039/c4sc03425b

4. A. Dimonte, T. Berzina, A. Cifarelli, V. Chiesi, F. Albertini, V. Erokhin. - Conductivity patterning with Physarum polycephalum: Natural growth and deflecting. - *Physica Status Solidi (C) Current Topics in Solid State Physics,* **12**, (2015) 197-201.
doi: 10.1002/pssc.201400077

5. A. Cifarelli, T. Berzina, V. Erokhin. - Bio-organic memristive device: Polyaniline-Physarum polycephalum interface. - *Physica Status Solidi (C) Current Topics in Solid State Physics*, **12** (2015) 218-221.
DOI: 10.1002/pssc.201400191

6. T. Berzina, A. Dimonte, A. Cifarelli, V. Erokhin. - Hybrid slime mold - Containing systems for unconventional computing. - *AIP Conference Proceedings*, **1648**, (2015) art. no. 280003.
doi: 10.1063/1.4912532

7. T. Berzina, A. Dimonte, A. Cifarelli, V. Erokhin. - Hybrid slime mould-based system for unconventional computing. - *International Journal of General Systems*, **44** (3), (2015) 341-353.
doi: 10.1080/03081079.2014.997523

8. A. Dimonte, A. Cifarelli, T. Berzina, V. Chiesi, P. Ferro, T. Besagni, F. Albertini, A. Adamatzky, V. Erokhin. - Magnetic Nanoparticles-Loaded Physarum polycephalum: Directed Growth and Particles Distribution. - *Interdisciplinary Sciences: Computational Life Sciences*, **7** (2015) 373-381.
doi: 10.1007/s12539-015-0021-2

9. A. Cifarelli, T. Berzina, A. Parisini, V. Erokhin, and S. Iannotta.- Polysaccarides-based gels and solid-state electronic devices with memresistive properties: Synergy between polyaniline electrochemistry and biology. . *AIP Advances* **6**, (2016) 111302(1-8).
http://dx.doi.org/10.1063/1.4966559